

LASER PARTICULATE COUNTER CALIBRATION
TO A MICRO-ORIFICE UNIFORM-DEPOSIT IMPACTOR

by

Benjamin Fredrich Seely

A thesis

submitted in partial fulfillment

of the requirements for the degree of

Master of Science in Civil Engineering

Boise State University

December 2011

© 2011

Benjamin Fredrich Seely

ALL RIGHTS RESERVED

BOISE STATE UNIVERSITY GRADUATE COLLEGE

DEFENSE COMMITTEE AND FINAL READING APPROVALS

of the thesis submitted by

Benjamin Fredrich Seely

Thesis Title: Laser Particulate Counter Calibration to a Micro-Orifice Uniform-Deposit Impactor

Date of Final Oral Examination: 21 October 2011

The following individuals read and discussed the thesis submitted by student Benjamin Fredrich Seely, and they evaluated his presentation and response to questions during the final oral examination. They found that the student passed the final oral examination.

Sondra M. Miller Ph.D., P.E. Chair, Supervisory Committee

George A. Murgel, Ph.D., P.E. Member, Supervisory Committee

Dale Stephenson, Ph.D., CIH Member, Supervisory Committee

The final reading approval of the thesis was granted by Sondra M. Miller, Ph.D., P.E., Chair of the Supervisory Committee. The thesis was approved for the Graduate College by John R. Pelton, Ph.D., Dean of the Graduate College.

ACKNOWLEDGEMENTS

I would like to thank the professors and instructors I worked with during my time at Boise State University: Dr. Murgel, my undergraduate advisor, who always took the time to encourage me to push myself and take on new challenges, Dr. Stephenson who provided me much needed technical support and the equipment necessary for me to perform my research, and most notably, my graduate advisor Dr. Sondra Miller, who deserves special thanks for providing me the opportunity to perform the research culminating in this thesis. She encouraged me to seek out solutions and answers on my own while teaching me to have confidence as an engineer.

Despite the single author on the title page, no thesis is written alone. This paper was possible due to the unending support of my family. My parents offered ceaseless support while my brother, Kevin, was constantly pushing me along, motivating me to complete the work. Most of all, I want to say thank you to my wife, Amy, who quietly sacrificed more than anyone else, myself included, to make this possible. Lastly, I want to thank my son, Remington, he gave up a lot of playtime while dad completed his homework.

This work was funded through a grant from the NASA Idaho Space Grant Consortium (NASA Award Number: NNG05GG29H).

ABSTRACT

In semi-arid regions, like southwest Idaho, snowmelt is a significant source of water. Anthropogenic activities continue to increase demand for this vital natural resource. Water resource managers must be able to quantify both the timing and quality of snowmelt. Atmospheric contaminants can deposit on the snow, altering its physical properties. For example, deposition of atmospheric particulate matter (PM) can cause snow to darken, thereby increasing radiative forcing on the snowpack, potentially causing a change in snowmelt timing.

This research is to calibrate a laser particulate counter (LPC) to a federal reference standard. The LPC provides real-time PM concentration data and can potentially be deployed in a wireless network of atmospheric sensors to measure temporal and spatial distributions. This calibration model will then be used to calibrate other LPCs for use in the network. This work will improve our understanding of the environment through real-time atmospheric monitoring in remote locations and over heterogeneous topography.

TABLE OF CONTENTS

ACKNOWLEDGEMENTS.....	iv
LIST OF TABLES.....	ix
LIST OF FIGURES.....	xi
INTRODUCTION.....	1
Motivation.....	1
Scope.....	3
LITERATURE REVIEW.....	4
Background.....	4
Particulate Matter Monitoring Equipment.....	7
OPC Performance Comparison with Cascade Impactors.....	9
Data Analysis and Inversion Techniques.....	10
MATERIALS AND METHODS.....	12
Setting.....	12
Laser Particle Counter.....	14
Micro-Orifice Uniform-Deposit Impactor (MOUDI).....	18
Calibration of MOUDI Air Flow.....	25
High Volume Air Sampler.....	28
Cascade Impactor.....	33
Data Analysis.....	35

RESULTS	42
General Results	42
LPC and MOUDI Comparison	43
LPC to MOUDI Calibration.....	49
LPC and Hi-Vol Comparison.....	53
MOUDI 1 and MOUDI 2 Comparison	61
Time Step Analysis.....	64
LPC 2 to LPC 1 Calibration.....	66
CONCLUSION.....	72
REFERENCES	76
APPENDIX A.....	84
Sample Calculation of LPC Count to Concentration	84
APPENDIX B	87
Calibration Data Provided by MSP for MOUDI Eff Curves	87
APPENDIX C	90
Same Calculations of MOUDI Concentration	90
APPENDIX D.....	92
Original Data from BIOS Testing.....	92
APPENDIX E	94
Calibration Calculations and Charts for Hi-Vols.....	94
APPENDIX F.....	105
Kernel Functions.....	105
APPENDIX G.....	119

Sample RPD Calculation	119
APPENDIX H.....	121
Sample Calculation of LPC 1 to LPC 2 Calibration, Stat Sheets, and Charts	121
APPENDIX I	140
Student T-Test Trip Blank Results	140
APPENDIX J	146
Student T-Test Trip Blank Results	146

LIST OF TABLES

Table 1	Instruments Used During Calibration	14
Table 2	Example of LPC Channel Sizing	16
Table 3	Aerodynamic Cutoff Diameters, D_{50} , for MOUDI Stages (13 L/min)	21
Table 4	MOUDI Model 100 Steepness Values, MSP Corp., St. Paul, MN.....	22
Table 5	Aerodynamic Cutoff Diameters for Hi-Vol Cascade Impactor Series 230	35
Table 6	Results from Data Inversion	46
Table 7	LPC and Inverted MOUDI PM Calibration Concentrations.....	47
Table 8	LPC and Inverted MOUDI PM Validation Concentrations.....	48
Table 9	Calibration PM Concentrations from LPC and MOUDI	50
Table 10	Validation Data Set	52
Table 11	Stage Equivalents Between LPC and Hi-vol	56
Table 12	Regression Analyses for Individual Cut Sizes (LPC 1 and LPC 2).....	70
Table A.1	Flow calibration for LPC	86
Table A.2	Statistical test results of pump flow rate between LPC and BIOS flow meter.	86
Table B.1	Original Calibration Data Provided by MSP Corp. for MOUDI 100/110 Stages 10 to 7	88
Table B.2	Original Calibration Data Provided by MSP Corp. for MOUDI 100/110 Stages 6 to 3	89
Table B.3	Original Calibration Data Provided by MSP Corp. for MOUDI 100/110 Stages 6 to 3 (continued).....	89

Table F.1	Kernel Function Results.....	108
Table F.2	Kernel Function Results (cont.)	109
Table F.3	Kernel Function Results (cont.)	110
Table F.4	Kernel Function Results (cont.)	111
Table F.5	Kernel Function Results (cont.)	112
Table F.6	Kernel Function Results (cont.)	113
Table F.7	Kernel Function Results (cont.)	114
Table F.8	Kernel Function Results (cont.)	115
Table F.9	Kernel Function Results (cont.)	116
Table F.10	Kernel Function Results (cont.)	117
Table F.11	Kernel Function Results (cont.)	118
Table H.1	Mann-Whitney Rank Sum Test Results for 0.5 μm , 5 min interval.	123
Table H.2	Mann-Whitney Rank Sum Test Results for 0.7 μm , 5 min interval.	125
Table H.3	Mann-Whitney Rank Sum Test Results for 1.0 μm , 5 min interval.	128
Table H.4	Mann-Whitney Rank Sum Test Results for 2.0 μm , 5 min interval.	130
Table H.5	Mann-Whitney Rank Sum Test Results for 3.0 μm , 5 min interval.	132
Table H.6	Mann-Whitney Rank Sum Test Results for 5.0 μm , 5 min interval.	134
Table H.7	Mann-Whitney Rank Sum Test Results for 7.0 μm , 5 min interval.	137
Table H.8	Mann-Whitney Rank Sum Test Results for 10.0 μm , 5 min interval.	139
Table J.1	Hi-vol trip blank results	147
Table J.2	T-Test.....	147

LIST OF FIGURES

Figure 1	Map of Boise, Surrounding Area, DCEW, and BSU.....	13
Figure 2	Equipment Used During Calibration Process, from Left to Right, MOUDIs, LPC, and Hi-vol.....	13
Figure 3	LPC with Cover Removed (Met One, Grants Pass, OR).....	15
Figure 4	LPC with Cover Removed (Met One, Grants Pass, OR).....	15
Figure 5	Cross-Section View of Typical MOUDI Stage (Images from Model 100/110 MOUDI User Guide, MSP Corp, St. Paul MN)	19
Figure 6	MOUDI Model 100 Collection Efficiency Curves (MSP Corp., St. Paul, MN).....	23
Figure 7	BIOS DryCal Air Flow Meter, Aircon 520 Air Sampling Pump, and MOUDI.....	25
Figure 8	Comparison of BIOS and Pump 1975 Flow Rates	26
Figure 9	Calibration of Pump 1828 with a BIOS Flow Meter	27
Figure 10	Hi-vol Diagram (Image from Hi-vol Operation Manual) [49]	29
Figure 11	Hi-vol Outfitted with a Rootsmeter Variable Flow Orifice (Wedding and Associates, Fort Collins, CO)	31
Figure 12	Image of Cascade Impactor Exploded View (Image from Hi-vol Operation Manual) [49]	34
Figure 13	Kernel Functions for the MOUDI Model 100/110	39
Figure 14	LPC and MOUDI Average Concentrations	44
Figure 15	LPC, MOUDI 1, and Inverted MOUDI PM Calibration Concentrations .	46
Figure 16	LPC, MOUDI 1, and Inverted MOUDI PM Validation Concentrations ..	48

Figure 17	Calibration of LPC Concentrations to Inverted MOUDI Concentrations	50
Figure 18	Validation of LPC Concentrations to Inverted MOUDI Concentrations..	52
Figure 19	LPC and Hi-vol (Unit B) During Summer of 2010	55
Figure 20	Stage 2 Concentrations for LPC 1, LPC 2, and Hi-vol.....	58
Figure 21	TSP Concentrations Measured by LPC 1, LPC 2, and the Hi-vol.....	58
Figure 22	Average Cut Size Concentration for the LPC, MOUDI, and Hi-vol	59
Figure 23	TSP Concentrations Measured Using the LPC, MOUDI, and Hi-vol	60
Figure 24	MOUDI 1 and MOUDI 2 Average Concentration Comparison.....	63
Figure 25	MOUDI 1 and MOUDI 2 Average Concentration by Cut Size.....	63
Figure 26	RPD Normalized by Hour for the LPC and MOUDI	65
Figure 27	LPC 1 and LPC 2 TSP Comparison.....	67
Figure 28	Regression Analyses for 0.50 μm (LPC 1 and LPC 2).....	68
Figure 29	Regression Analyses for 10.0 μm (LPC 1 and LPC 2).....	68
Figure 30	LPC 1 and LPC 2 Calibration Results for 0.50 μm Cut Size.....	70
Figure 31	LPC 1 and LPC 2 calibration results for 10.0 μm Cut Size.....	71
Figure A.1	Hand Calculations of LPC Count to Calculation.....	85
Figure B.1	Calibration Data Provided by MSP for MOUDI Eff Curves.....	88
Figure C.1	Hand Calculations of MOUDI Concentration	91
Figure D.1	Original Data from BIOS Testing.....	93
Figure E.1	Calibration Calculations and Charts for Hi-Vols.....	95
Figure E.2	Calibration Worksheet	96
Figure E.3	Air Pollution Monitoring Equipment Graph.....	97
Figure E.4	Calibration of Hi-vol Samples Hand Calculations.....	98

Figure E.5	Calibration of Hi-vol Samples Hand Calculations (cont.)	99
Figure E.6	Test Run of Hi-Vols Hand Calculations	100
Figure E.7	Particular Profiler Calibration Hand Calculations	101
Figure E.8	Particular Profiler Calibration Hand Calculations (cont.).....	102
Figure E.9	Particular Profiler Calibration Hand Calculations (cont.).....	103
Figure E.10	Particular Profiler Calibration Hand Calculations (cont.).....	104
Figure F.1	Kernel Function Hand Calculations.....	106
Figure F.2	Kernel Function Hand Calculations (cont.)	107
Figure H.1	LPC 1 vs LPC 2 Particulate Count Comparison (0.5 μm , 5 min Interval)	122
Figure H.2	LPC 1 and LPC 2 Sample Particulate Count (0.5 μm , 5 min Interval) ..	122
Figure H.3	LPC 1 vs LPC 2 Particulate Count Comparison (0.7 μm , 5 min Interval)	124
Figure H.4	LPC 1 and LPC 2 Sample Particulate Count (0.7 μm , 5 min Interval) ..	124
Figure H.5	LPC 1 vs LPC 2 Particulate Count Comparison (1.0 μm , 5 min Interval)	126
Figure H.6	LPC 1 and LPC 2 Sample Particulate Count (1.0 μm , 5 min Interval) ..	126
Figure H.7	LPC 1 vs LPC2 Particulate Count Comparison (2.0 μm , 5 min Interval)	129
Figure H.8	LPC 1 and LPC2 Sample Particulate Count (2.0 μm , 5 min Interval) ...	129
Figure H.9	LPC 1 vs LPC2 Particulate Count Comparison (3.0 μm , 5 min Interval)	131
Figure H.10	LPC 1 and LPC 2 Sample Particulate Count (3.0 μm , 5 min Interval) ..	131
Figure H.11	LPC 1 vs LPC2 Particulate Count Comparison (5.0 μm , 5 min Interval)	133
Figure H.12	LPC 1 and LPC2 Sample Particulate Count (5.0 μm , 5 min Interval) ...	133

Figure H.13	LPC 1 vs LPC2 Particulate Count Comparison (7.0 μm , 5 min Interval)	135
Figure H.14	LPC 1 and LPC2 Sample Particulate Count (7.0 μm , 5 min Interval) ...	135
Figure H.15	LPC 1 vs LPC2 Particulate Count Comparison (10.0 μm , 5 min Interval)	138
Figure H.16	LPC 1 and LPC2 Sample Particulate Count (10.0 μm , 5 min Interval) .	138
Figure I.1	LPC 1, LPC 2, and Hi-vol Concentrations for Stage 5.....	141
Figure I.2	LPC 1, LPC 2, and Hi-vol Concentrations for Stage 4.....	141
Figure I.3	LPC 1, LPC 2, and Hi-vol Concentrations for Stage 3.....	143
Figure I.4	LPC 1, LPC 2, and Hi-vol Concentrations for Stage 2.....	143
Figure I.5	LPC 1, LPC 2, and Hi-vol Concentrations for Stage 1.....	145
Figure I.6	TPS Concentrations for LPC 1, LPC 2, and Hi-vol.....	145

INTRODUCTION

Motivation

Population growth continues to increase demand on natural resources, especially water. Snowmelt is a significant source of water for millions of people in the western United States. Snowmelt in a semi-arid region, like that of southwest Idaho, is a critical driver for local stream flows and groundwater levels. It is vital that scientists, water resource managers, and community leaders are able to understand both the timing and quality of this water source. Contaminants in snow threaten water quality because they can be transported into local tributaries and aquifers.

Decreased air quality may result in a corresponding decrease of snow quality in a watershed. Increased anthropogenic activities have resulted in changes to regional air quality, including higher levels of criteria pollutants such as particulate matter (PM), O₃, SO₂, NO_x, CO, and Pb. These contaminants can be scavenged from the atmosphere and deposited on snow [1]. It is important to monitor contaminant deposition in watersheds with significant snow cover as this is the mechanism by which contaminants often first enter the ecosystem [2]. Quantifying the transport of atmospheric contaminants to a snowpack requires understanding their size, mass, chemical composition, as well as their temporal and spatial distribution. It is also important to understand the physical processes by which contaminants are deposited on snow.

PM and gaseous compounds are scavenged from the atmosphere by wet (rain and snow) and dry deposition [3]. Studies have shown that over half of the total PM deposition may occur during snow events [2]. Contaminant deposition can result when PM accumulates on the snow surface, which in turn decreases the snow albedo [4]. Albedo is a measure of the reflectivity of a substance. Pure snow is very reflective with albedo values near 1.0, indicating almost all light is reflected. Changes in albedo will increase radiative forcing on snow due to a darkening effect from PM accumulation, which may cause snowmelt to occur sooner [5]. In the San Juan Mountains of southwestern Colorado, increased radiative forcing was estimated to shorten snow cover duration by as much as 18 to 35 days [6]. A change in snowmelt timing due to particulate contamination also risks decoupling snowmelt from seasonal temperatures. In areas where average temperatures are below freezing, this effect is minimal, but at elevations where temperatures fluctuate near freezing this can impact phenological events [7].

It can be difficult to remotely sense contaminants, such as PM, due to their simultaneous presence in both the atmosphere and snow [8]. There are very few locations equipped to directly and accurately measure either albedo or PM concentration in the western United States and more are required [9-11]. A network of sensors could be deployed to various locales ranging from remote watersheds to urban centers in a temporary or permanent configuration. Currently, methods to monitor PM concentrations in remote locations are limited to aerochem-style precipitation collectors, providing only average concentrations for excessively long time scales on the order of days or weeks [12, 13]. Deposition levels of PM vary by topography, landcover, and precipitation

amount [14-17]. Capturing these trends requires a large number of sensors deployed in a region. These networks would dramatically improve current monitoring programs.

Quantifying the relationship between atmospheric contaminants and changes in snowpack albedo could be used to verify the accuracy of remotely sensed data. Ground verification requires sensors that are able to monitor PM levels in real time while spatially distributed throughout a sampling area. The location of ground verification is dependent upon the flight time and path of orbiting satellites and a sensor network could be aligned to any specific flight path.

Scope

The hypothesis of this research is that a laser particulate counter (LPC), designed to estimate PM concentrations in real time, can be calibrated to a federal reference standard. Testing this hypothesis was accomplished by completing three research stages. The first stage was to operate a LPC and a Micro-Orifice Uniform-Deposit Impactor (MOUDI) simultaneously to collect calibration data. The sample runs included varying time intervals as well as duplicate MOUDI and LPC samples. Also, a high volume air sampler (hi-vol), outfitted with a cascade impactor, was used to further validate the LPC and MOUDI results.

The second stage was to analyze the data to ensure compatibility between these different measurement processes. This included performing a data inversion of the MOUDI results. Lastly, this calibrated LPC was used to calibrate a second LPC thereby demonstrating the reproducibility of deploying a series of particle counters throughout a watershed and other remote or distributed networks without the need for a long, labor-intensive calibration process.

LITERATURE REVIEW

Background

The complex effects of atmospheric PM deposition on a watershed snowpack have been studied extensively by researchers over the past 50 years. This work includes analyzing the effect of PM deposition on snowpack albedo as well as its spatial and temporal distributions, composition, and monitoring methods. Recently, different analysis algorithms have been developed to better quantify PM concentration data collected in the field. Though the breadth of this work is extensive, it illustrates a need for improved monitoring methods. The field-testing and calibration of a LPC is a fundamental step for deploying new leading-edge research equipment to the field.

Albedo, the reflective power of a surface, is calculated as the ratio of incident to reflected sunlight. It is an important descriptive parameter in both energy balance and snowmelt models. In 1980, Wiscombe and Warren developed a model to measure the spectral albedo of snow; this research has become a seminal work, spawning a multitude of subsequent studies [18, 19]. These studies identify key parameters affecting snow albedo, including: snow depth, solar angle, snow grain size, and ratio of diffuse to direct incoming solar radiation. The albedo of snow containing a variety of contaminants was measured in an attempt to explain the variation between experimental albedo and theoretical albedo.

Increasing snowmelt rates, corresponding to decreasing snowpack albedo, were reported as early as 1981 by Drake et al. This work showed that increased dust deposition on a snowpack resulted in up to an order of magnitude change to snowmelt timing. A thin dust layer, coupled with high solar radiation and low wind speeds, resulted in an advanced snowmelt rate [20]. By relating the changes in atmospheric PM concentration to corresponding changes in snow albedo, a link can be made between PM concentration and snowmelt rate.

In 1997, Ranalli et al. [13] studied PM deposition in a remote, high-alpine watershed. Bulk deposition collectors were used because real-time atmospheric monitoring instruments had prohibitive power and labor requirements. The following year, Lovett et al. [12] demonstrated that deposition in a complex watershed is dependent on topographical features such as landcover, aspect, and elevation. These works illustrate the need to monitor PM concentrations in remote locations using instruments capable of providing spatial and temporal distributions without excessive power or labor requirements.

The need to monitor PM concentrations in remote locations is further supported by the works of Heuer et al. [15] and Turk et al. [21]. Heuer's team demonstrated that PM could be transported long distances. For example, PM originating in the southwestern United States was deposited on the snowpacks in Colorado. Turk's team examined this PM and found it to be a potentially significant source of contaminants within the snowpack. This is because PM, in addition to being a contaminant, also provides a location for organic contaminants to sorb to before being transported to remote locations.

It is important to quantify the changes to both snowmelt rate and timing resulting from PM deposition. Painter et al. [22] estimated a change in snow cover duration between 18 and 35 days in the San Juan Mountains of the western United States. These changes were attributed to increased radiative forcing on the snowpack indicated by decreased albedo values measured during dust deposition events. The results also indicated an increased snowmelt rate of up to 40%. Although these values were attributed to decreased albedo during deposition events, corresponding changes in atmospheric PM concentration were not measured. These measurements could have provided a quantifiable link between atmospheric PM concentration and snowmelt rate. One reason these measurements were not taken was because the current air monitoring instruments were not suitable for remote location monitoring (e.g., excessive power requirements) nor do they offer sufficient time-scale resolution.

PM deposition is not the sole cause of change to snowmelt rate. For example, atmospheric PM blocks solar radiance from reaching the snowpack, this is referred to as dimming. Simultaneously, atmospheric PM absorbs solar radiance causing the troposphere to warm, increasing the temperature above the snowpack and resulting in a higher snowmelt rate (solar heating). Flanner et al. [5] found the effects of snowpack-bound particulates outweighed the effects of solar heating and dimming by six-fold. They outlined differences in model-observation trends while highlighting potentially significant sources of error. Some modeling problems include inaccurate observational data and insufficient aerosol distribution data. Both of these shortcomings would be greatly improved using real-time PM monitoring.

Particulate Matter Monitoring Equipment

A variety of instruments are available for estimating and measuring PM concentration. Each instrument operates by applying a different measurement theory, resulting in unique benefits and shortcomings. It is important to understand and correct for these differences before comparing results made using different instruments.

Optical particle counters (OPC) count and size particles based on the frequency and magnitude of a reflected laser beam passing through a stream of air. They provide real-time measurements but are susceptible to counting artifacts at higher concentrations. LPCs, such as the ones used in this research, are a class of OPCs.

Cascade impactors measure concentration based on gravimetric analysis. Particles are sized according to their behavior in an air stream, resulting in an aerodynamic diameter. One of the most common types of impactors is the Micro-Orifice Uniform-Deposit Impactor (MOUDI). A high volume air sampler (hi-vol) can also be outfitted with a cascade impactor. Impactors are very reliable and capable of producing accurate PM measurements. Because impactors physically collect PM on a substrate, they can require long sample times to meet minimum detection limits (MDLs).

Differential mobility analyzers (DMA) size particles based on their behavior in an electric field. A significant drawback to many of these devices (MOUDI, DMA, and hi-vol) is an excessive power requirement, often hindering field deployment. All of these devices, including the OPCs, offer the ability to size segregate PM.

Multiple studies have been performed using an OPC to estimate atmospheric concentrations of PM in a laboratory setting where concentrations are typically low.

Improvements in OPC performance have allowed their use in the field. Hughes et al. [23] simultaneously operated an OPC, DMA, and MOUDI to monitor and characterize atmospheric PM in Pasadena, CA during the winter of 1996. The results of this study showed strong agreement between number concentrations estimated by the OPC and the MOUDI (assuming a spherical particle with a density of 1.7 g/cm^3). These results were found by averaging 24 hr sample times.

Kleeman and Schauer [24] used an OPC, DMA, and MOUDI to characterize PM in vehicle exhaust. In this study, the air source was diluted to prevent coincidence errors that OPCs are prone to experience under high PM concentrations. When operating simultaneously, all instruments measured similar particle-size distributions. PM monitoring often requires the assumption of ideal, homogenous physical particle characteristics. Because the operating principles of each particular device vary, they can measure different magnitudes of PM concentration. It was recommended by these authors that multiple instruments be used to monitor atmospheric PM.

Field measurements have been made using an electrical low-pressure impactor (ELPI) in conjunction with different particle counters. The agreement between measurements was good, except for lower particle sizes (7 to 30 nm). The authors found that comparison of number, mass, and size distributions made using a high-volume air sampler, OPC, and ELPI did not follow a Gaussian distribution and therefore were evaluated using a Spearman's rank correlation coefficient. A very strong agreement, between the OPC and ELPI, was found when considering all stages. Individual stage comparisons were not provided [25].

OPC Performance Comparison with Cascade Impactors

OPC concentration measurements have been compared to concentration measurements from gravimetric analysis in a variety of studies. These comparisons are critical because gravimetric analysis is the federal reference standard for mass based air quality standards [26]. The LPC used in this work is a specific type of OPC used to estimate PM concentrations.

In 1995, Hand et al. [27], working in the Great Smokey Mountains, analyzed differences between OPC and MOUDI measurements. The MOUDI mass concentrations were first converted to number concentrations to allow direct comparison to OPC number counts. These number concentrations typically agreed within 30% and the standard deviations were within 8%. Discrepancies were attributed to MOUDI data inversion artifacts, lower size resolution of the MOUDI data, and OPC counting methods. This research illustrates a level of agreement that can be expected from these different sampling methodologies. In 1998, Hughes et al. [23] compared results from a pair of MOUDIs, a DMA, and an OPC. Again, MOUDI mass concentrations were converted to number counts. Comparisons were made for particle number distributions, mass concentrations, and chemical compositions. Although the results generally showed agreement, only the total number concentrations between the OPC and MOUDI were compared.

An Anderson cascade impactor, operating under the same physical principles as a MOUDI, was used to compare total suspended particulate (TSP) mass concentrations to those estimated with an OPC [28]. The impactor underreported concentrations due to particle bounce and carryover between stages. The OPC performed well when estimating

relative mass concentration, as compared to the impactor, but due to calibration factors did not provide an absolute concentration measurement. This indicates a need to calibrate or compare OPC concentrations to a measurement standard.

In 2009, Wang et al. [26] developed an OPC to estimate mass concentration. The testing demonstrated that OPCs are capable of very accurately counting particles present in low concentration but sensors can be overwhelmed during periods of high concentration. OPCs measure optical particle diameter, a size based on a calibration aerosol. The authors performed a linear regression comparing the OPC results to those obtain by a Tapered Element Oscillating Microbalance (TEOM). They found good agreement from results taken in ambient air, although not as good as those from a laboratory. The agreement was stronger for smaller particle sizes. This indicates that a linear regression comparison can be used to compare the results between an OPC and a gravimetric-based analysis method.

Data Analysis and Inversion Techniques

MOUDIs size segregate PM by collecting individual particles on a series of impactor stages. This collection method produces a discrete data set with each impactor stage representing an individual data point. Generally, this data is reported as a histogram. A complete analysis and calibration requires a numerical inversion to transform the discrete data into a continuous distribution function [29]. Numerous methods exist to perform this type of inversion [30-34].

The Twomey algorithm is a nonlinear, iterative algorithm used for data inversions. This algorithm was specifically adapted for use on cascade impactor results by Winklmayr et al. [30]. This adaptation incorporates the use of smooth kernel functions

that are based on impactor stage cut-off diameters as well as weighting functions and stopping criteria (convergence and boundary conditions).

Atmospheric PM concentrations are bimodal and lognormally distributed. Dzubay and Hasan [33] successfully fit this complex distribution to cascade impactor data. One assumption, critical during analysis, was that the geometric standard deviations of each mode were assumed equal. This work also showed the importance of determining the correct cut size of each stage, as a change of 10% to the theoretical cut size may introduce bias into the inversion results.

An iterative inversion algorithm will potentially have multiple solutions. Therefore, it is important to select the appropriate stopping criteria [35]. Successful application of an iterative inversion algorithm is achieved when the predicted stage mass agrees with the experimental mass within 5% and the number of iterations is limited (<100). In practice, convergence usually occurs within 5 to 20 iterations [29, 30]. Dong et al. [31] demonstrated that this inversion process could be applied in situations when the mass concentration of a particular mode or the total mass are unknown. These works demonstrate the applicability of applying an adapted Twomey algorithm to cascade impactor data. The inversion allows for the inter-stage estimation of PM concentration, which is critical to this thesis.

MATERIALS AND METHODS

Setting

Prior to field deployment, the LPC was calibrated. The calibration was performed by operating a LPC concurrently with both a MOUDI and a hi-vol. Calibration sampling was performed on the roof of the Micron Engineering Center (MEC) located on Boise State University's (BSU) engineering campus, affording easy, secure access to the equipment, including an adequate power supply. This locale represented an urban setting along the Boise River near the Dry Creek Experimental Watershed (DCEW) (see Figure 1 and Figure). A variety of equipment, as well as their functions (listed in Table 1), was used during sampling.

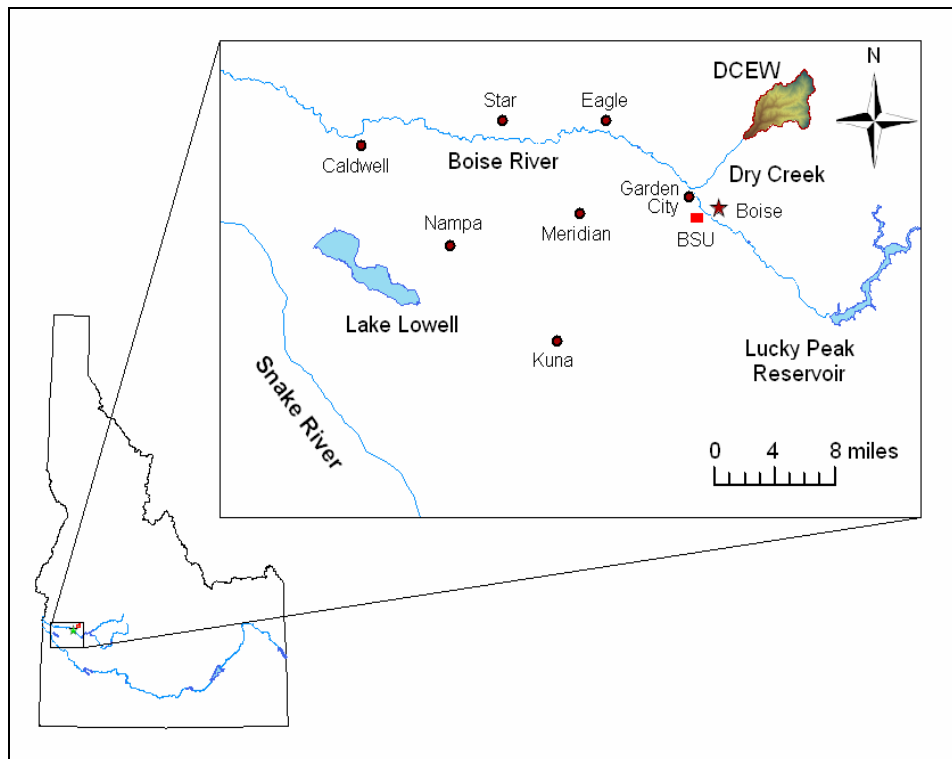


Figure 1 Map of Boise, Surrounding Area, DCEW, and BSU

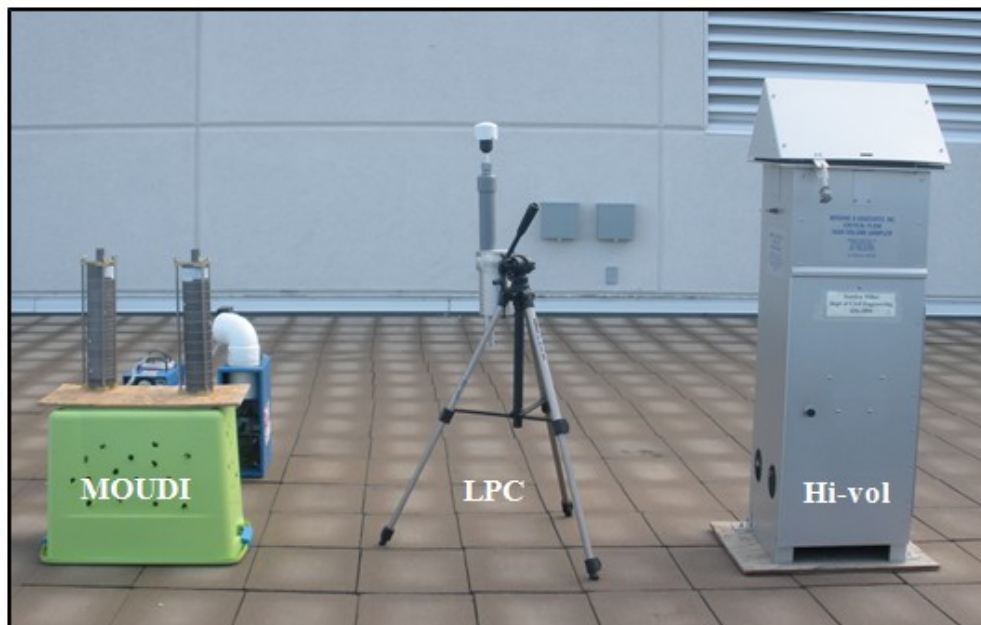


Figure 2 Equipment Used During Calibration Process, from Left to Right, MOUDIs, LPC, and Hi-vol

Table 1 Instruments Used During Calibration

Instrument	Manufacturer	Model	Function
Hi-vol	Wedding and Associates	Critical Flow High-Volume Air Sampler	Samples airborne particulate
Cascade Impactor	Tisch Environmental, Inc	Series 230	Samples and size fractionates airborne particulate
MOUDI	MSP Corp	Model 100	Samples and size fractionates airborne particulate
Laser Particulate Counter	Met One Instruments, Inc	212-1	Counts and size fractionates airborne particulate
Rootsmeter	Anderson Instruments, Inc	G28A	Calibration of hi-vol
BIOS DryCal	BIOS International Corp	DC-Lite	Calibration of air sampling pumps

Laser Particle Counter

Laser particulate counters, such as the Ambient Particulate Profiler Model 212-1 (Met One Instruments), are a class of light scattering optical sensors that use a reflected laser beam to count and size particulate, see Figure 3 and Figure 3. This LPC uses 8 programmable channels to report different particle sizes, ranging from 0.5 μm to 10.0 μm , while providing real-time estimations of atmospheric particulate.

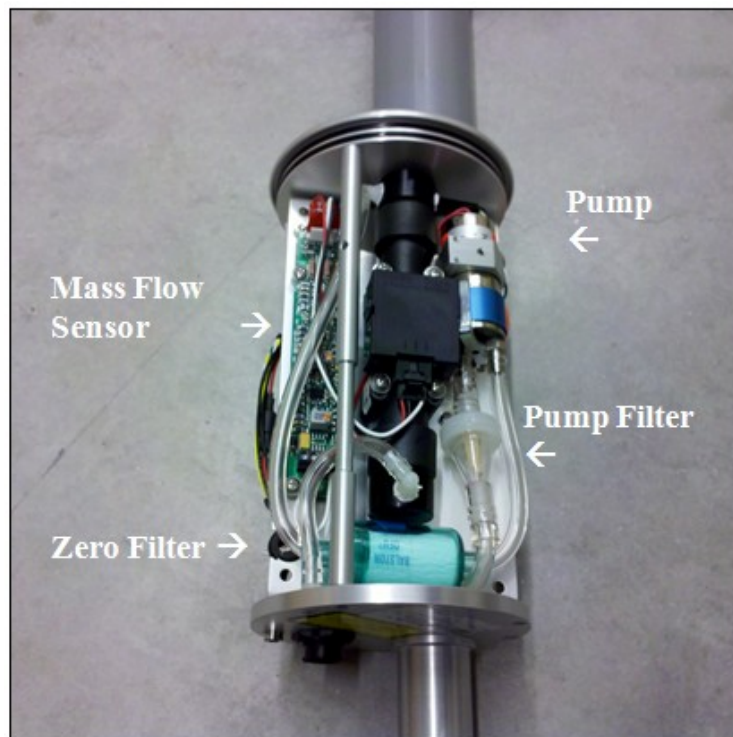


Figure 2 **LPC with Cover Removed (Met One, Grants Pass, OR)**

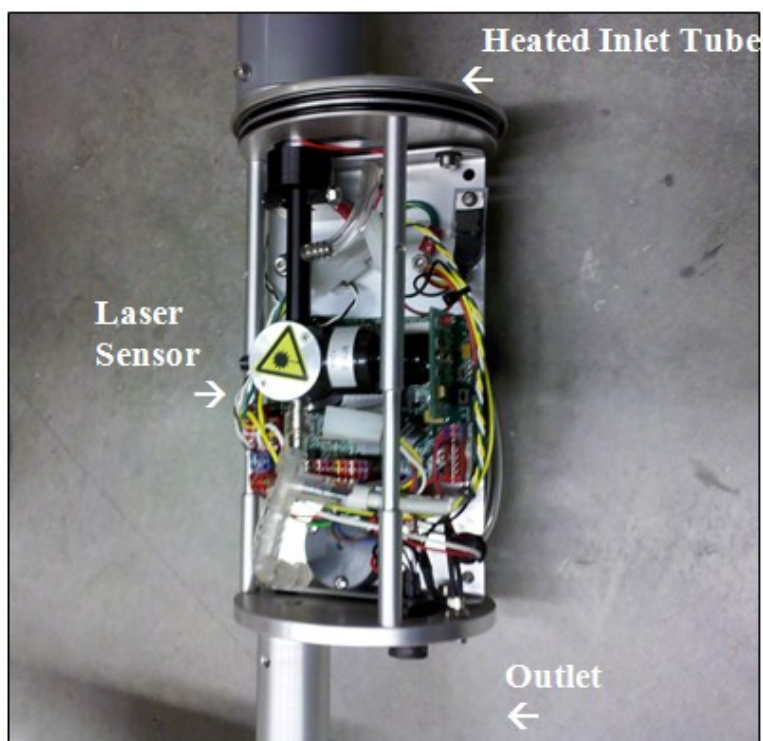


Figure 3 **LPC with Cover Removed (Met One, Grants Pass, OR)**

The LPC draws in air at a rate of 3.0 L/min using an internal rotary vane pump. Two-thirds of the air stream is filtered and used as sheathed air to contain the remaining one-third of the air stream. It is this unfiltered one-third of the air stream that is subsequently sampled. The sheathed air acts as a clean boundary surrounding the sampling stream, thus eliminating edge effects as well as preventing particles from leaving the sampling stream. A laser beam, collimated through the recombined air stream, is scattered by particulate. The magnitude of the scattering is proportional to the cross-sectional area of the particulate. The scattered light signal is collected and focused onto a photo diode, which converts the return signal to a voltage. The amplitude of this voltage is compared to eight predetermined, programmable voltages (Table 2). An internal counter is increased each time the voltage exceeds the programmed level so that the LPC reports a count of particles exceeding a specific cut size.

Table 2 Example of LPC Channel Sizing

Channel	Size (µm)	Mean Size (µm)
1	0.5	0.60
2	0.7	0.85
3	1.0	1.5
4	2.0	1.5
5	2.5	2.25
6	3.0	4.0
7	5.0	7.5
8	10.0	10.0

The LPC is outfitted with a total suspended particulate (TSP) inlet hood, matching the inlet configuration of the MOUDI and hi-vol. This hood is configured to allow all sizes of particles to enter the instrument. Particle size can change due to humidity as particles absorb moisture. The air stream was heated during periods of high humidity, ensuring a relative humidity below 50% and reducing this sampling artifact.

Optical particle counters, such as this LPC, are susceptible to sampling errors at high concentrations when particles shield other particles from the laser beam. The PM concentrations sampled during this work remained well below the maximum concentration level for the LPC. High concentration artifacts are therefore assumed to be insignificant. The LPC specifications are: maximum concentration up to 250,000 particles per m^3 , sensitivity is $0.5 \mu\text{m}$, and accuracy $\pm 10\%$. Particles greater than $10.0 \mu\text{m}$ were counted but sized as $10.0 \mu\text{m}$. The LPCs were operated using Windows[®] based PCs and data was acquired using Microsoft Excel[®] software. Statistical analysis of the results was made using SigmaPlot[®] software (Systat Software Inc. San Jose, CA).

The LPC provides a number count concentration of the particles in the air stream that must be converted to a mass concentration before comparison to the MOUDI or hi-vol data. This conversion assumes a uniform, spherical particle shape with a density of 1.0 g/cm^3 . Identical assumptions for shape and density were made for the MOUDI and hi-vol. The conversion from number count to mass concentration was made using Equations 1 and 2.

$$Count = \frac{particles}{Liter} \quad (1)$$

$$C_{LPC} = Count * Q * \rho * V \quad (2)$$

Where:

Q = flow rate (m^3/s)

ρ = particle density ($\mu g/m^3$)

V = particle volume (m^3)

C_{LPC} = concentration from LPC ($\mu g/m^3$)

The flow through the LPC was confirmed using a BIOS DryCal[®] DC-lite Primary Air Flow Meter (Bios International Corporation, Butler, NJ) primary flow meter. There was no statistical difference between the flow through the LPC and flow meter. A sample calculation with unit conversions and flow calibration results are provided in Appendix A.

Micro-Orifice Uniform-Deposit Impactor (MOUDI)

Micro-Orifice Uniform-Deposit Impactors (Model 100, MSP Corporation, Minneapolis, MN) were used to collect and size segregate atmospheric particulate during two sampling sessions (summer 2010 and fall 2010) [23, 36]. The two MOUDIs were operated in parallel using identical configurations and collection substrates. MOUDIs are inertial impactors that collect particulate by directing a particle-containing jet of air over and around flat impaction plates. Larger particles, with lower inertia, become trapped on the upper impaction plates while smaller particles, with a higher inertia, are carried past to the lower plates as illustrated in Figure [36].

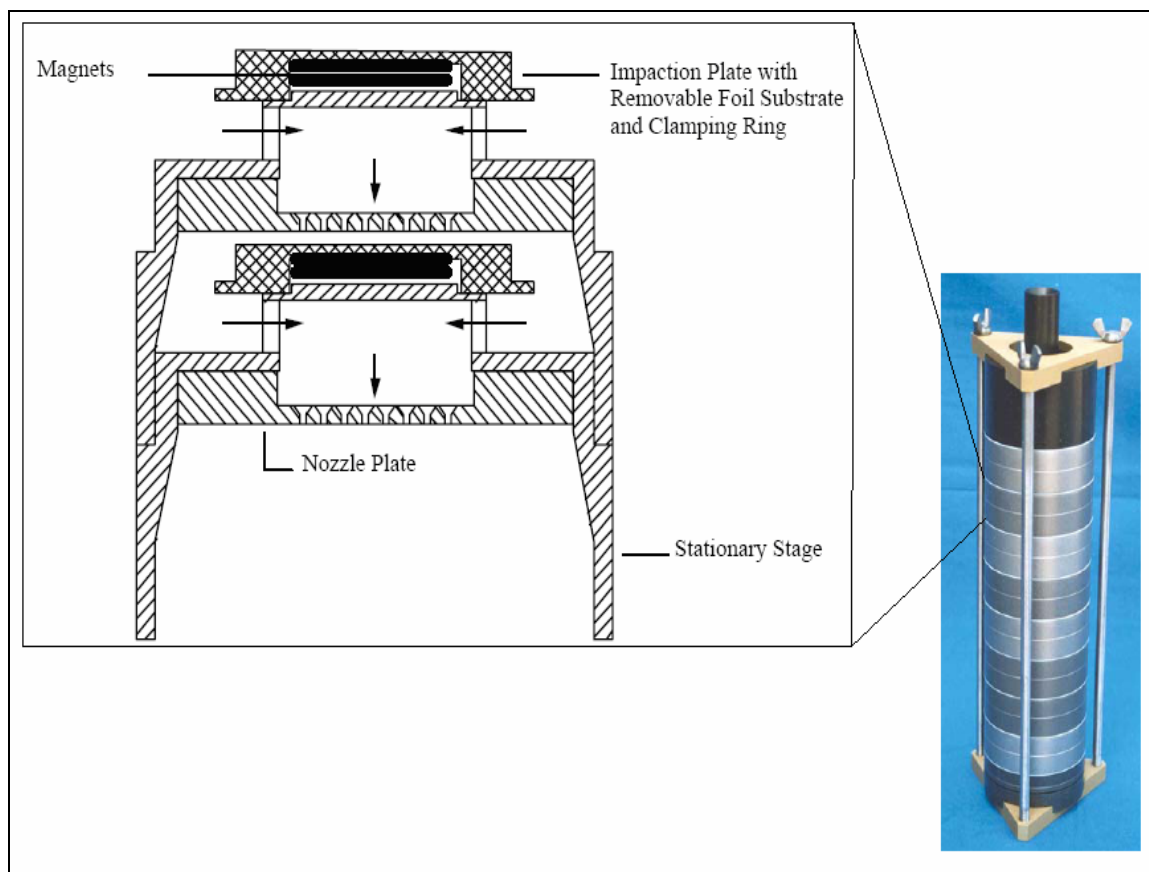


Figure 5 Cross-Section View of Typical MOUDI Stage (Images from Model 100/110 MOUDI User Guide, MSP Corp, St. Paul MN)

The particle-size distribution is, in part, a function of the airflow rate through the MOUDI. The particles are sized according to their behavior in the air stream, based on their aerodynamic diameter. The aerodynamic diameter is the diameter of an irregularly shaped particle, with a unit density that behaves the same as the diameter of a perfect spherical particle. Stokes law governs particle behavior in a fluid stream. The Stokes number (Sk), as defined in Equation 3, is a dimensionless parameter used to predict

whether a particle will leave an airstream and impact on a collection substrate or remain suspended in the airstream.

$$Sk = \frac{\rho_p CV_o D_p^2}{9\mu W} \quad (3)$$

Where:

ρ_p = particle density (g/cm³)

C = Cunningham slip correction factor (dimensionless)

W = nozzle diameter (μm)

D_p = particle diameter (μm)

μ = air viscosity (g/(cm·s))

V_o = air velocity (g/(cm·s))

The Stokes number is based on particle properties, airflow rate, and impactor geometry [37]. Furthermore, the Stokes number can be related to aerodynamic diameter using Equation 4.

$$D_{p50} = \sqrt{\frac{9\mu W}{\rho_p CV_o}} \sqrt{Sk_{50}} \quad (4)$$

For a MOUDI, Sk_{50} is defined as the square root of the Sk corresponding to a particle size collected with 50% efficiency on a particular impaction stage. $D_{p,50}$ is the particle diameter retained on an individual impactor stage and collected with 50% efficiency. As evident by Equations 3 and 4, the only value that can be altered to adjust

the cut size of an impactor stage is the air velocity. The flow rate was 13 L/min, resulting in the fifty percent aerodynamic cutoff diameters (D_{50}) shown in Table 3 [38].

Table 3 Aerodynamic Cutoff Diameters, D_{50} , for MOUDI Stages (13 L/min)

Impactor Stage	Size (μm)
Inlet	51
1	32
2	20
3	12
4	8
5	4.8
6	2.8
7	1.7
8	0.94
9	0.53
10	0.30

Particle collection and size fractionation are characterized by collection efficiency curves and the individual cut size of each impactor stage. The collection efficiency curves represent the probability of a particular sized particle being retained on an individual impaction stage. Cascade impactors with “steep” collection efficiency curves perform well collecting and size fractionating particulates. This MOUDI displayed steep efficiency curves, indicating a lower probability of multi-stage impaction by identically sized particles. Steepness values were determined by fitting calibration data provided by the manufacturer to Equation 5 and the results are presented in Table (individual values for $E_{i,j}$ are provided in **Error! Reference source not found.**).

$$E_{i,j} = \left[1 + \left(\frac{(D_{50})_i}{D_{pj}} \right)^{2B_i} \right]^{-1} \quad (5)$$

Where:

$E_{i,j}$ = stage collection efficiency

$D_{50,I}$ = cutoff diameter of stage i

B_i = steepness of the collector efficiency curve at stage i

$D_{p,j}$ = diameter of particle j.

Table 4 MOUDI Model 100 Steepness Values, MSP Corp., St. Paul, MN

Stage	D ₅₀	Steepness
10	0.056	1.93
9	0.097	3.94
8	0.174	5.21
7	0.299	5.67
6	0.543	7.81
5	0.952	9.55
4	1.733	10.06
3	3.088	14.30
2	6.145	5.89
1	9.825	4.23
inlet	18.097	2.73

The collection efficiency curves were generated using the initial calibration data **(Error! Reference source not found.)** provided by the MSP Corporation [39, 40] and are displayed in Figure 4. The curves for the inlet and stages 1, 9, and 10 are less steep

than curves 2 through 8. These lower steepness values are indicative of collection artifacts, including boundary layer effects such as blow through and particle bounce or the use of a non-monodisperse particulate during initial calibration [41-43]. It was assumed that these artifacts did not affect the final experiment results because these stages were not used during the analysis. These stages were excluded because they did not correspond with any LPC or hi-vol stages.

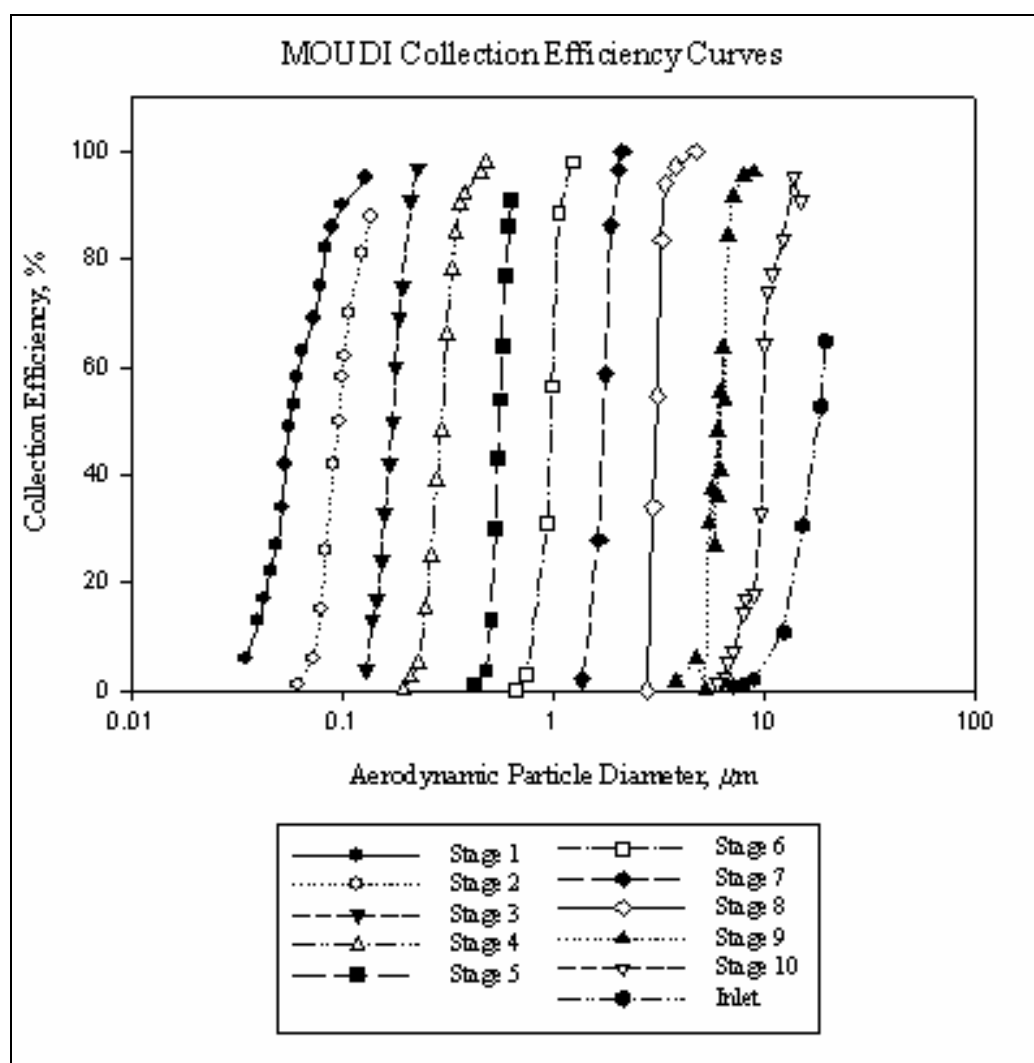


Figure 4 MOUDI Model 100 Collection Efficiency Curves (MSP Corp., St. Paul, MN)

Gravimetric analysis is the federal reference standard for mass-based air quality standards and was therefore used to determine the mass collected on each impactor plate. Particulate was collected on aluminum foil substrates (47-mm nominal diameter, MSP Corp., St. Paul, MN). These substrates were allowed to equilibrate for >24 hrs in a desiccator both before and after sampling. Particulate mass was determined for each stage using a Mettler Toledo XP56 ultra-microbalance (0.001 mg, Columbus, OH). These mass measurements were converted to a concentration using Equation 6. A sample calculation is provided in **Error! Reference source not found.**

$$C_{MOUDI,i} = m_{MOUDI,i} * Q * t \quad (6)$$

Where:

$C_{MOUDI,i}$ = concentration on impactor stage i ($\mu\text{g}/\text{m}^3$)

$m_{MOUDI,i}$ = mass collected on stage i ($\mu\text{g}/\text{m}^3$)

Q = MOUDI flow rate (m^3/min)

t = collection time (min)

Humidity was assumed to have a negligible effect on the PM mass accumulated on each MOUDI stage. The pressure drop through the MOUDI minimizes the effect of humidity. In addition, studies have shown that measurement artifacts occur on the lowest stage during periods of high humidity [44]. Samples collected during high humidity (>90%) were not used in during this study.

Calibration of MOUDI Air Flow

A pair of Aircon 520 AC air sampling pumps (referred to as pump 1975 and pump 1828, Sensidyne, Clearwater, FL) were selected to provide airflow to the MOUDIs, see Figure 5. The airflow rate for each pump required calibration before use. A BIOS DryCal[®] DC-lite Primary Air Flow Meter (Bios International Corporation, Butler, NJ) was the primary flow standard used for calibration [45, 46].



Figure 5 BIOS DryCal Air Flow Meter, Aircon 520 Air Sampling Pump, and MOUDI

Pump calibration was performed in a laboratory environment. The BIOS DryCal flow meter (BIOS) was placed in line with the pump and MOUDI. Pump 1975 and Pump

1828 were equipped with a rotameter to indicate flow rate. Airflow was varied between 5.0 L/min and 15.0 L/min, spanning the operational range of the pump. At each interval, five BOIS flow rates were averaged and compared to the corresponding rotameter flow, the results of which are graphed in Figure 6. Leak tests were performed on each pump and no leaks were detected. Test results are provided in **Error! Reference source not found.**

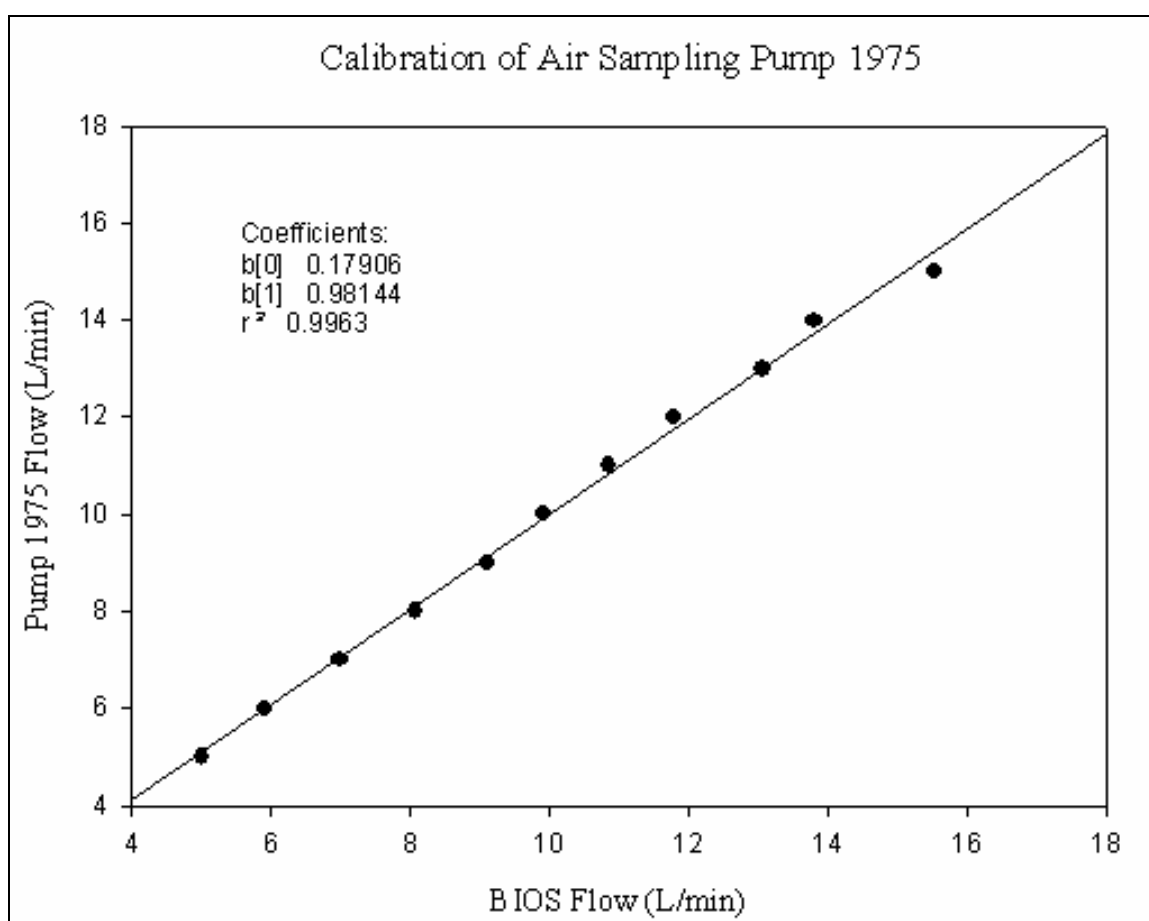


Figure 6 Comparison of BIOS and Pump 1975 Flow Rates

Pump 1975 performed extremely well with a near unity slope of 0.98, an offset of only 0.18 L/min, and root mean squared error (RMSE) of 0.192 L/min. The rotameter and

BIOS flow rates compared very well as indicated by a linear regression coefficient of determination (r^2) value of 0.9963 (Figure 8). Differences between pump 1975 and BIOS flowrates were not significant at the 95% confidence level using the student's t-test.

The flow rate of Pump 1828 also compared well to the BIOS flow rate as shown in Figure 7. The r^2 was 0.9808, the slope was near unity (0.99). An offset of 1.36 L/min through the MOUDI was measured and flow was adjusted to accommodate this offset. The RMSE was 1.43 L/min. The differences were not statistically significant at the 95% confidence level using the student's t-test.

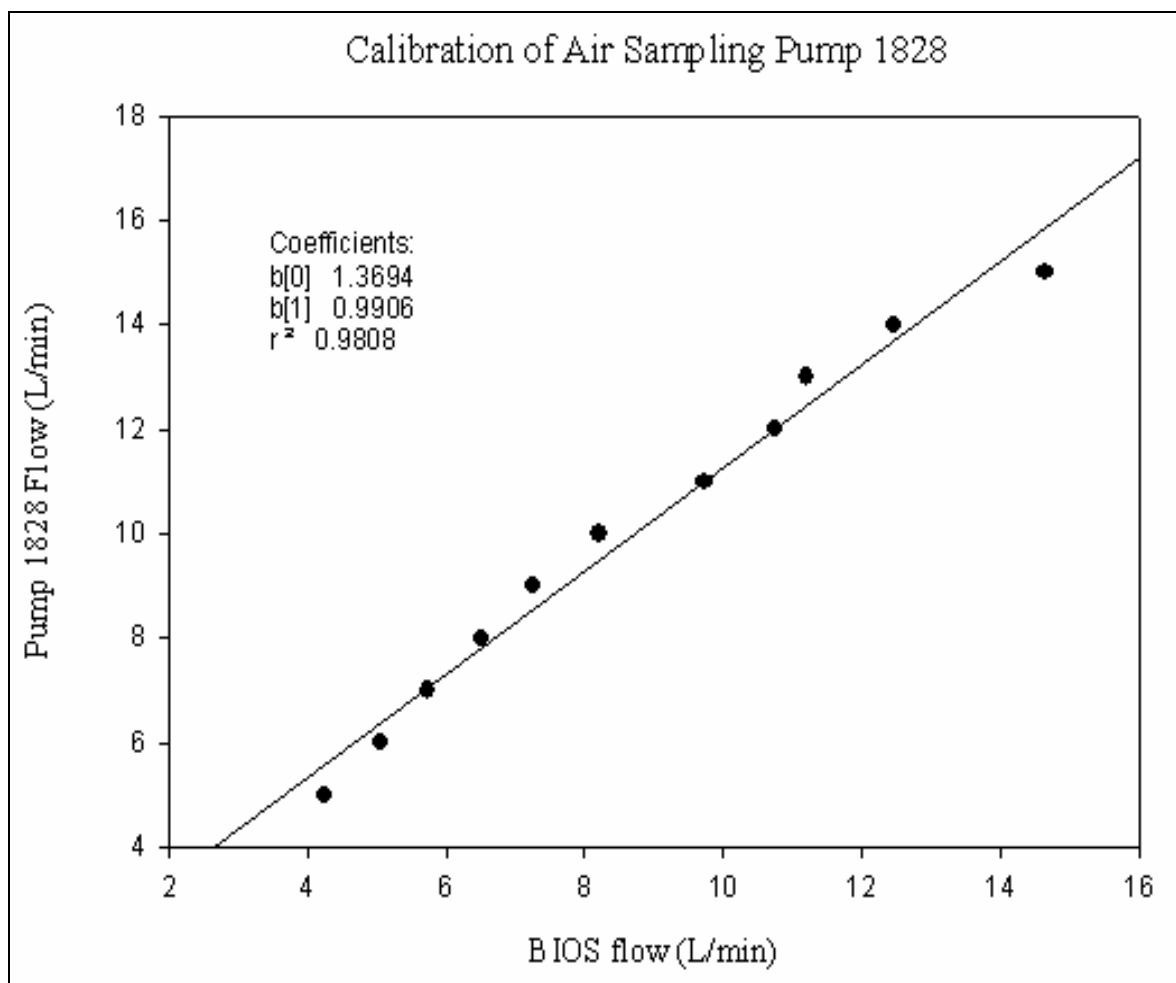


Figure 7 Calibration of Pump 1828 with a BIOS Flow Meter

High Volume Air Sampler

Total suspended particulate (TSP) concentrations were measured using a Wedding and Associates Critical Flow High-Volume Air Sampler (hi-vol). Although, this hi-vol outfitted with a cascade impactor is a federal reference standard for size fractionating PM, it lacks sufficient temporal resolution [47, 48] for real-time monitoring. The hi-vol TSP concentrations were used to validate TSP concentrations measured by the MOUDI and LPC.

Hi-vols consist of three major components: a size selective inlet hood, a collection filter, and a blower assembly, see Figure 8. The inlet hood can act as a preliminary screen for specific sized particles such as PM_{10} , $PM_{2.5}$, or TSP. A TSP hood was selected to correspond to the inlet hoods used on the MOUDI and LPC.

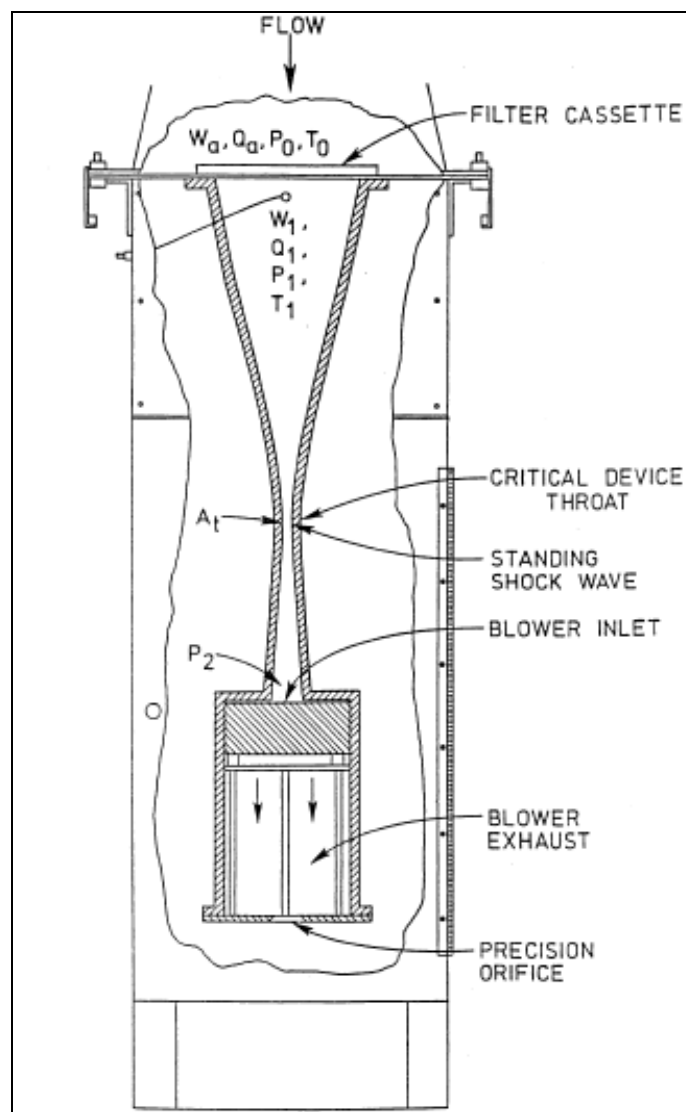


Figure 8 Hi-vol Diagram (Image from Hi-vol Operation Manual) [49]

The hi-vol drew air through a filter and the accumulated PM mass was gravimetrically determined. Coupling this mass to a known volume of air and sample time, a total concentration of particulate was determined using Equation 7.

$$C_{hi-vol,i} = m_{hi-vol,i} * Q * t \quad (7)$$

Where:

$C_{hi-vol,i}$ = concentration on impactor stage i ($\mu\text{g}/\text{m}^3$)

$m_{hi-vol,i}$ = mass collected on stage i ($\mu\text{g}/\text{m}^3$)

Q = hi-vol flow rate (m^3/min)

t = collection time (min)

Whatman 8 inch x 10 inch quartz microfiber filters (QMF, Tisch Environmental, Cleaves, OH) were used as the collection substrate. Quartz fiber filters were selected because they are not sensitive to changes in temperature or humidity [50]. Each filter was allowed to equilibrate in a desiccator for >24 hours before initial and final weighing. The filters were weighed using a Mettler Toledo (Model AB104, 0.1 mg, Columbus, OH) top loading balance.

The hi-vol is designed to operate with an airflow rate of approximately 1.13 m^3/min . This flow rate is maintained by a volumetric flow control (VFC) system. The VFC is simply a choked venturi tube attached to a blower motor. Air is pulled through the venturi tube where it accelerates until maximum velocity is achieved. This maximum velocity is a function of tube geometry, ambient air pressure, and temperature. Therefore a reliable, steady flow is provided, assuming sufficient downstream pressure is maintained.

The airflow rate was determined by performing a multipoint calibration using a variable flow orifice called a rootsmeter (Anderson Instruments, Inc., Smyrna, GA). The rootsmeter is a National Institute of Standards and Technology (NIST) calibration tool

allowing fully variable flow rates through the hi-vol (see Figure 9). This calibration established a numerical relationship between the volumetric flow rate through the hi-vol and both the stagnation pressure and ambient air pressure [51]. The stagnation pressure is the area of low pressure directly behind the filter, labeled P_1 in Figure 8 [49, 52].

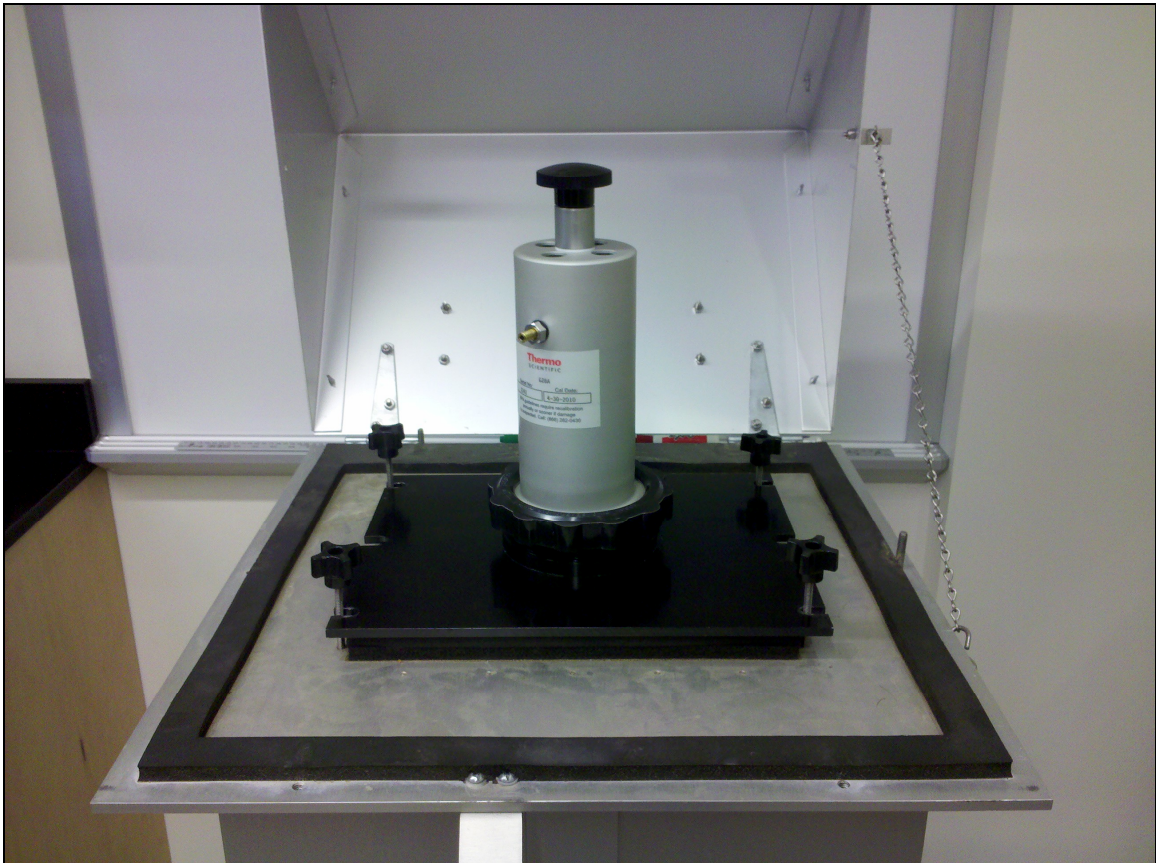


Figure 9 Hi-vol Outfitted with a Roots meter Variable Flow Orifice (Wedding and Associates, Fort Collins, CO)

The calibration process was performed by operating hi-vol while the airflow was varied by the rootsmeter as shown in Figure 9. Flow rates were then measured for five different flows and the corresponding change in pressure through the rootsmeter were recorded. Airflow through the rootsmeter was determined using Equations 8-10.

Calibration curves for the rootsmeter are provided in **Error! Reference source not found.**

$$Q_r = \frac{\sqrt{\Delta P_r \frac{T_a}{P_a} - b_r}}{m_r} \quad (8)$$

Where:

Q_r = flow through the rootsmeter (m³/min)

ΔP_r = pressure change through rootsmeter (in H₂O)

T_a = air temperature (K)

P_a = ambient air pressure (in H₂O)

b_r = y-intercept from rootsmeter calibration curve

m_r = slope from rootsmeter calibration curve

$$X = \frac{Q_r}{\sqrt{T_a}} \quad (9)$$

$$Y = P_{rat} = \frac{P_a - \Delta P_{stg}}{P_a} \quad (10)$$

Where:

P_{rat} = pressure ratio

P_{stg} = pressure at the stagnation point (in H₂O)

The X and Y values were graphed and linear regression was used to generate a calibration curve. The slope (m_c) was 6.526 and the y-intercept (b_c) was 0.5061. The r^2

value was 0.9987, which was acceptable [53]. The actual flow through the hi-vol could then be determined using Equation 11.

$$Q_{act} = \frac{(P_{rat} - b_c) \sqrt{T_a}}{m_c} \quad (11)$$

Where:

Q_{act} = flow through the hi-vol (m³/min)

P_{rat} = pressure ratio

b_c = y-intercept from calibration curve

m_c = slope from calibration curve

The calibration chart and sample calculations for hi-vol (blower motor B) are provided in **Error! Reference source not found..** Once calibrated, the airflow was determined in the field by using a manometer to measure the stagnation pressure immediately behind the filter. Flow measurements were taken at the beginning and end of each sampling period and averaged to determine flow. Time-weighted average temperatures were obtained from the National Weather Service at the nearby Boise Airport.

Cascade Impactor

The hi-vol was outfitted with a High Volume Cascade Impactor Series 230 (Tisch Environmental, Cleves, OH), which was used to size fractionate airborne particulate. The impactor operates by directing an air stream through a series of staggered openings on aluminum plates as shown in Figure 10. As air travels between the plate openings,

particles with sufficient inertia are retained on filters while smaller particles pass by. The cascade impactor size fractionates the particulate into the 5 stages shown in Table 4.

Particles smaller than $0.49\ \mu\text{m}$ were retained on a back-up filter. The operating flow rate was approximately 1.13 L/min.

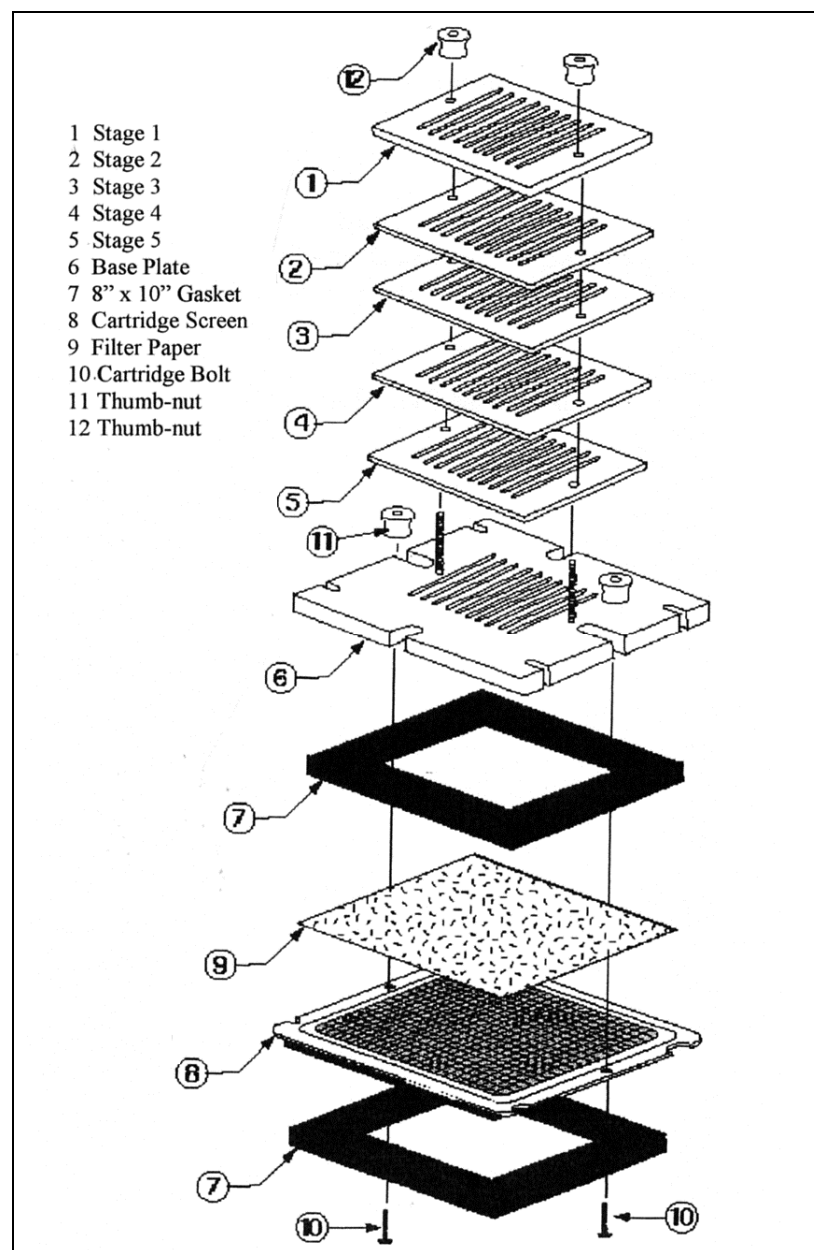


Figure 10 Image of Cascade Impactor Exploded View (Image from Hi-vol Operation Manual) [49]

Table 4 Aerodynamic Cutoff Diameters for Hi-Vol Cascade Impactor Series 230

Impactor Stage	Size (μm)
Back up filter	< 0.49
1	0.49
2	0.95
3	1.5
4	3.0
5	> 7.2

This style of cascade impactor may be susceptible to high blow through and particle bounce. Blow through occurs when a particle bypasses the appropriate impaction plate and impacts on a later stage. Particle bounce occurs when a particle dislodges from the appropriate impactor stage and is re-entrained in the air stream. Particles that bounce tend to stay in the air stream before being retained on the back up filter [54]. The particle distribution, as a percent of TSP, can be compared to other impactors when blow through and bounce rates are high.

Data Analysis

Because of the differences in measurement methodologies, extensive data analysis was required to calibrate a LPC to a MOUDI and sub-sequentially a second LPC. The analysis was divided into four activities: (1) data inversion of the MOUDI results, (2) calibration of a LPC to a MOUDI, (3) time-step analysis, and (4) calibration of a second LPC using the original LPC. These sections, taken together, were used to develop an algorithm for calibrating LPCs before they are integrated into a wireless network.

The initial step in calibration was the data analysis, which required comparing the LPC and MOUDI results. Two problems had to be overcome before this was possible. First, the instruments had unique cut sizes, making direct comparison of concentrations impossible. For example, the LPC had a mid-range cut size of 4.0 μm while the corresponding MOUDI cut size was 4.8 μm . Second, inter-stage estimation of particle concentrations from the MOUDIs is difficult as identically sized particles can impact on different stages. These two issues were overcome by performing a data inversion on the MOUDI results.

The data inversion was the most computationally intensive portion of the calibration process. Gravimetric analysis was initially used to determine mass accumulated on each MOUDI stage, producing a discrete data set. This data is generally presented as a histogram [30, 35]. A fundamental issue with this style of data display is that it does not account for particles of the identical diameters depositing on multiple stages. To account for this disparity, as well as inter-stage losses, a data inversion was performed to convert these discrete results into a continuous function [29, 32, 44]. This continuous function was then used to estimate inter-stage concentrations, allowing for direct comparison between the LPC and MOUDI.

Aerosol measurements typically display a bi-modal, lognormal distribution which results from aerosols having a nuclei and an accumulation mode [55]. The data inversion process outlined in Dong et al. (2004), as shown in Equation 12, was applied [31].

$$W_i = \sum_{j=1}^M K_{i,j} \left\{ \frac{W_f \exp \left[\frac{-(\log D_{pj} - \log D_{gf})^2}{2(\log \sigma_{gf})^2} \right]}{\sqrt{2\pi} \log \sigma_{gf}} + \frac{(W_T - W_f) \exp \left[\frac{-(\log D_{pj} - \log D_{ga})^2}{2(\log \sigma_{ga})^2} \right]}{\sqrt{2\pi} \log \sigma_{ga}} \right\} \Delta \log D_p \quad (12)$$

Where:

W_i = concentration of PM mass on stage i ($\mu\text{g}/\text{m}^3$)

D_p = particle diameter (μm)

D_{gf} = geometric mean diameter, first mode (μm)

D_{ga} = geometric mean diameter, second mode (μm)

W_f = mass concentration, first mode ($\mu\text{g}/\text{m}^3$)

W_T = total mass concentration, both modes ($\mu\text{g}/\text{m}^3$)

σ_{gf} = geometric standard deviation, first mode (μm)

σ_{ga} = geometric standard deviation, second mode (μm)

$K_{i,j}$ = kernel function

This inversion method was selected because it accounts for either a bi-modal, lognormal distribution or can be adapted to a uni-modal, lognormal distribution. Values for W_i and W_T were measured experimentally while the values of the five remaining parameters (D_{gf} , D_{ga} , W_f , σ_{gf} , and σ_{ga}) were determined through the inversion process. W_i measurements were determined for seven of the impactor stages, leaving the inversion equation with five unknown parameters. These parameters were determined using a system of equations and Solver in Microsoft Excel[®] software (Frontline Systems Inc.,

Incline Village, NV) [56]. The inter-stage losses were accounted for through the use of kernel functions [31].

Kernel functions are important because they show the particle distributions between impactor stages [37, 57]. These functions, also known as response functions, are critical when converting discrete impactor data to a continuous function as the collection of particles on individual impactor stages is not perfect. This means some particles of a specific size are captured on previous stages while others are allowed to pass through. Accounting for this imperfect collection involves graphing the collection efficiency of each impactor stage with particle diameter [41, 44, 56]. Steep efficiency curves, such as those of the MOUDI, indicate efficient impactor collection, making it a good calibration standard. These functions are shown in Figure 11. Sample calculations and complete results are provided in **Error! Reference source not found.**

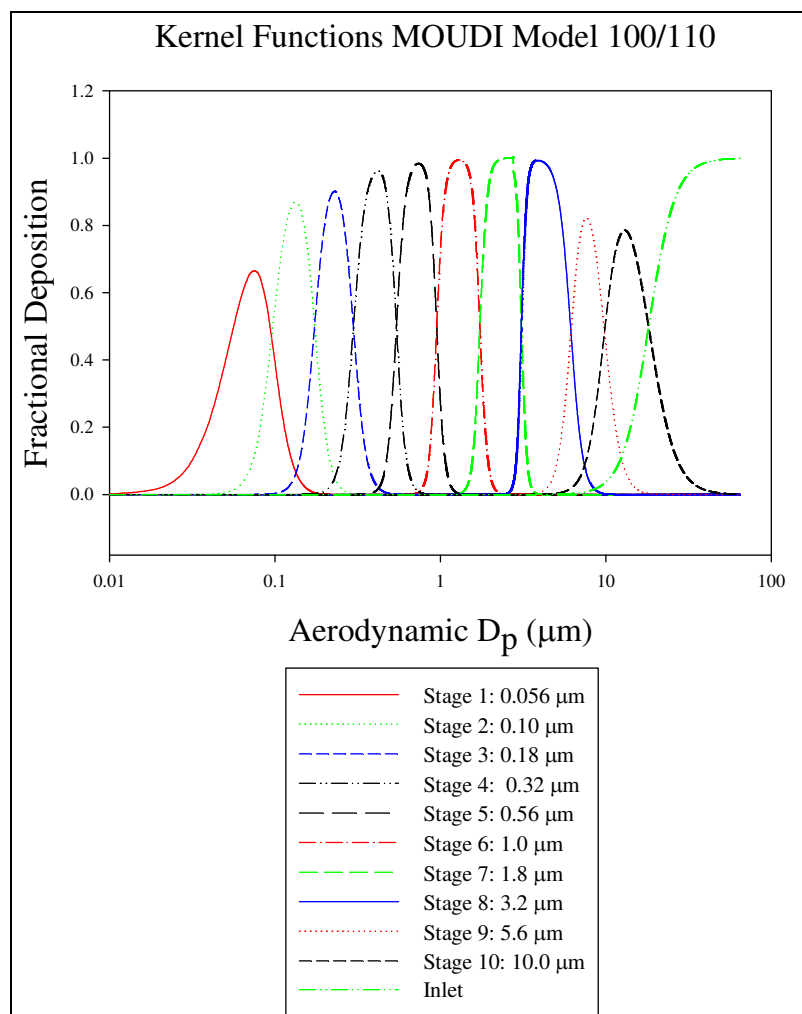


Figure 11 Kernel Functions for the MOUDI Model 100/110

The second stage, upon completion of the data inversion, was the calibration of the LPC to the MOUDI. The sampling data set was divided into two portions, a calibration and a validation set. Standard regression analysis was performed to compare the LPC and MOUDI concentrations. The magnitude of the LPC measurements were adjusted to better fit the magnitude of the MOUDI concentrations. These same adjustments were then applied to the validation data set. An analysis of variance (ANOVA) was used to determine if the changes made during calibration were necessary

or significant. A one-way ANOVA can be used to test the hypothesis that the mean from two groups is equivalent. The data collected had large, unequal variances (due to differences in concentration magnitudes) and was not normally distributed. These conditions met the standards for applying a Kruskal-Wallis analysis of variance on ranks. This test is a non-parametric version of a one-way ANOVA [58].

Third, a time-step analysis was required because the LPC sampled in real time while the MOUDI time steps ranged between 18 hr and 48 hr. The MOUDIs required substantial accumulation of mass on a substrate and as such, despite having access to an ultra-microbalance (i.e., measurements to 0.001 mg), long sample times were required to meet MDLs. This work required demonstrating that calibration standard occurring on a scale of hours or days could be applied to a sensor capable of real-time measurements. The relative percent difference of the TSP concentration measurements was calculated using Equation 13.

$$RPD = \frac{|C_{LPC} - C_{MOUDI}|}{\frac{C_{LPC} + C_{MOUDI}}{2}} * 100 \quad (12)$$

Where:

RPD = relative percent difference (%)

C_{LPC} = LPC TSP concentration ($\mu\text{g}/\text{m}^3$)

C_{MOUDI} = MOUDI TSP concentration ($\mu\text{g}/\text{m}^3$)

These results were then normalized by hour. This process was used to show that measurements made in real time by the LPC could be summed to correspond to the long

sample times of the MOUDI. Sample calculations are provided in **Error! Reference source not found.**

Finally, the initial LPC (labeled unit 1) was used to calibrate an additional LPC (labeled unit 2). The LPCs were operated simultaneously under both laboratory and field conditions. A student's t-test was used to determine if the differences between concentrations estimated for each instrument were statistically significant. This process was done to develop an algorithm for integrating future LPCs into a wireless sensor network. Sample calculations are provided in **Error! Reference source not found.**

RESULTS

General Results

Two sampling sessions were conducted to measure PM concentrations using a combination of LPCs, MOUDIs, and hi-vols. The first session, during the summer of 2010, used two LPCs and two hi-vols. This session was used to test the feasibility of calibrating a LPC to a hi-vol outfitted with a cascade impactor, and using one LPC to calibrate a second LPC. The second sampling period, during the fall of 2010, included a LPC, a hi-vol, and a pair of MOUDIs. This sampling period was used to calibrate a LPC to a MOUDI, compare PM concentration measurements made using all three instruments, and evaluate the effects of different collection time steps on the results.

The three instruments showed varying levels of agreement depending on the sampling methodology and the collection time. As expected, the instruments often measured different concentration magnitudes but similar concentration distributions [24]. The agreement between devices was validated using different statistical methods (student t-test, ANOVA, Kruskal-Wallis ANOVA, and Mann-Whitney Rank Sum test) depending on the type of data collected. Because of the different concentration magnitudes, the corresponding data often exhibited unequal variances requiring use of the non-parametric ANOVA testing. Five comparisons were made of PM concentrations: LPC and MOUDI, LPC and hi-vol, MOUDI replicate testing, time-step analysis, and LPC 1 and LPC 2.

LPC and MOUDI Comparison

The LPC and MOUDI data were collected during the fall sampling session. Each device was operated for an identical time period so that the concentrations measurements were comparable. The complete data set was divided into two groups, one for calibration and one for validation. The MOUDI data was inverted, allowing for inter-stage concentration estimation and a direct comparison to the LPC data. Following the calibration of the LPC, an ANOVA was performed, which showed no statistically significant difference between the LPC and MOUDI concentration measurements.

Both the LPC and MOUDI size fractionated particulate into different cut sizes, making the direct comparison of the results difficult. It is customary to present cascade impactor data (average concentration measurements) as a histogram because these concentrations represent a collection of particles within a specific size range. Also, the use of a histogram accounts for the deposition of identically sized particles on different impaction plates. The LPC is not susceptible to the same collection artifacts as a cascade impactor and as such a standard curve could be fitted to this discrete data. The LPC and MOUDI results are shown in

Figure 12 and for clarity these results are limited to the cut sizes used during the data inversion and calibration processes. The size distribution of the LPC curve mirrors that of the histogram, albeit with different magnitudes. The calibration process was used to adjust for these differences of magnitude.

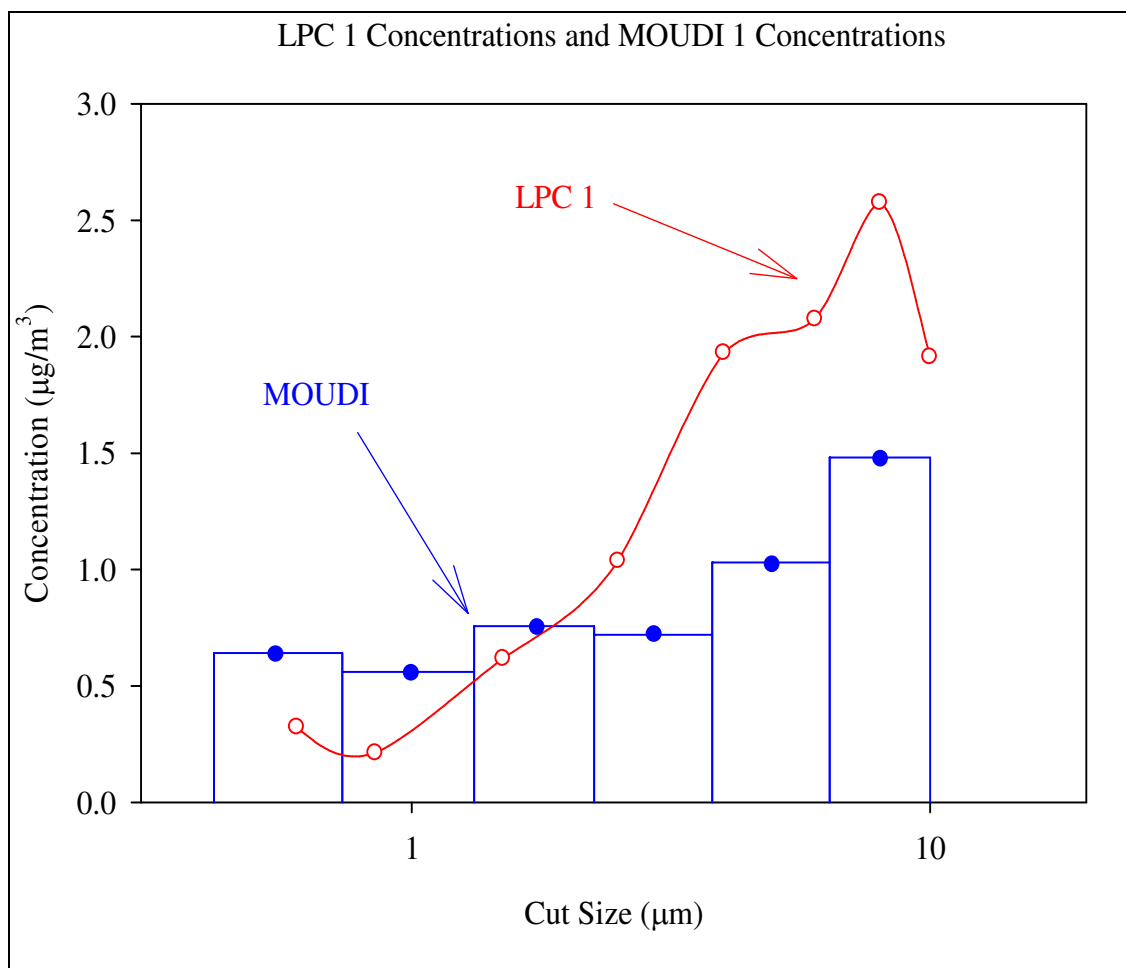


Figure 12 LPC and MOUDI Average Concentrations

In Figure 14, the MOUDI results were also maintained as discrete points (each point is an impactor stage at the midway point of the histogram), while the LPC results are presented as both discrete and continuous functions. This graph illustrates how the cut sizes between the LPC and MOUDI do not directly align, preventing calibration. Because standard curve fitting techniques are inadequate to fit a continuous function to the MOUDI data, a data inversion was applied to convert this discrete MOUDI data into a continuous function.

The PM concentration measurements displayed a bi-modal, lognormal distribution [55]. The inversion process as outlined in Dong et al. (2004) [31] and adapted from the Twomey algorithm was performed on the MOUDI data. This inversion process required solving for the unknown parameters in Equation 15.

PM concentration was determined for seven of the MOUDI stages (W_i) and were selected because they span the same operating range as the LPC. The software Solver (Frontline Systems Inc., Incline Village, NV and Microsoft Excel[®]) was used to fit this measured data to Equation 12 by optimizing the difference between a set of modeled concentrations with measured concentrations.

This inversion technique required minimizing the root mean squared error (RMSE) between measured (W_i) concentrations and modeled (W_c) concentrations. Because there were seven solutions and six unknowns numerous solutions were possible. By applying specific stopping criteria, an acceptable solution set was achieved [35]. The stopping criteria included rapid convergence, specific boundary conditions, and the difference between measured and model sample weight is less than 5%. The solution converged quickly (<15 trials) and the solutions were bounded using the following constraints: $W_f < 5.0 \mu\text{g}$ (mass concentration of first mode), $D_{gf} < 0.50 \mu\text{m}$ (average diameter of the first mode), $\sigma_{gf} > 1.01$ (standard deviation of the first mode), $\sigma_{gf} < 10.0$ (standard deviation of second mode), $\sigma_{gf} = \sigma_{ga}$, $D_{gf} < D_{ga}$, and $D_{gf} > 2.5 \mu\text{m}$ (average diameter of second mode). This inversion was performed on both the calibration and the validation data sets with the unknown parameter values shown in Table 5. The PM concentrations made by the LPC and MOUDI 1 are superimposed on the inverted

MOUDI concentrations in Figure 13 and Table 6. The values shown in Table 6 were used during calibration.

Table 5 Results from Data Inversion

Equation Parameter	Calibration Data Set	Validation Data Set
W_f	5.00 μg	4.99 μg
W_t	13.58 μg	9.11 μg
D_{gf}	5.16 μm	5.17 μm
D_{ga}	12.56 μm	10.0 μm
σ_{gf}	3.41	3.39
σ_{ga}	3.41	3.39

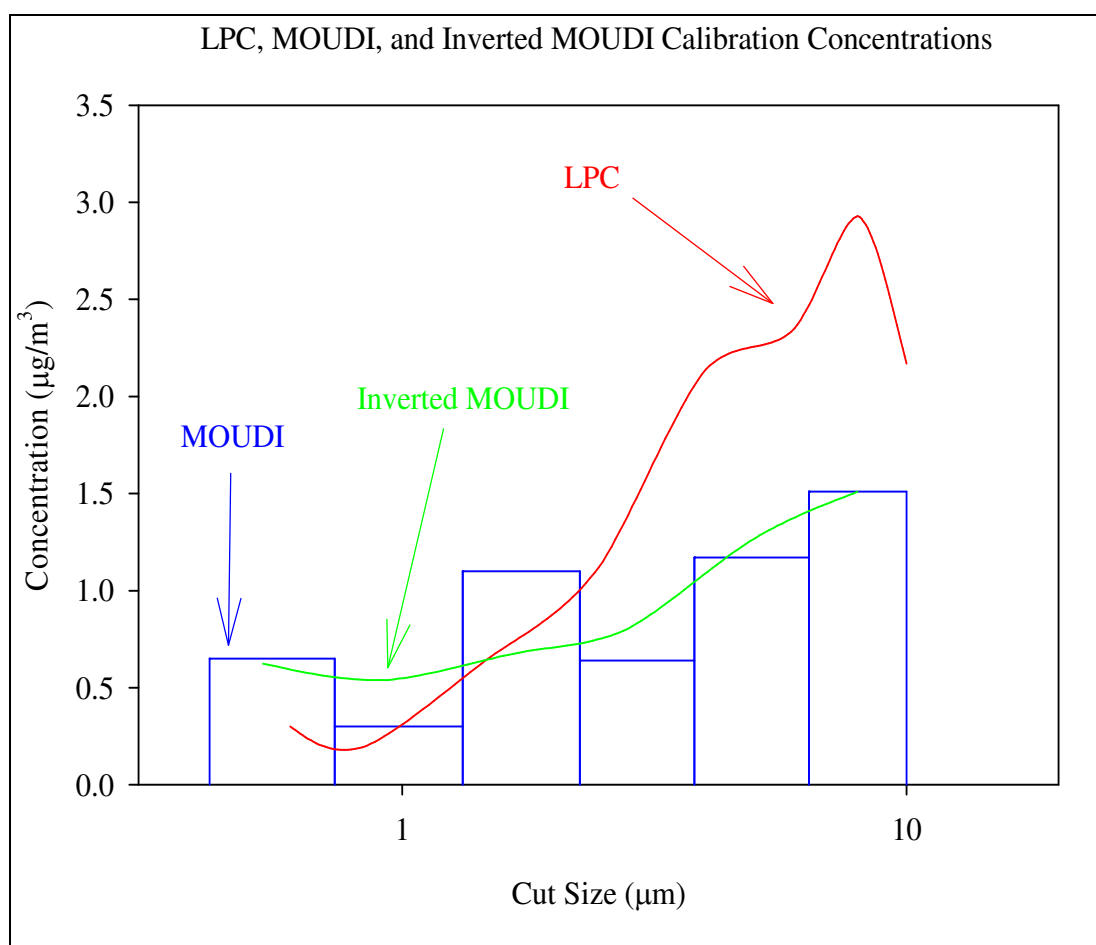


Figure 13 LPC, MOUDI 1, and Inverted MOUDI PM Calibration Concentrations

Table 6 **LPC and Inverted MOUDI PM Calibration Concentrations**

Cut Size (μm)	LPC Concentration ($\mu\text{g}/\text{m}^3$)	Inverted MOUDI ($\mu\text{g}/\text{m}^3$)
0.60	0.30	0.593
0.85	0.20	0.541
1.50	0.66	0.645
2.5	1.15	0.755
4.0	2.14	1.078
6.0	2.35	1.375
8.0	2.17	1.510

The RMSE between the calibrated LPC concentrations and validation MOUDI concentrations was optimized (minimized) using identical methods and constraints as the calibration data set. Again, convergence was achieved quickly (< 20 trials). The difference between the sampled and model weight was less than 5%. The values are shown in Figure 14 and Table 7. The graph shows a higher estimation of particulate near the 1.0 μm and slightly lower concentrations near the 0.6 μm and 2.0 μm .

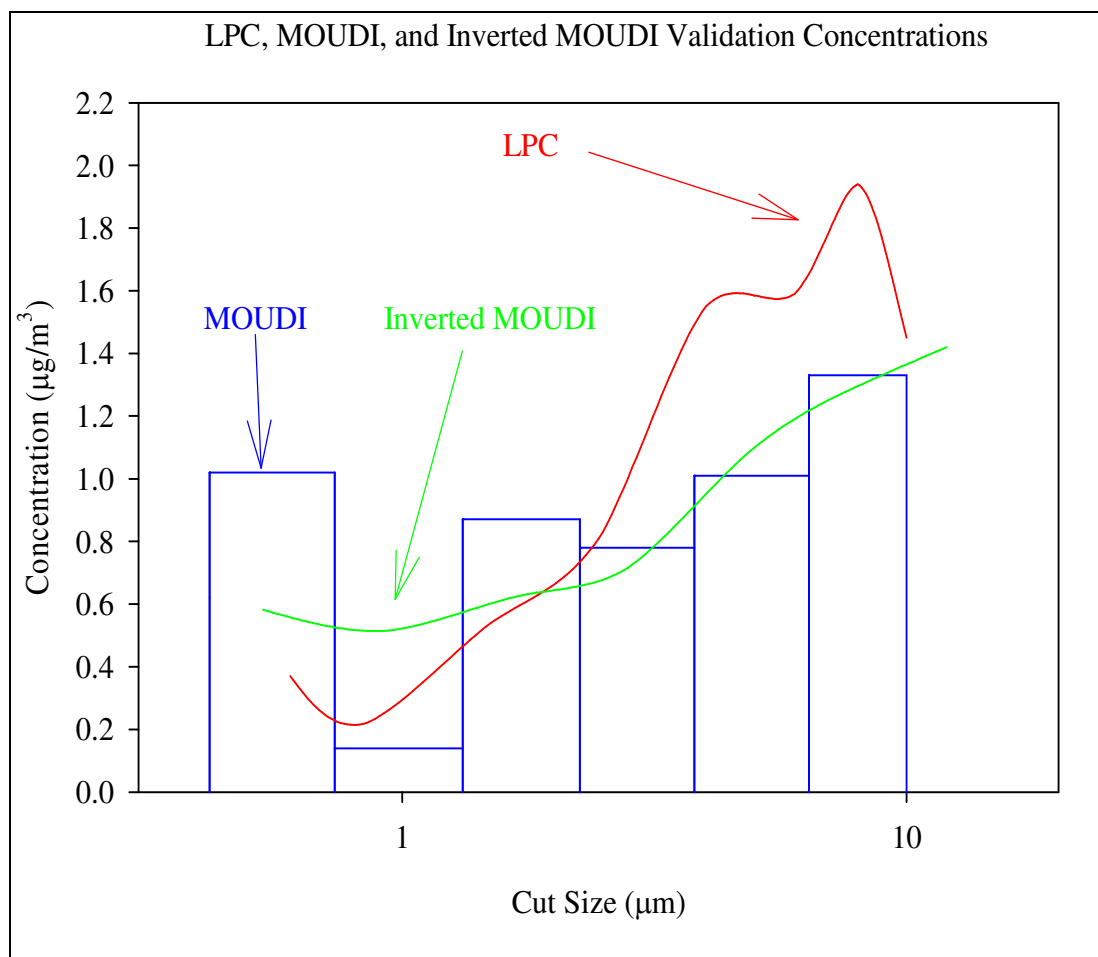


Figure 14 LPC, MOUDI 1, and Inverted MOUDI PM Validation Concentrations

Table 7 LPC and Inverted MOUDI PM Validation Concentrations

Cut Size (µm)	LPC Concentration (µg/m³)	Inverted MOUDI Concentration (µg/m³)
0.60	0.37	0.559
0.85	0.22	0.517
1.50	0.54	0.599
2.5	0.83	0.678
4.0	1.55	0.959
6.0	1.59	1.194
8.0	1.94	1.286

LPC to MOUDI Calibration

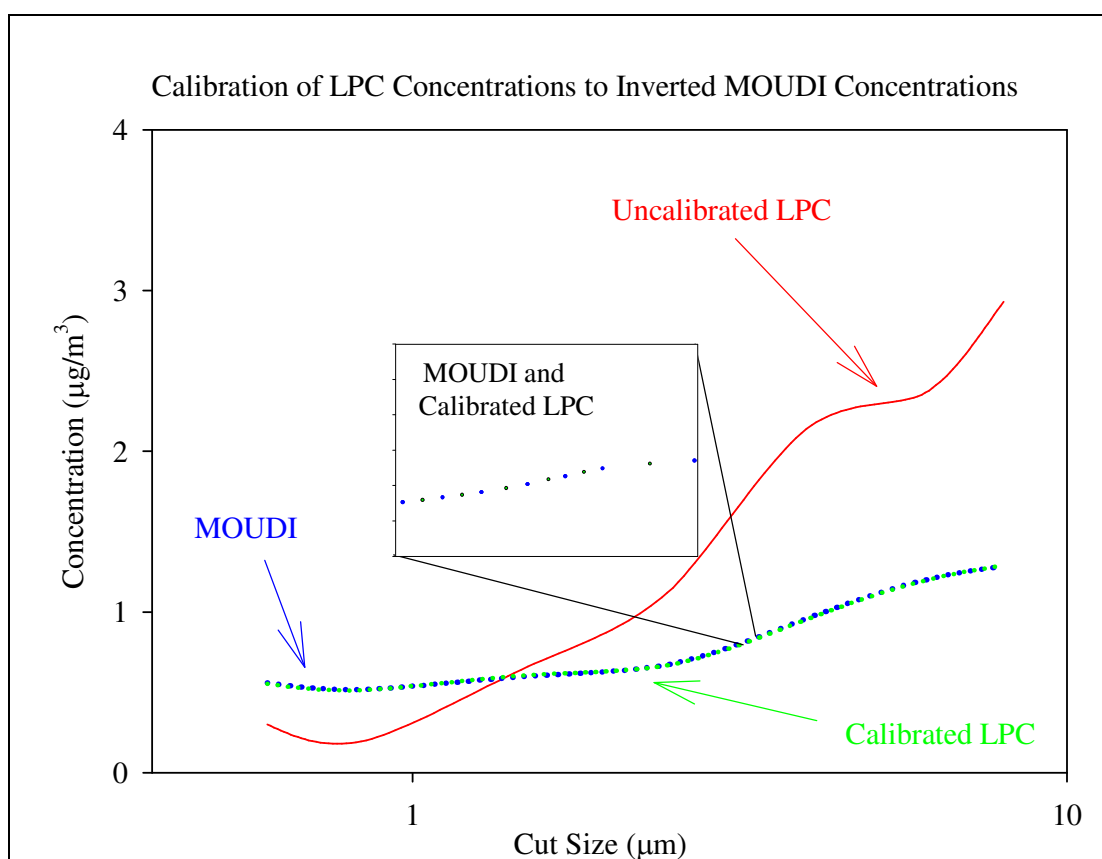
Following the data inversion process, a direct comparison between the LPC and the MOUDI concentrations was performed. Based on these results, a calibration of the LPC to the MOUDI was completed to adjust for the different concentration magnitudes. The calibration was performed on a subset of the data generated during the fall sampling session while the unused data was reserved for validation. Statistical testing was performed during each step of the calibration process to measure the significance of the adjustments.

The calibration was performed on individual LPC cut sizes, 0.60 μm , 0.85 μm , 1.50 μm , 2.5 μm , 4.0 μm , 6.0 μm , and 8.0 μm . First, the LPC and MOUDI concentrations were averaged for each cut size. Next, the relative percent difference between the concentrations was calculated and ranged from a low of 9.2% (1.50 μm) to a high of 158.5% (0.85 μm). The magnitude of each LPC cut size concentration was adjusted by this percent difference as shown in

Table 8. The original LPC concentrations, inverted MOUDI concentrations, and adjusted LPC concentrations are graphed in Figure 15. The LPC consistently underestimated the concentrations below 2.0 μm while overestimating concentrations above this cut size. Therefore, the magnitude of the lower cut sizes was increased and upper cut size magnitudes decreased. These same adjustments (% change by cut size) were then applied accordingly to each LPC concentration in the validation set.

Table 8 Calibration PM Concentrations from LPC and MOUDI

Cut Size (μm)	LPC Concentration ($\mu\text{g}/\text{m}^3$)	Inverted MOUDI Concentration ($\mu\text{g}/\text{m}^3$)	% Difference	LPC Concentration Calibrated ($\mu\text{g}/\text{m}^3$)
0.60	0.30	0.56	86.3	0.56
0.85	0.20	0.52	158.5	0.52
1.50	0.66	0.60	-9.2	0.60
2.50	1.15	0.68	-41.0	0.68
4.0	2.14	0.96	-55.2	0.96
6.0	2.35	1.19	-49.2	1.19
8.0	2.93	1.29	-56.1	1.29

**Figure 15 Calibration of LPC Concentrations to Inverted MOUDI Concentrations**

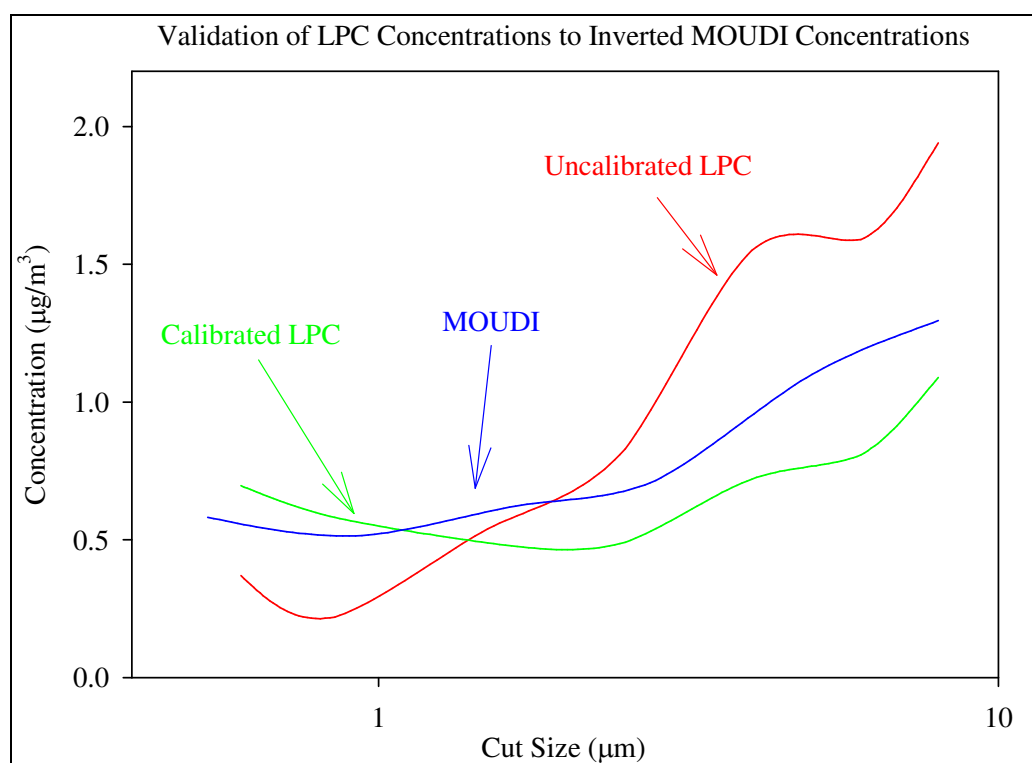
An ANOVA was used to determine the significance of the differences between the mean values of each cut size before and after calibration. This statistical measure was applied twice on the calibration data and twice on the validation data. The first application compared the raw LPC data and MOUDI inverted data (from the calibration group). A successful application of a one-way ANOVA required the data set to have equal variance, which this data set did not. The unequal variance was expected because of the different concentration magnitudes. Although, a non-parametric ANOVA, the Kruskal-Wallis one way ANOVA on rank test could be applied, a more robust ANOVA (parametric) was desired for calibration. The ANOVA was rerun on the calibrated LPC data and inverted MOUDI data. There were no statistically significant differences at the 95% confidence interval between the results, which was expected because the LPC was specifically adjusted to match the MOUDI data.

The results from this calibration process required validation; therefore, the second half of the data generated during the fall sampling session was reserved for this purpose. The adjustments made to each cut size concentration were applied to the LPC validation data set as shown in

Table 9. The LPC concentrations, inverted MOUDI concentrations, and adjusted LPC validation concentrations are graphed in Figure 16. This illustrates the improvement made to the magnitude of the LPC concentrations. There is marked improvement in the agreement below and above the 2.0 μm cut size. The general distribution of the LPC concentrations is maintained throughout the calibration process and generally agrees with the MOUDI distributions.

Table 9 Validation Data Set

Cut Size (μm)	LPC Concentration ($\mu\text{g}/\text{m}^3$)	Inverted MOUDI Concentration ($\mu\text{g}/\text{m}^3$)	% Adjusted	LPC Concentration Calibrated ($\mu\text{g}/\text{m}^3$)
0.60	0.37	0.67	86.3	0.69
0.85	0.22	0.62	158.5	0.57
1.50	0.54	0.90	-9.2	0.49
2.50	0.83	0.40	-41	0.49
4.0	1.55	0.87	-55.2	0.69
6.0	1.59	0.78	-49.2	0.81
8.0	1.94	1.15	-56.1	1.08

**Figure 16** Validation of LPC Concentrations to Inverted MOUDI Concentrations

The same ANOVA testing was repeated twice more on the validation results. First on the non-calibrated LPC validation data and MOUDI inverted validation sets, once

again the ANOVA failed due to unequal variance concentrations. This was expected because the LPC data set had yet to be calibrated but represented the need to improve the compatibility between the instruments. As with the calibration data, set a non-parametric ANOVA was possible but not robust enough for a calibration. Finally, the ANOVA was performed to compare the calibrated LPC data to the inverted MOUDI data. The test passed and showed there was no statistically significant difference between the data sets ($p=0.05$). A key result here is that the calibrated data set passed the equal variance test. Because there is no longer a statistically significant difference between the LPC and MOUDI concentrations, this LPC can potentially act as a master LPC used to calibrate future LPCs.

LPC and Hi-Vol Comparison

Three hi-vols (labeled A, B, and C) were operated concurrently with two LPCs during the summer and fall sampling sessions. The summer session tested the feasibility of calibrating a LPC to a hi-vol outfitted with a cascade impactor. The fall sampling session was used to validate the results obtained using the MOUDI and LPC. Because both the hi-vol and MOUDI are federal reference standards for measuring PM concentration, it is valuable to determine how these measurements compare.

During both sampling sessions, the LPCs and hi-vols were situated such that their inlet hoods were at identical heights and configured to capture TSP. The instruments were located a minimum of 15 feet from the nearest building or wall and aligned perpendicular to the prevailing wind direction. Hi-vol B was outfitted with a cascade impactor and used to size segregate particulate into five sizes: 0.50 μm , 0.95 μm , 1.5 μm ,

3.0 μm , and 7.2 μm and larger. Hi-vols A and C used standard collection filters to measure TSP concentrations, as described in Chapter 3.

During the summer testing, hi-vols A and B were operated with the LPC 1 and LPC 2 (see Figure 17, Unit B and LPC 1 shown). Unfortunately, the blower on hi-vol A failed during testing, rendering the results from this instrument inconclusive. The unit remained in the field where it was converted to test trip blanks. The trip blank testing was performed by loading hi-vol filters but not operating the hi-vol during the testing period. The filters were stored and weighed using identical methods as hi-vol B. Any change in filter weight could be indicative of testing artifacts. The results from these trip blanks were favorable with no statistically significant differences in the change in filter weights at the 95% confidence level (student t-test). The results of the trip tests are provided in Appendix J.

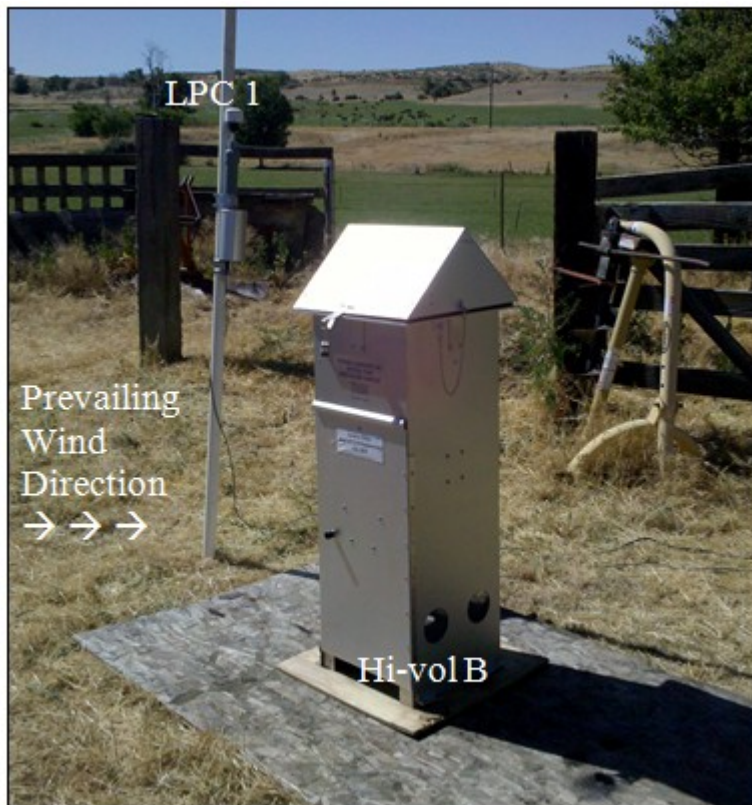


Figure 17 LPC and Hi-vol (Unit B) During Summer of 2010

As with the MOUDI and LPC, the hi-vol and LPC used different detection methodologies to measure PM concentrations. The cascade impactor and LPCs also segregated particulate into different cut sizes, making the direct comparison of concentrations difficult except when comparing TSP. Attempts were made to invert the hi-vol data (using the Twomey Algorithm) to allow for interstage estimation of PM concentrations. The cascade impactor used five stages, each stage representing a solution to the data inversion. The inversion process required solving for six unknown parameters. Five solutions with six unknowns is inadequate to solve a system of equations. Despite this difficulty, the sampling was not without merit. The hi-vol was still used to compare TSP results in lieu of its use as a calibration standard.

PM concentrations measured using LPC 1, LPC 2, and hi-vol B were compared. The first comparison was between the individual impactor stages and LPC 1 stages. Before comparison, the LPC's individual sizes were combined to better align with the hi-vol. For example, impactor stage 3 collected particles ranging in size from 1.5 μm to 3.0 μm . The LPC counts particles ranging from 1.5 μm to 2.5 μm using stage 3 and stage 4, hence the results from these were combined into a single stage. Stage combinations and the corresponding hi-vol stage are shown in Table 10.

Table 10 Stage Equivalents Between LPC and Hi-vol

Stage Equivalents			
LPC Stage	LPC Median Size	Impactor Range	Impactor Stage
10	10	7.2 and up	1
7	8.5		
5	6	3.0 to 7.2	2
3	4		
2	2.5	1.5 to 3.0	3
1	1.5		
0.7	0.85	0.95 to 1.5	4
0.5	0.6	0.5 to .95	5

The concentrations from the hi-vol and LPC are graphed. The results for stage 2 are shown in Figure 18 (remaining stages are provided in **Error! Reference source not found.**). The concentrations between the two LPCs compared very well, each showing similar size distribution and magnitude. This was expected because each device sampled for the same time period, under identical conditions, and using similar cut sizes. Figure 19 is the graph of TSP concentrations showing the strong agreement between LPC and hi-vol concentrations.

The LPC and hi-vol concentrations showed similar size distribution but different magnitudes. There were two primary reasons for this difference. First, the cut stages were not properly aligned. Second is that the cascade impactor used in this study was susceptible to high blow through. Blow through occurs when particles are initially entrapped on a substrate but break loose and become re-entrained in the air stream. These particles are carried past the correct impaction stage and then deposited on subsequent stages. This was confirmed by the high levels of particulate accumulated on the back up filters.

The three instruments compared favorably for TSP concentration. The non-parametric A Kruskal-Wallis one way ANOVA ranks test was performed because the mean concentrations did not have equal variances. The unequal variances were expected due to the difference in magnitude between the LPC and hi-vol concentrations. The Kruskal-Wallis test was performed on each individual cut size and the differences were found to be statistically significant ($p=0.05$). This test was repeated using TSP concentrations and the differences were no longer statistically significant ($p=0.05$). This agreement was expected; TSP concentrations included the back-up filters so all particles were accounted for by each instrument. This agreement indicates that the LPC and hi-vol are both measuring the same particulate but estimating different size distributions due to operating differences. The hi-vol would be a good measurement standard to calibrate the LPC using TSP but not robust enough for individual cut sizes.

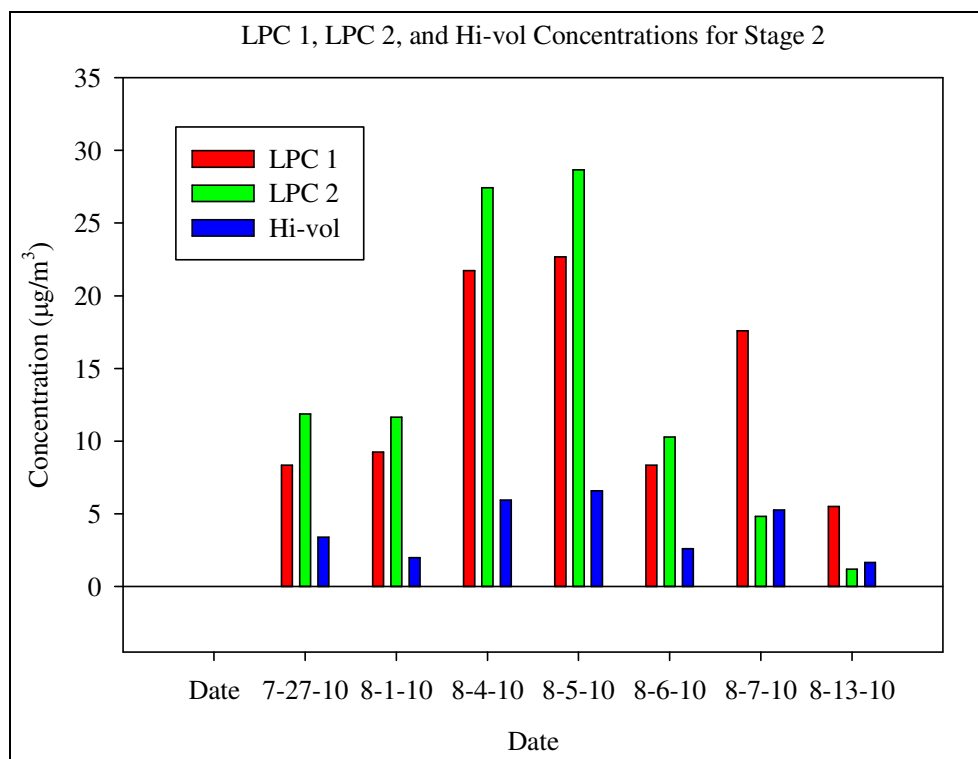


Figure 18 Stage 2 Concentrations for LPC 1, LPC 2, and Hi-vol

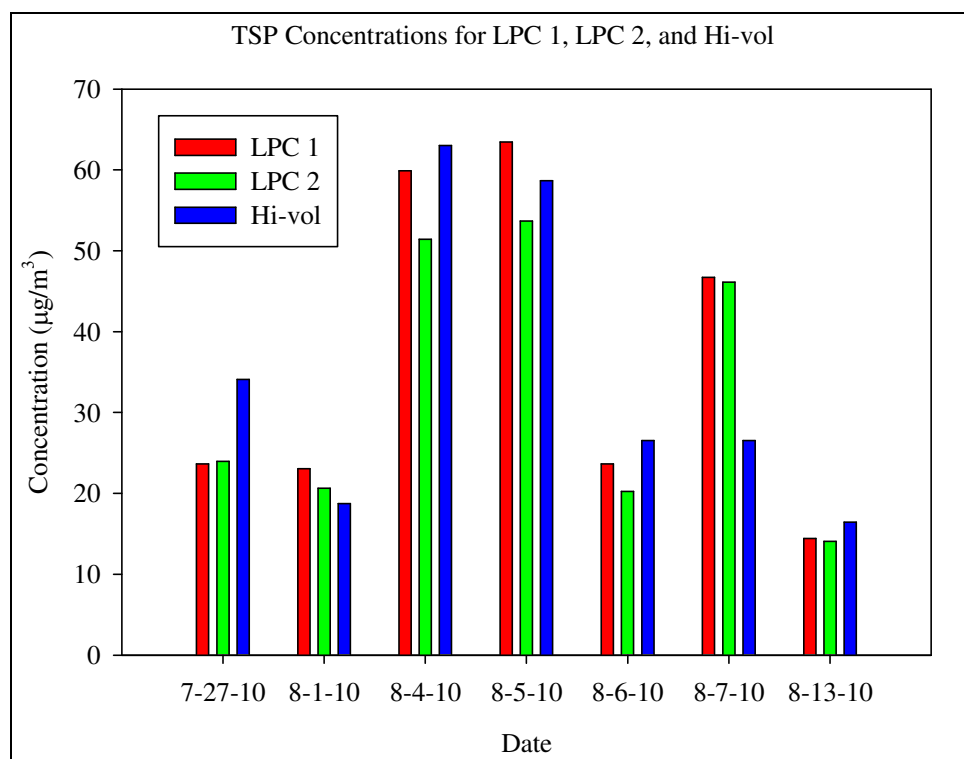


Figure 19 TSP Concentrations Measured by LPC 1, LPC 2, and the Hi-vol

The results from the fall testing were analyzed by comparing both individual cut size concentrations and TSP concentrations from the LPC, hi-vol, and MOUDI. The average concentrations are graphed in Figure 20 by curve fitting the LPC concentrations and presenting the hi-vol and MOUDI results as histograms. Although, direct comparison of individual points is not possible (due to low number of impactor stages for the hi-vol), the three instruments displayed similar size distributions. For example, each instrument displayed peak concentrations between 8.0 μm to 10.0 μm . The LPC and MOUDI demonstrated a similar PM concentration magnitudes while the hi-vol consistently measured significantly higher concentrations. This result also occurred when comparing the TSP concentrations for each device as shown in Figure 21.

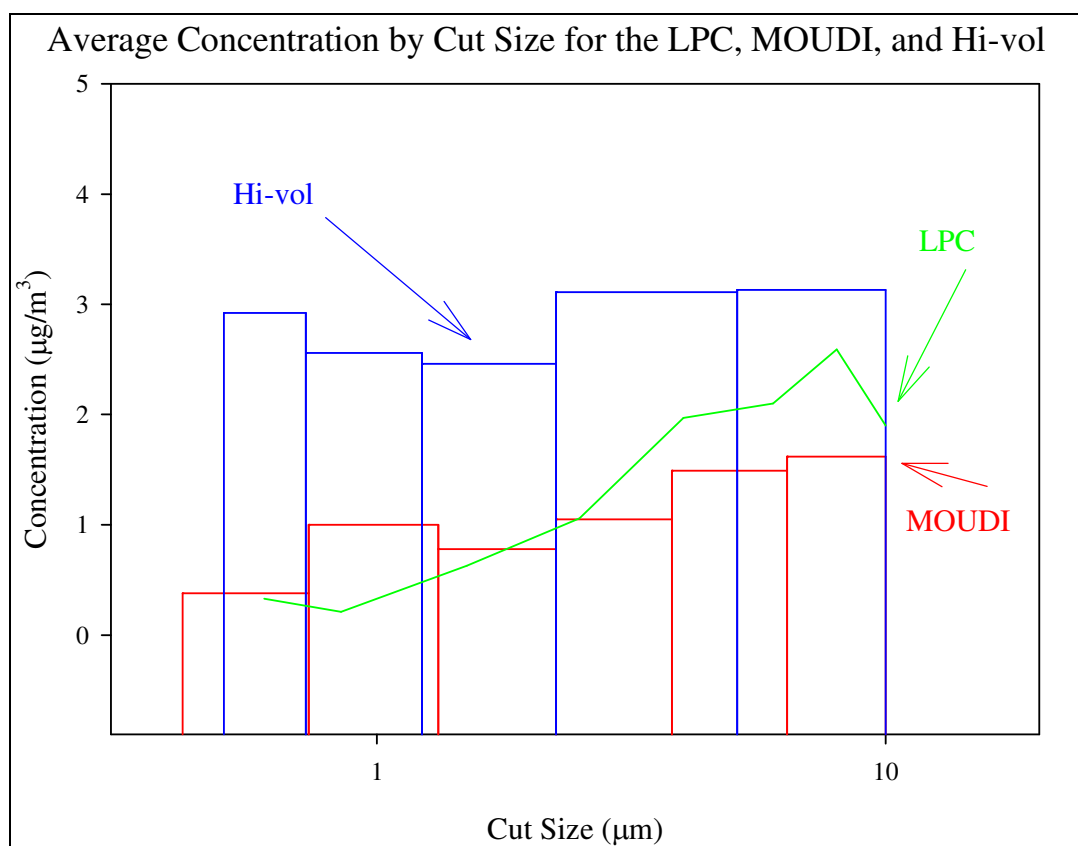


Figure 20 Average Cut Size Concentration for the LPC, MOUDI, and Hi-vol

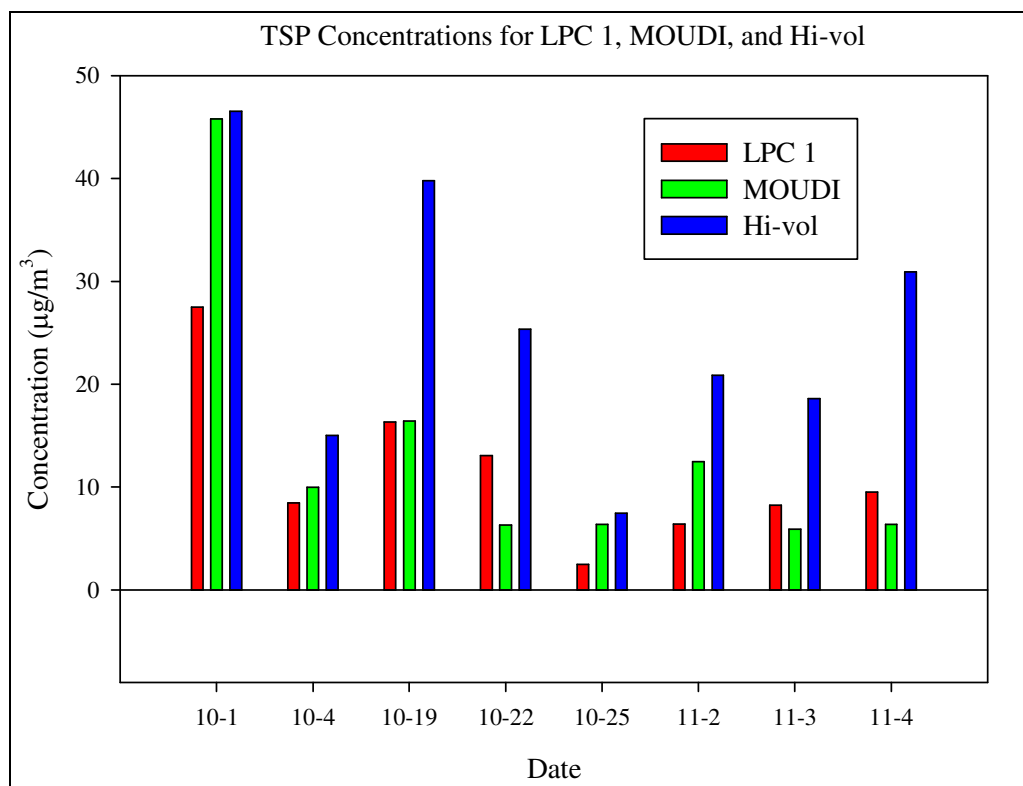


Figure 21 TSP Concentrations Measured Using the LPC, MOUDI, and Hi-vol

Although direct comparison between individual cut sizes was not feasible, the TSP concentrations were analyzed using an ANOVA. The results did not compare favorably. A Kruskal-Wallis one-way ANOVA ranks test was performed and it was determined that the differences between concentrations were statistically significant ($p=0.05$). The lack of agreement was because the hi-vol typically measured higher concentrations than the LPC or MOUDI. There are a few possible reasons for the higher hi-vol concentrations.

First, mechanical failure and power outages limited the number of days that each device sampled during the same time period so that there were only eight sample periods during which all three instruments were operated simultaneously. Unlike the summer

testing session, the sample time steps were varied significantly during the fall testing. These sample times ranged from 18 to 48 hours. The greatest variation between the hi-vol and the other two instruments (on 10/19/10 and 11/4/10) corresponded to the 18 hr sample periods. The higher agreement tended to occur during the longer sample periods (10/04/10 and 10/25/10). This could be indicative of small measurement artifacts being masked during longer sample times. Unfortunately, there were insufficient samples during each of the time steps to determine if this cause was significant. Second, the hi-vol sampled at a higher flow rate (30 L/min) than the MOUDI (13 L/min), allowing it to reach MDLs quickly. The shorter sample times prevented the MOUDI from reaching MDLs of the smaller cut sizes. This was indicated by a lack of measurable difference in change of weight on the stages of the MOUDI.

Despite the lack of definitively positive results during the fall testing campaign, there was enough agreement during the summer testing that more extensive testing with the hi-vol is recommended. Once calibrated, the cut sizes on the LPC could be adjusted to align with the cascade impactor. Also, further testing could be performed using improved sampling periods, allowing the MOUDI and hi-vol to reach MDLs. Further testing could also be used to determine if the percent composition of each impactor stage can be related to a percent composition of stages for the LPC or MOUDI.

MOUDI 1 and MOUDI 2 Comparison

During the fall testing period, duplicate sampling was performed using MOUDI 1 and MOUDI 2 to ensure reproducibility. The MOUDIs were placed at identical heights and spaced approximately 2 m apart. The average concentrations and linear regression are displayed in Figure 22 and Figure 25. The correlation was 0.896, indicating good

agreement. The offset was just 0.087 and the slope of the regression line was near unity at 1.03. The high coefficient of determination indicates an agreement between the instruments; small differences were attributed to particle bounce or the natural heterogeneity of particulate concentration that occurs for two instruments located 2 m apart.

The average concentrations by cut size for each MOUDI are displayed in Figure 25. Both devices showed a slight bimodal distribution of particulate concentration with peaks near the 0.53 μm and 20 μm . MOUDI 1 and MOUDI 2 consistently measured similar concentrations and differences could be a result of measuring artifacts due to instrument location. The measurement differences tended to be greater at the lower and higher cut sizes although, all measurements are within the confidence intervals ($p = 95\%$) shown in the graph. A student t-test was performed and MOUDI 1 had a mean of 3.969 ($\mu\text{g}/\text{m}^3/\text{dlogd}$) and a standard deviation of 2.386 while MOUDI 2 had a mean of 3.922 ($\mu\text{g}/\text{m}^3/\text{dlogd}$) and a standard deviation of 2.184. These differences were not statistically significant ($p=0.05$). These results demonstrate that good testing and operating procedures were followed.

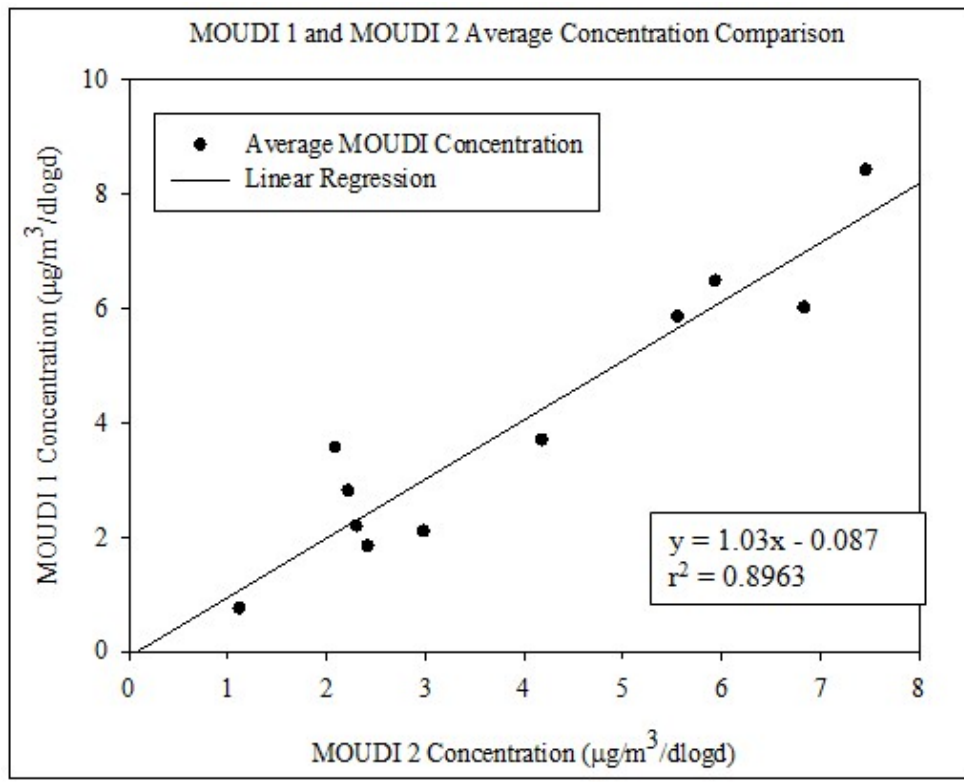


Figure 22 MOUDI 1 and MOUDI 2 Average Concentration Comparison

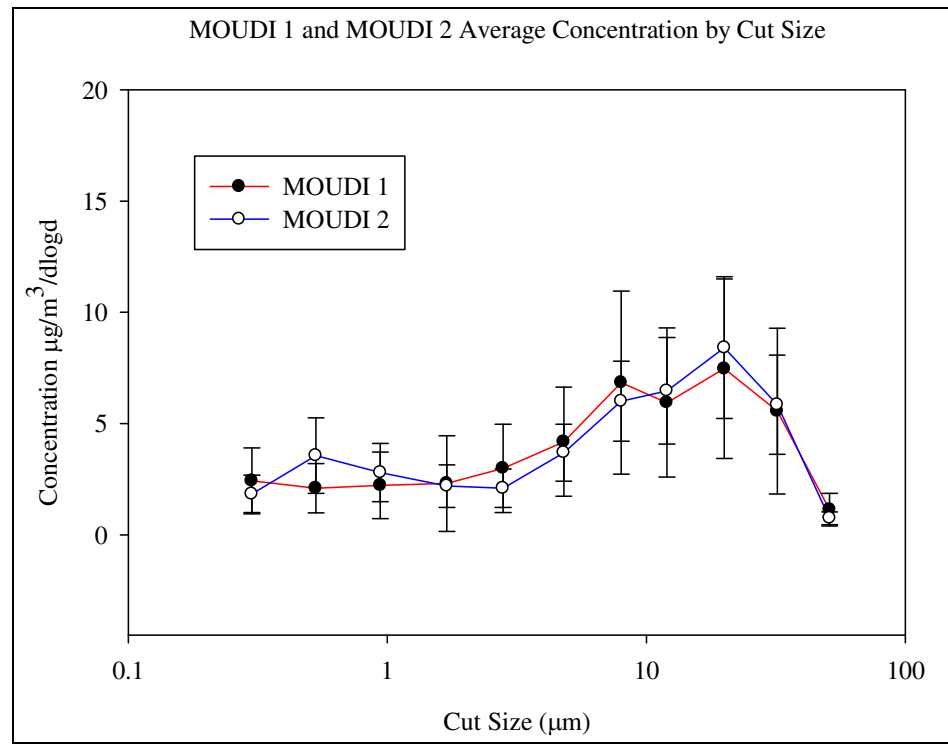


Figure 23 MOUDI 1 and MOUDI 2 Average Concentration by Cut Size

Time Step Analysis

The LPC and MOUDI each operated using different sampling or collection time-steps. The LPC operated in real time while the MOUDI collected particulate over a long sampling period. Therefore, the fall collection sampling times were varied between 18 hours and 48 hours. The long sample periods ensured enough particulate mass was collected by the MOUDI to meet MDLs. A second reason was to examine the compatibility between the different collection time steps of the MOUDI and LPC. The MOUDI operates by collecting particulate over a long sample time, resulting in an average concentration during that time. Meanwhile, the estimated LPC concentrations were the result of a series of small, real-time measurements summed and averaged over the duration of the total collection period. Therefore, the hypothesis was that short time step measurements made using a LPC were equivalent to a single MOUDI measurement made over a long period of time. To answer this, a comparison was made of the relative percent difference (RPD) normalized by hour between the MOUDI and LPC as shown in Figure 24.

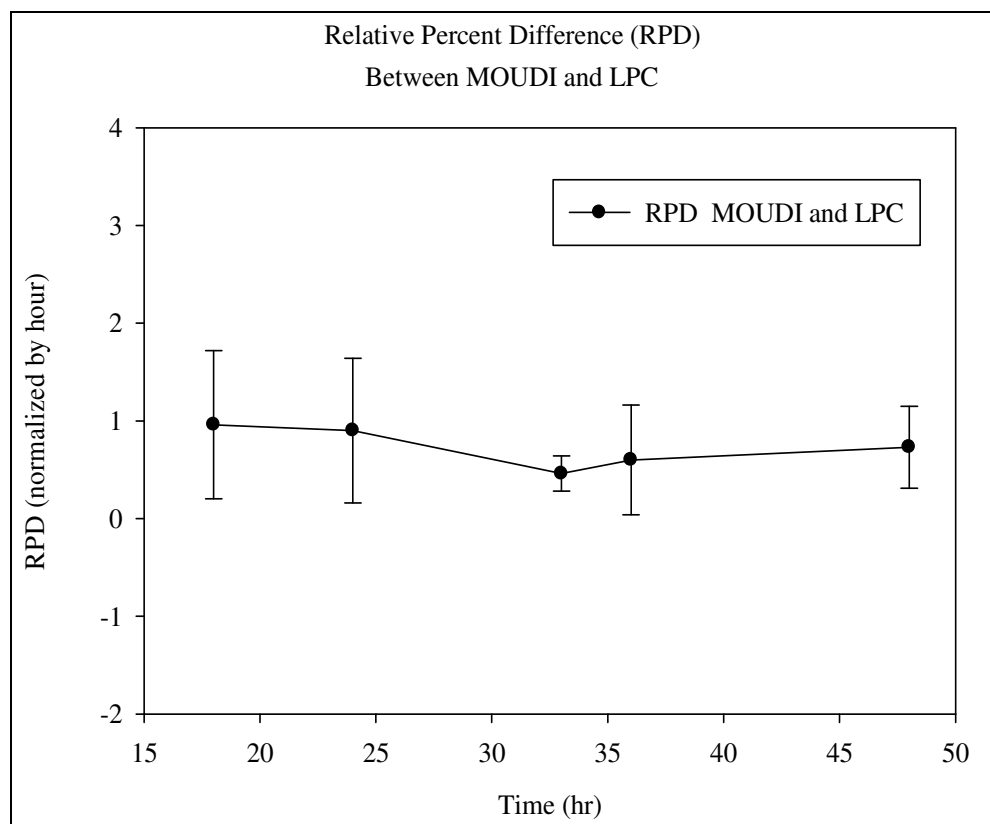


Figure 24 RPD Normalized by Hour for the LPC and MOUDI

The RPD between the instruments was small. The magnitude is fairly constant, consistently near 1% with an error range of approximately +/- 1%. A student's t-test was performed to determine if this difference between the mean was significant. The LPC had a mean of $22.71 \mu\text{g}/\text{m}^3$ and a standard deviation of $8.263 \mu\text{g}/\text{m}^3$ compared to the MOUDIs mean of $23.79 \mu\text{g}/\text{m}^3$ and standard deviation of $8.166 \mu\text{g}/\text{m}^3$. There was no statistically significant difference between the measurements at the 95% confidence level. This indicates that it was acceptable to use the long time steps required by the MOUDI to calibrate the real-time measurements made with the LPC.

LPC 2 to LPC 1 Calibration

After the initial LPC was calibrated to a MOUDI, it could act as a master LPC used to calibrate future LPCs as they are added to a wireless sensor network. This would enable rapid integration of LPCs without the need for a long, labor-intensive calibration process. Two LPCs were operated concurrently during a laboratory sampling session to test the feasibility of this concept.

A pair LPCs (labeled LPC 1 and LPC 2) were set up in a laboratory located in the first floor of the Engineering Technology building on the BSU campus. The LPCs sampled for approximately 12 hrs under identical conditions. The number concentrations were converted to mass concentrations by assuming the particulate was spherically shaped with a unit density of 1.0 g/cm^3 . The LPCs were positioned so that the inlet hoods were located at identical heights, approximately 1.0 m apart.

Both TSP and individual cut size concentrations were compared, generally agreeing. The TSP concentrations ($\mu\text{g/m}^3$) presented in Figure 25 illustrate that both devices respond similarly to changing particulate concentration while also recording similar concentration magnitude. Although the graph illustrates strong agreement between these LPCs, this was not enough to preclude the calibration of individual cut sizes of LPC 2 to LPC 1.

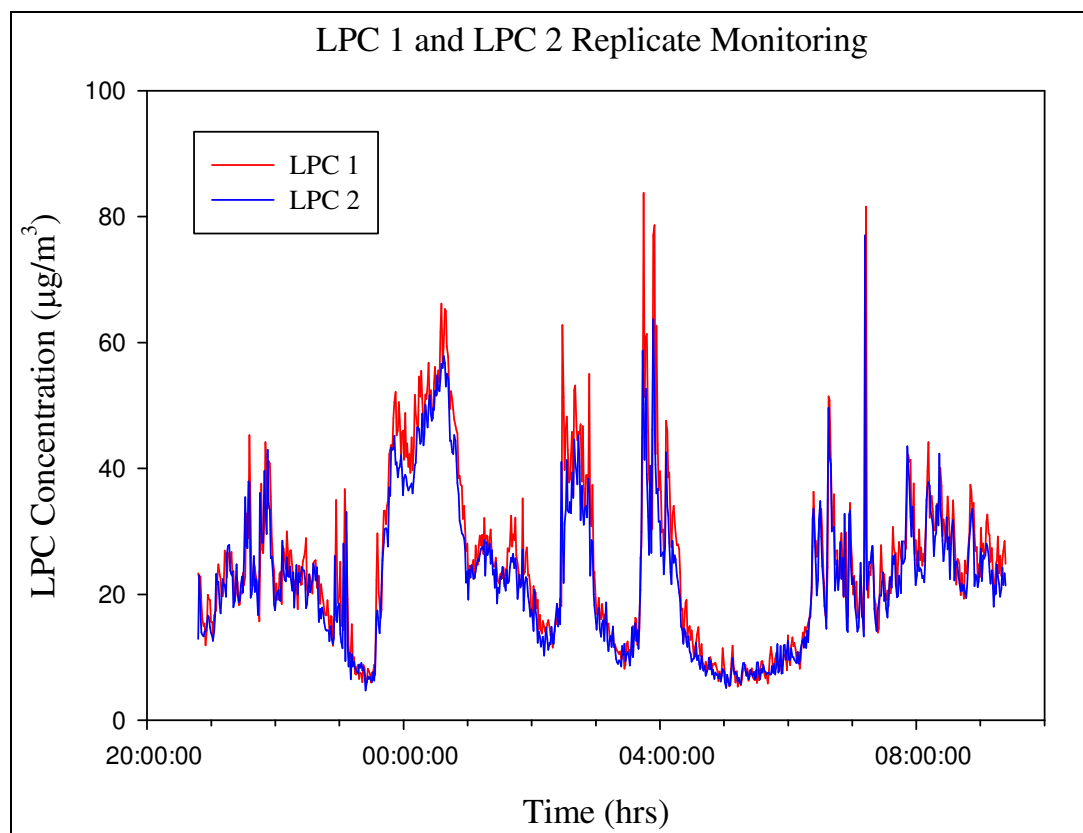


Figure 25 LPC 1 and LPC 2 TSP Comparison

Some individual cut size concentrations agreed well enough that calibration was not required and small adjustments were made to the magnitude of the remaining cut size concentrations. The LPCs were configured to size segregate particulate according to cut sizes: 0.5 µm, 0.70 µm, 1.0 µm, 2.0 µm, 3.0 µm, 5.0 µm, 7.0 µm, and 10.0 µm. The individual stage comparison included both a regression analysis and student's t-test. The regression analysis results are shown Figure 26 and Figure 27 for the 0.5 µm and 10.0 µm and the remaining cut sizes graphs are provided in **Error! Reference source not found.**

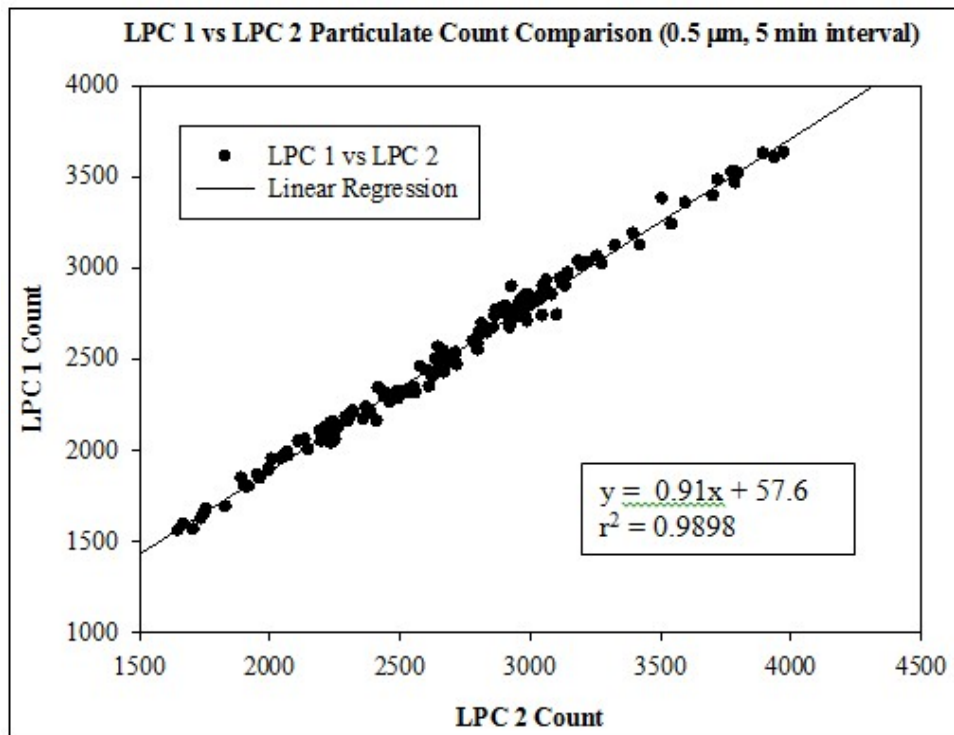


Figure 26 Regression Analyses for 0.50 μm (LPC 1 and LPC 2)

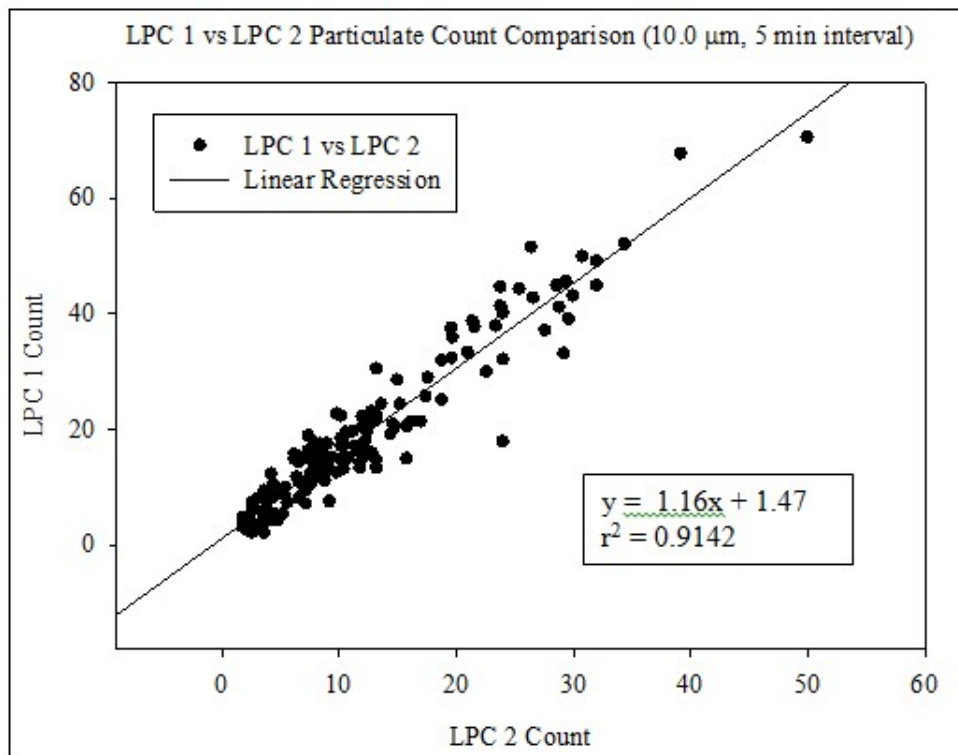


Figure 27 Regression Analyses for 10.0 μm (LPC 1 and LPC 2)

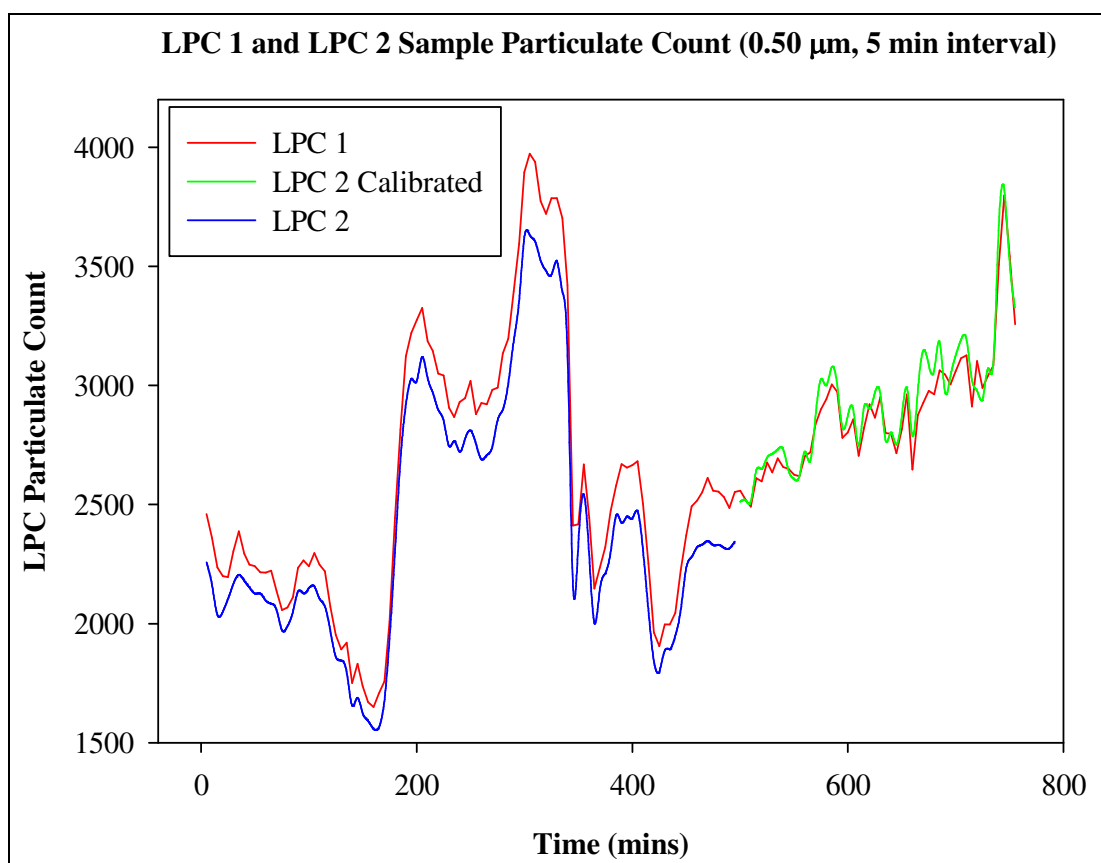
Table 11 contains the regression analysis results for each cut size. The r^2 ranged from a low of 0.9142 (10.0 μm) to a high of 0.9898 (0.5 μm). This indicates a very strong agreement between the measurements made by each LPC. The slope ranged from a low of 0.7002 at the 5.0 μm size to a high of 1.830 at the size 7.0 μm . The slopes were near 1.000, indicating that both devices are capturing similar concentration levels. A high (+/-) y-intercept value can be indicative of measurement or instrument bias. The intercept ranged from a low of -14.0 to a high of 57.0, which demonstrates an absence of significant measurement or instrument bias.

Student t-tests were performed on the individual cut sizes and the results are provided in

Table 11. The differences were not significant ($p=0.05$) for the 1.0 μm and 2.0 μm cut size and as such no adjustments were made to those cut sizes on LPC 2. The remaining cut sizes had unequal variances, therefore the Mann-Whitney Rank Sum test, a non-parametric t-test, was used, showing that the differences for the remaining cut sizes were statistically significant. Each cut size for LPC 2 was calibrated to LPC 1 by adjusting the measurements according to the offset from LPC 1. This offset was applied to a validation data set and the Mann-Whitney test was rerun. The differences were not statistically significant for the remaining cut sizes. The calibrated and original results are shown in the graphs in Figure 28 and Figure 29 for cut sizes 0.5 μm and 10.0 μm and the remaining cut size graphs are provided in **Error! Reference source not found.** The graphs and statistical tests both show very good agreement between LPC 1 and LPC 2 post calibration.

Table 11 Regression Analyses for Individual Cut Sizes (LPC 1 and LPC 2)

Size (μm)	Agreement (r^2)	Slope (m)	Intercept (b)	Statistically Significant Student t-test	Statistically Significant Mann-Whitney Rank Sum Test Calibrated
0.50	0.9898	0.9134	57.76	Yes	No
0.70	0.9659	0.7355	-14.00	Yes	No
1.0	0.9837	0.9968	3.094	No	No
2.0	0.9794	1.014	2.448	No	No
3.0	0.9792	0.8917	0.7990	No	No
5.0	0.9593	0.7002	2.758	Yes	No
7.0	0.9326	1.830	2.403	Yes	No
10.0	0.9142	1.155	1.472	Yes	No

**Figure 28 LPC 1 and LPC 2 Calibration Results for 0.50 μm Cut Size**

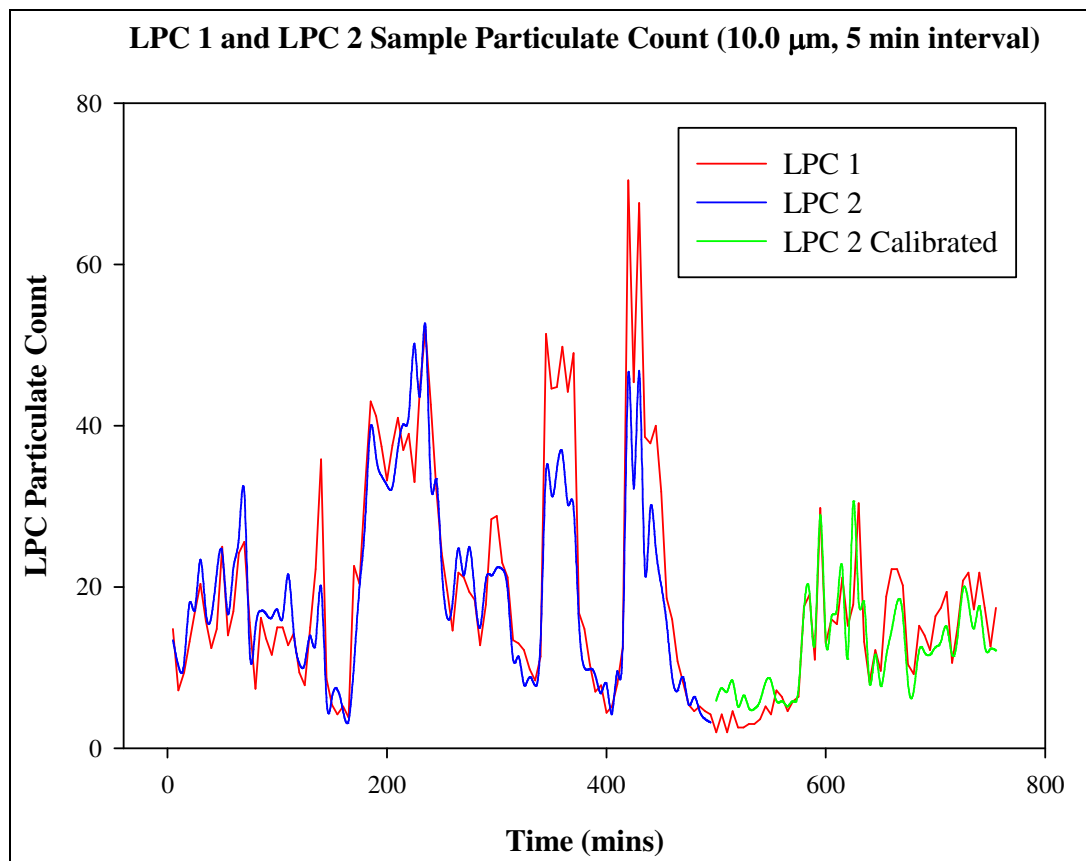


Figure 29 LPC 1 and LPC 2 calibration results for 10.0 μm Cut Size

CONCLUSION

Water is a vital natural resource in a semi-arid region like the western United States. It is imperative that scientists and water resource managers are able to quantify both its quantity and quality. PM scavenged from the atmosphere by snow can alter the physical properties of the snow. Understanding the link between PM and snow requires real-time monitoring of PM, ideally using multiple sensors in a networked array. This research demonstrated the applicability of LPCs to fulfill those requirements. Ultimately, this research provides a valuable link between atmospheric quality and water quality in a watershed. By understanding how atmospheric contaminants affect water runoff, we can better manage this valuable resource.

The hypothesis of this research was that a LPC, designed to estimate PM concentrations in real time, could be calibrated to a federal reference standard. This was accomplished by completing three research stages. First, a LPC was operated concurrently with a MOUDI and a hi-vol (outfitted with a cascade impactor). The PM concentrations estimated by the LPC and those made using the MOUDI and hi-vol were compared and analyzed using a variety of statistical testing. The initial results showed that size distributions of the PM concentrations were similar but the concentration magnitudes were significantly different. The magnitudes of the LPC concentrations were adjusted to match the MOUDI concentrations. The LPC concentrations were then

validated and an ANOVA was performed. The differences between the MOUDI and LPC mass concentrations were no longer statistically significant.

Next, the data was analyzed to ensure compatibility between the different measurement processes. This required performing a data inversion of the MOUDI results. The different measurement time steps between the LPC and MOUDI were compared. These differences were not significant, indicating that real-time measurements made using a LPC were equivalent to the long collection process used by the MOUDI.

Finally, two LPCs were operated simultaneously to compare their performance. The two devices measured very similar size distributions and magnitudes. The initial LPC was used to calibrate a second LPC, thereby demonstrating the reproducibility of deploying a series of particle counters throughout a watershed and other remote or distributed networks without the need for a long, labor-intensive calibration process.

This work was successful in demonstrating the applicability of field deploying LPCs in a wireless sensor network. The next stage of research could be to deploy the LPCs in a remote location such as the Dry Creek Experimental Watershed (DCEW). Currently, there are two aerochem-style precipitation collectors located in the watershed to collect particulate. These collectors and the LPCs could be used to study the relationship between atmospheric concentrations of PM and its deposition.

Further testing of the LPCs could be conducted to better understand their performance and reliability. One shortcoming of the current research was the inability to precisely identify the causes for each device measuring different magnitudes. Operating a LPC and a MOUDI in a controlled environment, such as a laboratory, could be used to better identify operating and measurement differences between the instruments. For

example, the instruments could be exposed to particulates of a single, specific size. This would allow researchers to better quantify measurement artifacts such as blow through.

One feature of the LPC, that was not fully tested, was the ability to alter the sampling cut sizes. The devices have the capability of adjusting the cut size between 0.5 μm and 10 μm . This offers the possibility to compare LPC concentrations to those made by other devices with predetermined cut sizes. This would allow the LPC to be operated concurrently with a TEOM to measure 2.5 μm .

As reported in this research, the size distribution of particulate between the hi-vol and LPC was similar. Studies have indicated that the percent composition of the hi-vol could be correlated with the LPC concentrations and initial results from this study support that. A hi-vol outfitted with a cascade impactor could be used to further verify the results obtained using a LPC. This is valuable because hi-vols can be configured to collect particulate and used to determine particle composition, a feature LPCs lack.

Finally, the LPC could be used in conjunction with local research and environmental monitoring. The Geoscience department at BSU is studying snowpack albedo in the DCEW. These LPCs could be used to establish a link between changing atmospheric PM concentrations and changing snowpack albedo. The link could be crucial to predicting changes to snow melt rates.

These LPC were field tested by operating them concurrently to both a MOUDI and hi-vol. They performed as expected and the concentrations generally compared well to reference standards. The measurement differences were statistically insignificant

following a calibration to the MOUDI. The LPCs are ready for field deployment to a remote location such as the DCEW.

REFERENCES

1. Zeller, K., Harrington, D., Riebau, A., and Donev, E., 2000. Annual Wet and Dry Deposition of Sulfur and Nitrogen in the Snowy Range, Wyoming. *Atmos. Environ.* **34** (11), 1703-1711.
2. Douglas, T.A. and Sturm, M., 2004. Arctic Haze, Mercury and the Chemical Composition of Snow Across Northwestern Alaska. *Atmos. Environ.* **38** (6), 805-820.
3. Thimonier, A., Schmitt, M., Waldner, P., and Rihm, B., 2005. Atmospheric Deposition on Swiss Long-Term Forest Ecosystem Research (LWF) Plots. *Environ. Monit. Assess.* **104** (1-3), 1-3.
4. Wiscombe, W.J. and Warren, S.G., 1980. A Model for the Spectral Albedo of Snow I: Pure Snow. *Proc SPIE Int Soc Opt Eng* **134**, 2712-2733
5. Flanner, M.G., Hess, P.G., Mahowald, N.M., Rasch, P.J., Zender, C.S., Painter, T.H., and Ramanathan, V., 2009. Springtime Warming and Reduced Snow Cover From Carbonaceous Particles. *Atmos. Chem. Phys.* **9** (7), 2481-2497.
6. Painter, T.H., Barrett, A.P., Landry, C.C., Neff, J.C., Cassidy, M.P., Lawrence, C.R., McBride, K.E., and Farmer, G.L., 2007. Impact of Disturbed Desert Soils on Duration of Mountain Snow Cover *Geophys Res Lett* **34** (12), L12502.

7. Steltzer, H., Landry, C., Painter, T.H., Anderson, J., and Ayres, E., 2009. Biological Consequences of Earlier Snowmelt from Desert Dust Deposition in Alpine Landscapes. *Proc. Nat. Acad. Sci. U.S.A.* **106** (28), 11629-11634.
8. Dozier, J. and Painter, T.H., 2004. Multispectral and Hyperspectral Remote Sensing of Alpine Snow Properties. *Ann. Rev. of Earth and Planetary Sci.* **32**, 465-494.
9. Bales, R.C., Molotch, N.P., Painter, T.H., Dettinger, M.D., Rice, R., and Dozier, J., 2006. Mountain Hydrology of the Western United States. *Wat. Res. Research* **42** (8), 1-32.
10. Samet, J., Wassle, R., Holmes, K.J., Abt, E., and Bakshi, K., 2005. Research Priorities for Airborne Particulates Matter in the United States. *Environ. Sci. Tech.* **39** (14), 299-304.
11. Lovett, G.M., Bowser, J.J., and Edgerton, E.S., 1997. Atmospheric Deposition to Watersheds in Complex Terrain. *Hydro. Proc.* **11** (7), 645-654.
12. Lovett, G.M., Bowser, J.J., and Edgerton, E.S., 1997. Atmospheric Deposition to Watersheds in Complex Terrain. *Hydrol. Process.* **11** (7), 645-654.
13. Ranalli, A.J., Turk, J.T., and Campbell, D.H., 1997. The use of Bulk Collectors in Monitoring Wet Deposition at High-Altitude Sites in Winter. *Water, Air & Soil Poll.* **95** (1/4), 237-255.
14. Nanus, L., Campbell, D.H., Ingersoll, G.P., Clow, D.W., and Alisa Mast, M., 2003. Atmospheric Deposition Maps for the Rocky Mountains. *Atmos. Environ.* **37** (35), 4881-4892.

15. Heuer, K., Tonnessen, K.A., and Ingersoll, G.P., 2000. Comparison of Precipitation Chemistry in the Central Rocky Mountains, Colorado, USA. *Atmos. Environ.* **34** (11), 1713-1722.
16. Weathers, K.C., Lovett, G.M., Likens, G.E., and Lathrop, R., 2000. The Effect of Landscape Features on Deposition to Hunter Mountain, Catskill Mountains, New York. *Eco. Appl.* **10** (2), 528-540.
17. Weathers, K.C., Simkin, S.M., Lovett, G.M., and Lindberg, S.E., 2006. Empirical Modeling of Atmospheric Deposition in Mountainous Landscapes. *Eco. Appl.* **16** (4), 1590-1607.
18. Warren, S.G. and Wiscombe, W.J., 1980. A Model for the Spectral Albedo of Snow. II: Snow Containing Atmospheric Aerosols. *J. of Atm. Sci.* **37** (12), 2734-2745.
19. Wiscombe, W.J. and Warren, S.G., 1980. A Model for the Spectral Albedo of Snow. I: Pure Snow. *Proc. SPIE Int. Soc. Opt. Eng.* **134**, 2712-2733.
20. Drake, J.J., 1981. The Effects of Surface Dust on Snowmelt Rates. **13** (2), 219-223.
21. Turk, J.T., Taylor, H.E., Ingersoll, G.P., Tonnessen, K.A., Clow, D.W., Mast, M.A., Campbell, D.H., and Melack, J.M., 2001. Major-ion chemistry of the Rocky Mountain snowpack, USA. **35** (23), 3957-3966.
22. Painter, T.H., Barrett, A.P., Landry, C.C., Neff, J.C., Cassidy, M.P., Lawrence, C.R., McBride, K.E., and Farmer, G.L., 2007. Impact of Disturbed Desert Soils on Duration of Mountain Snow Cover. *Geophys. Res. Lett.* **34** (12), L12502.

23. Hughes, L.S., Cass, G.R., Gone, J., Ames, M., and Olmez, I., 1998. Physical and Chemical Characterization of Atmospheric Ultrafine Particles in the Los Angeles Area. *Environ. Sci. and Tech.* **32** (9), 1153-1161.
24. Kleeman, M.J. and Schauer, J.J., 2000. Size and Composition Distribution of Fine Particulate Matter Emitted from Motor Vehicles. **34** (7).
25. Kinsey, J.S., Mitchell, W.A., Squier, W.C., Linna, K., King, F.G., Logan, R., Dong, Y., Thompson, G.J., and Clark, N.N., 2006. Evaluation of Methods for the Determination of Diesel-Generated Fine Particulate Matter: Physical Characterization Results. *J. of Aerosol Sci.* **37** (1), 63-87.
26. Wang, X., Chancellor, G., Evenstad, J., Farnsworth, J., Hase, A., Olson, G., Sreenath, A., and Agarwal, J., 2009. A Novel Optical Instrument for Estimating Size Segregated Aerosol Mass Concentration in Real Time. *Aerosol Sci. & Tech.* **43** (9), 939-950.
27. Hand, J.L., Kreidenweis, S.M., Kreisberg, N., Hering, S., Stolzenburg, M., Dick, W., and McMurry, P.H., 2002. Comparisons of aerosol properties measured by impactors and light scattering from individual particles: refractive index, number and volume concentrations, and size distributions. **36** (11), 1853.
28. Park, J.M., Rock, J.C., Wang, L., Seo, Y.C., Bhatnagar, A., and Kim, S., 2009. Performance Evaluation of Six Different Aerosol Samplers in a Particulate Matter Generation Chamber. *Atmos. Environ.* **43** (2), 280-289.
29. Keywood, M.D., Ayers, G.P., Gras, J.L., Gillett, R.W., and Cohen, D.D., 1999. Relationships Between Size Segregated Mass Concentration Data and Ultrafine

- Particle Number Concentrations in Urban Areas. *Atmos. Environ.* **33** (18), 2907-2913.
30. Winklmayr, W., Wang, H.C., and John, W., 1990. Adaptation of the Twomey Algorithm to the Inversion of Cascade Impactor Data. *Aerosol Sci. and Tech.* **13** (3), 322-331.
 31. Dong, Y., Hays, M.D., Dean Smith, N., and Kinsey, J.S., 2004. Inverting Cascade Impactor Data for Size-Resolved Characterization of Fine Particulate Source Emissions. *J. Aerosol Sci.* **35** (12), 1497-1512.
 32. Kandlikar, M. and Ramachandran, G., 1999. Inverse Methods for Analysing Aerosol Spectrometer Measurements. *J. Aerosol Sci.* **30** (4), 413-437.
 33. Dzubay, T.G. and Hasan, H., 1990. Fitting Multimodal Lognormal Size Distributions to Cascade Impactor Data. *Aerosol Sci. and Tech.* **13** (2), 144-150.
 34. Baron, P.A. and Willeke, K., *Aerosol Measurement : Principles, Techniques, and Applications*. 2001, New York: Wiley. 667-701.
 35. Wolfenbarger, K.J. and Seinfeld, J.H., 1990. Inversion of Aerosol Size Distribution Data. *J. Aerosol Sci.* **21** (2), 227-247.
 36. Marple, V.A., Rubow, K.L., and Behm, S.M., 1991. A Microorifice Uniform Deposit Impactor (MOUDI): Description, Calibration, and Use. *Aerosol Sci. and Tech.* **14** (4), 434-446.
 37. Marjamäki, M., Lemmetty, M., and Keskinen, J., 2005. ELPI Response and Data Reduction I: Response Functions. *Aerosol Sci. and Tech.* **39** (7), 575-582.

38. Wethington iii, D.M. and Hornbuckle, K.C., 2005. Milwaukee, WI, as a Source of Atmospheric PCBs to Lake Michigan. *Environ. Sci. and Tech.* **39** (1), 57-63.
39. MSP, *Model 100/110 MOUDI User Guide*. 2006, MSP Corporation: Shoreview, MN. p. 1-21.
40. Romay, R., *MOUDI Model 100*, B. Seely, Editor. 2010. p. 1.
41. Majoral, C., Le Pape, L., Diot, P., and Vecellio, L., 2006. Comparison of Various Methods for Processing Cascade Impactor Data. *Aerosol Sci. and Tech.* **40** (9), 672-682.
42. Wang, H.-C. and John, W., 1988. Characteristics of the Berner Impactor for Sampling Inorganic Ions. *Aerosol Sci. and Tech.* **8** (2), 157-172.
43. Kwon, S.B., Lim, K.S., Jung, J.S., Bae, G.N., and Lee, K.W., 2003. Design and Calibration of a 5-stage Cascade Impactor (K-JIST cascade impactor). *J. Aerosol Sci.* **34** (3), 289-300.
44. Howell, S., Pszenny, A.A.P., Quinn, P., and Huebert, B., 1998. A Field Intercomparison of Three Cascade Impactors. *Aerosol Sci. and Tech.* **29** (6), 475-491.
45. Middendorf, P.J., MacIntosh, D.L., Tow, L.V., and Williams, P.L., 2001. Performance of Electronic Flow Rate Meters Used for Calibration of Air Sampling Pumps. *AIHAJ* **62** (4).
46. M. McCawley, S. Martin, E. Moyer, M. Berakis, Hornsby-Myers, J., and Kent, M., 2002. Development of a Filter Assembly to Match the Deposition of Ultrafine Aerosol in the Lung: A Pilot

Study with Beryllium. *Ann Occ Hyg* **46** (1), 215-218.

47. Pennanen, A.S., Sillano, P., M., Hillamo, R., Quass, U., John, A.C., Branis, M., Hunov L, I., Meliefste, K., Janssen, N.A., and Koskentalo, T., 2007. Performance of a High-Volume Cascade Impactor in Six European Urban Environments: Mass Measurement and Chemical Characterization of Size-Segregated Particulate Samples. *Sci. of the Total Environ.* **374** (2-3), 297-310.
48. E.P.A., 1999, Sampling of Ambient Air for Total Suspended Particulate Matter (SPM) and PM₁₀ Using High Volume (HV) Sampler, U.S.E.P. Agency, Compendium of Methods for the Determination of Inorganic Compounds in Ambient Air, 1-78
49. Wedding, J.B. and Weigand, M.A., *Operations and Maintenance Manual The Wedding & Associates' PM₁₀ Critical Flow High-Volume Sampler*. 1993, Wedding & Associates: Fort Collins, Colorado.
50. Parekh, P.P., Khwaja, H.A., Khan, A.R., Naqvi, R.R., Malik, A., Shah, S.A., Khan, K., and Hussain, G., 2001. Ambient Air Quality of Two Metropolitan Cities of Pakistan and Its Health Implications. *Atmos. Environ.* **35** (34), 5971-5978.
51. Quality, S.o.I.D.o.E., 2003, Standard Operating Procedures for Air Quality Monitoring, Appendix A: PM₁₀ Graseby/Anderson/GMW Hi-Volume Sampler, S.o.I.D.o.E.Q.A.M.Q. Assurance, Monitoring, Modeling, and Emissions Inventory A1-A28

52. Munson, B.R., Young, D.F., and Okiishi, T.H., *Fundamentals of Fluid Mechanics*. 2006, Hoboken, NJ: J. Wiley & Sons.
53. Quality, I.D.o.E., 2001, Appendix A: PM10 Graseby/Anderson/GMW Hi-volume Sampler, E. Quality, A-1 - A-28
54. Hinds, W.C., *Aerosol Technology : Properties, Behavior, and Measurement of Airborne Particles*. 1982, New York: J. Wiley.
55. Seinfeld, J.H. and Pandis, S.N., *Atmospheric Chemistry and Physics : From Air Pollution to Climate Change*. 1998, New York: Wiley.
56. O'Shaughnessy, P.T. and Raabe, O.G., 2003. A Comparison of Cascade Impactor Data Reduction Methods. *Aerosol Sci. and Tech.* **37** (2), 187-200.
57. Lemmetty, M., Marjamäki, M., and Keskinen, J., 2005. The ELPI Response and Data Reduction II: Properties of Kernels and Data Inversion. *Aerosol Sci. and Tech.* **39** (7), 583-595.
58. Software, S., *SigmaPlot 11 Analyze and Graph Your Data with Unparalleled Ease and Precision*. User's Guide Part 2 Statistics. Vol. 2. 2008, San Jose: Systat Software Inc. 564.

APPENDIX A

Sample Calculation of LPC Count to Concentration

Appendix A Sample Calculation of LPC Count to Concentration

Ben Seely Sample Calculation to Convert Counts to Concentration

Given: counts made using laser particle counter
Flow = 1.0 L/min

① mean particle size = $\frac{\text{channel (n+1) Size} + \text{channel (n) Size}}{2}$

channel 1	0.5 μm	}	$\frac{0.5 \mu\text{m} + 0.7 \mu\text{m}}{2} = 0.6 \mu\text{m}$
channel 2	0.7 μm		

② Radius = $\frac{\text{mean particle size}}{2}$; $\frac{0.6 \mu\text{m}}{2} = 0.3 \mu\text{m} = r$

③ mean Particle Volume = $\frac{4}{3} \pi r^3$; $(0.3 \mu\text{m})^3 \pi (\frac{4}{3}) = 0.11316 = 0.1131 \mu\text{m}^3$

④ Assume Standard Particle density = 1.5 $\frac{\text{g}}{\text{cm}^3}$

⑤ mean particle mass (μg) = volume \cdot density;

$$1.5 \frac{\text{g}}{\text{cm}^3} \cdot 0.1131 \mu\text{m}^3 \times \frac{(10)^3 \text{m}^3}{(1.0 \times 10^6) \mu\text{m}^3} \times \frac{100^3 \text{cm}^3}{1.0 \mu\text{m}^3} = 1.696 \times 10^{-13} \frac{\text{g}}{\mu\text{m}^3} \times \frac{1.0 \times 10^6 \mu\text{g}}{1.0 \text{g}} = 1.696 \times 10^{-7} \mu\text{g} = \text{mean particle mass}$$

⑥ Differential Counts (sample counts used)

Range	channel count	Differential count
1	5307	3507
2	1800	

⑦ Differential counts per liter = $\frac{\text{Diff. count}}{\text{time}} \cdot \frac{60}{\text{L}} \cdot \frac{\text{min}}{\text{L}}$ ← flow rate

$$3507 \cdot \frac{60 \text{ sec}}{\text{min}} \cdot \frac{\text{min}}{1.0 \text{ L}} \cdot \frac{1}{\text{Sample time (sec)}} = \frac{3507}{\text{L}}$$

↑ 60 sec

⑧ Differential mass = $\frac{\text{counts}}{\text{Liter}} \cdot \text{mean particle mass} \cdot 1000$

$$\frac{3507 \text{ particles}}{\text{L}} \cdot 1.696 \times 10^{-7} \mu\text{g} = 5.9478 \times 10^{-4} \mu\text{g} / \text{L} \times \frac{1000 \text{ L}}{1 \text{ m}^3} = 0.595 \mu\text{g}/\text{m}^3$$

Figure A.1 Hand Calculations of LPC Count to Calculation

Table A.1 Flow calibration for LPC

LPC Flow (L/min)	BOIS Flow (L/min)
3.10	3.091
3.10	3.123
3.10	3.075
3.10	3.670
3.10	3.206
3.00	3.052

Table A.2 Statistical test results of pump flow rate between LPC and BIOS flow meter.

t-test

Wednesday, September 21, 2011, 5:34:10 PM

Data source: LPC Pump Calibration in LPC pump calibration.JNB

Normality Test: Passed (P = 0.176)

Equal Variance Test: Passed (P = 0.410)

Group Name	N	Missing	Mean	Std Dev	SEM
Col 1	7	1	3.083	0.0408	0.0167
Col 2	7	1	3.102	0.0563	0.0230

Difference -0.0190

t = -0.669 with 10 degrees of freedom. (P = 0.518)

95 percent confidence interval for difference of means: -0.0822 to 0.0442

The difference in the mean values of the two groups is not great enough to reject the possibility that the difference is due to random sampling variability. There is not a statistically significant difference between the input groups (P = 0.518).

Power of performed test with alpha = 0.050: 0.050

The power of the performed test (0.050) is below the desired power of 0.800.

Less than desired power indicates you are less likely to detect a difference when one actually exists.

Negative results should be interpreted cautiously.

APPENDIX B

Calibration Data Provided by MSP for MOUDI Eff Curves

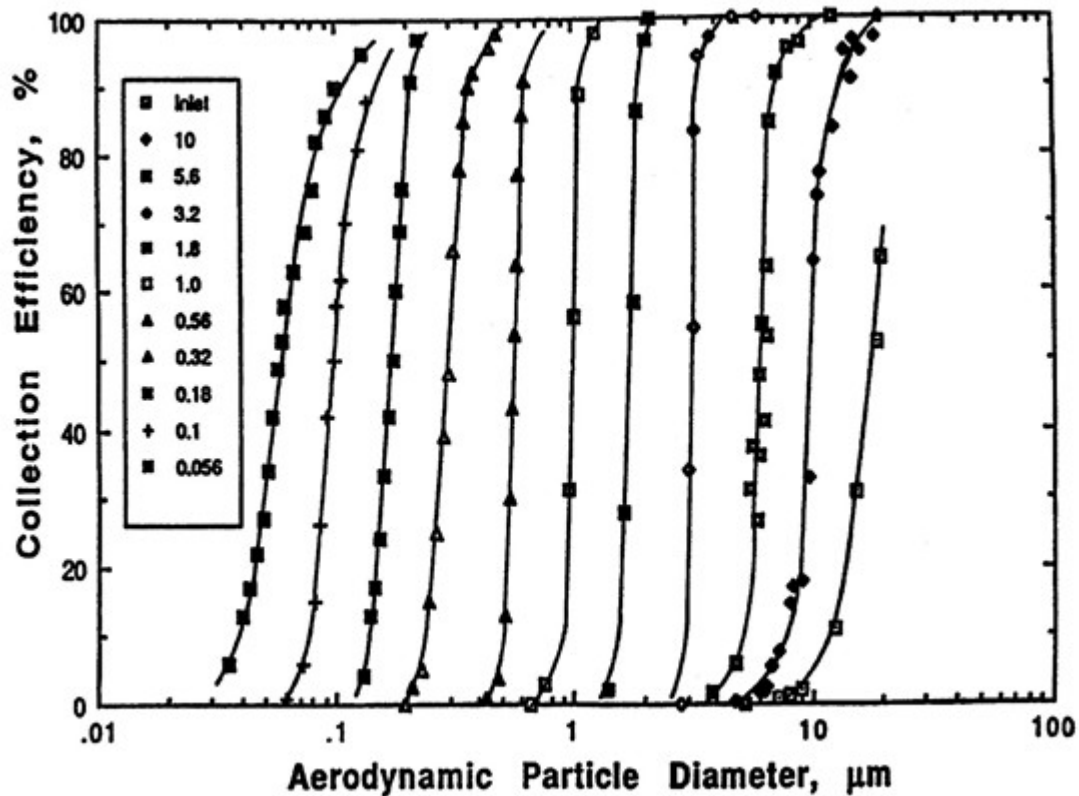


Figure B.1 Calibration Data Provided by MSP for MOUDI Eff Curves

Table B.1 Original Calibration Data Provided by MSP Corp. for MOUDI 100/110 Stages 10 to 7

Da St 10	Eff St 10	Da St 9	Eff St 9	Da St 8	Eff St 8	Da St 7	Eff St 7
0.035	6	0.062	1	0.13	4	0.195	0
0.04	13	0.073	6	0.139	13	0.213	2.3
0.043	17	0.08	15	0.146	17	0.23	4.9
0.046	22	0.084	26	0.153	24	0.247	15
0.049	27	0.091	42	0.159	33	0.264	25
0.052	34	0.097	50	0.167	42	0.28	39
0.054	42	0.1	58	0.174	50	0.297	48
0.056	49	0.103	62	0.179	60	0.313	66
0.059	53	0.108	70	0.186	69	0.33	78
0.061	58	0.124	81	0.192	75	0.346	85
0.065	63	0.138	88	0.211	91	0.361	90
0.073	69			0.228	97	0.377	92
0.079	75					0.451	96
0.083	82					0.477	98
0.09	86						
0.1	90						
0.13	95						

**Table B.2 Original Calibration Data Provided by MSP Corp. for MOUDI
100/110 Stages 6 to 3**

Da St 6	Eff St 6	Da St 5	Eff St 5	Da St 4	Eff St 4	Da St 3	Eff St 3
0.426	1	0.66	0	1.38	2.09	2.8	0
0.48	3.7	0.75	2.9	1.64	27.9	2.98	34
0.506	13	0.94	31	1.77	58.7	3.12	54.7
0.534	30	0.986	56.4	1.87	86.2	3.26	83.4
0.548	43	1.06	88.7	2.05	96.7	3.4	94
0.561	54	1.24	98	2.12	100	3.8	97.2
0.572	64					4.73	99.9
0.587	77						
0.614	86						
0.63	91						

**Table B.3 Original Calibration Data Provided by MSP Corp. for MOUDI
100/110 Stages 6 to 3 (continued)**

Da St 2	Eff St 2	Da St 1	Eff St 1	Da St 0	Eff St 0
8.91	96.2	14.9	90.8	19.4	64.7
7.98	95.6	13.8	95.1	18.5	52.7
7.15	91.5	12.3	83.7	15.2	30.6
6.69	84.5	10.9	77.2	12.3	10.8
6.45	53.7	10.4	74	8.91	2
6.32	63.6	9.99	64.4	7.98	1.1
6.2	41	9.63	32.9	7.15	0.8
6.11	55.1	8.91	17.7		
5.99	35.9	8.12	16.9		
5.95	47.9	7.98	14.7		
5.84	26.6	7.15	7.3		
5.61	37.3	6.69	5.2		
5.46	31.1	6.45	2.4		
5.25	0	6.2	1.6		
4.73	5.9	5.99	1.6		
3.8	1.6				

APPENDIX C

Same Calculations of MOUDI Concentration

	Bent Seely	
	<p>Hand calculation of MOUDI concentration</p> <p>End W (mg) - Start W (mg) = ΔW</p> <p>75.023 mg - 74.985 mg = 0.038 mg</p> <p>Run time = 1390 min</p> <p>Flow rate = 13.0 L/min</p> <p>$\Delta W \div \text{Run time} \div \text{Flow rate} = \text{Concentration}$</p> $\frac{0.038 \text{ mg}}{1} \cdot \frac{1}{1390 \text{ min}} \cdot \frac{\text{min}}{13.0 \text{ L}} \cdot \frac{1000 \text{ L}}{\text{m}^3} \cdot \frac{1000 \text{ } \mu\text{g}}{\text{mg}} = 2.103 \text{ } \mu\text{g}/\text{m}^3$ <p>Data taken from MOUDI 1, stage 0.187, 10-1-10.</p>	

Figure C.1 Hand Calculations of MOUDI Concentration

APPENDIX D

Original Data from BIOS Testing

Results for MOUDI Pump Flow Calibration

Pump 1975

Pump Flow L/min	BIOS Flow L/min
5.0	5.01
6.0	5.92
7.0	6.99
8.0	8.07
9.0	9.11
10.0	9.91
11.0	10.86
12.0	11.79
13.0	13.07
14.0	13.81
15.0	15.55

Pump 1828

Pump Flow L/min	BIOS Flow L/min
5.0	4.26
6.0	5.06
7.0	5.74
8.0	6.51
9.0	7.26
10.0	8.22
11.0	9.73
12.0	10.75
13.0	11.20
14.0	12.46
15.0	14.65

All BIOS Flows are an average of 5 readings.

Figure D.1 Original Data from BIOS Testing

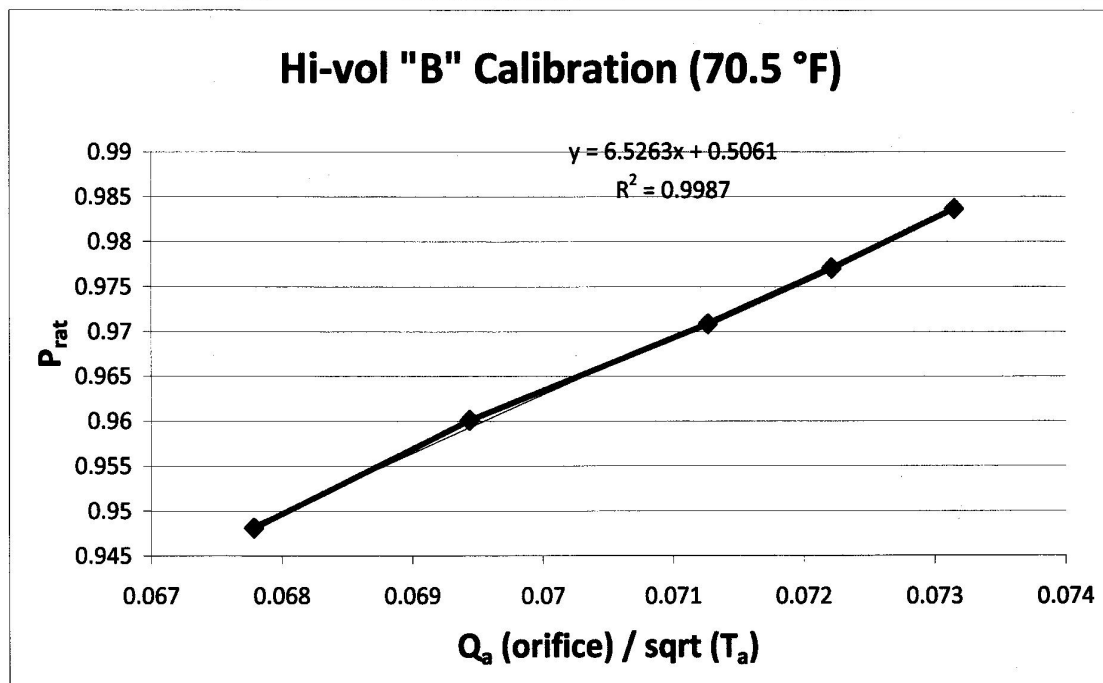
APPENDIX E

Calibration Calculations and Charts for Hi-Vols

Calibration of Hi-Vol Samplers
 Performed by Ben Seely on 05-12-2010

Lab Conditions		Q_a (m^3/min)		Q_{std} (m^3/min)	
T_a (K)	294.5	m=	0.9840	m=	1.5710
P_a (mm Hg)	692.3	b=	-0.015030	b=	-0.023585
		r=	0.999986	r=	0.999986

Hi-Vol "B"							
Run	ΔH_2O	Stag Port		Q_a	X-Axis	Y-Axis	P_{rat}
	in H_2O	in H_2O	mm Hg	orifice			
1	3.50	6.05	11.29	1.25538955	0.07314866	0.98369079	
2	3.41	8.50	15.86	1.23934138	0.07221357	0.97708624	
3	3.32	10.80	20.16	1.22307998	0.07126605	0.97088604	
4	3.15	14.80	27.62	1.19175093	0.06944058	0.96010309	
5	3.00	19.25	35.93	1.16339793	0.06778852	0.94810707	



For Q_{act} (across filter) use:

Where:

m= 6.5263

b= 0.5061

$$Q_{act} = \frac{(P_{rat} - b)\sqrt{T_a}}{m}$$

Figure E.1 Calibration Calculations and Charts for Hi-Vols

**W & A CRITICAL FLOW HIGH VOLUME SAMPLER
SINGLE- OR MULTI-POINT CALIBRATION WORKSHEET
FOR USE WITH MANOMETER OR W & A CALIBRATOR
RE: SECTIONS 5.2 AND 5.3
(TOP LOADING ORIFICE)**

Site lab Date 5-19-10 Time 2:00 Operator Ben Seely

Sampler Model "C" Serial Number _____ Motor Number _____

P₀ 762.96/30.01 mm Hg, in Hg T₀ 297.6 k K, R P̄₀ _____ mm Hg, in Hg T̄₀ _____ K

Orifice S/N 2141 (Model 628A) Orifice Cal. Date 4/30/10 W&A Cal. S/N NA Cal. Date NA

Comments: _____

Orifice Plate Number	(A) Manometer Readings		(B) P ₁ = P ₀ - ΔP _{cf} (in Hg)	W&A Cal V ₁ /V ₀ = P ₁ /P ₀	(C) Indicated Flow Rate from orifice cal (D)			Flow Rate From W&A Look-Up Table (E)			
	Top Orifice ΔP _{total} (LHS + RHS)	Critical Device ΔP _{cf} (LHS + RHS)			Q _{std}	Q ₀	Q̄ ₀	Q ₀ CFM	Q ₀ m ³ /min	Q̄ ₀ CFM	Q̄ ₀ m ³ /mi
18	2.46	24.65	28.20	0.9397							The Critical Flow Device volumetric flow rate values are given in the W & A Look-Up Table determined from previous calibration using a Root meter. Only the Single Point (Design Flow Rate) values are presented and should be equal to those determined herein.
13	2.42	25.25	28.15	0.9380							
10	2.33	26.75	28.04	0.9344							
7	2.21	28.75	27.90	0.9297							
5	2.13	29.90	27.81	0.9267							
None	3.52	6.00	29.57	0.9855							
Single Point (E)	X	20.95	28.47	0.9487							

Comments: _____

Note: Calculation of Q_{std}
 (1) in degrees R and in. Hg (1) $Q_{std} = \bar{Q}_0 \frac{\bar{P}_0}{T_0} \frac{537}{29.92}$ (2) $Q_{std} = \bar{Q}_0 \frac{\bar{P}_0}{T_0} \frac{298}{760}$
 (2) or degrees K and mm. Hg.

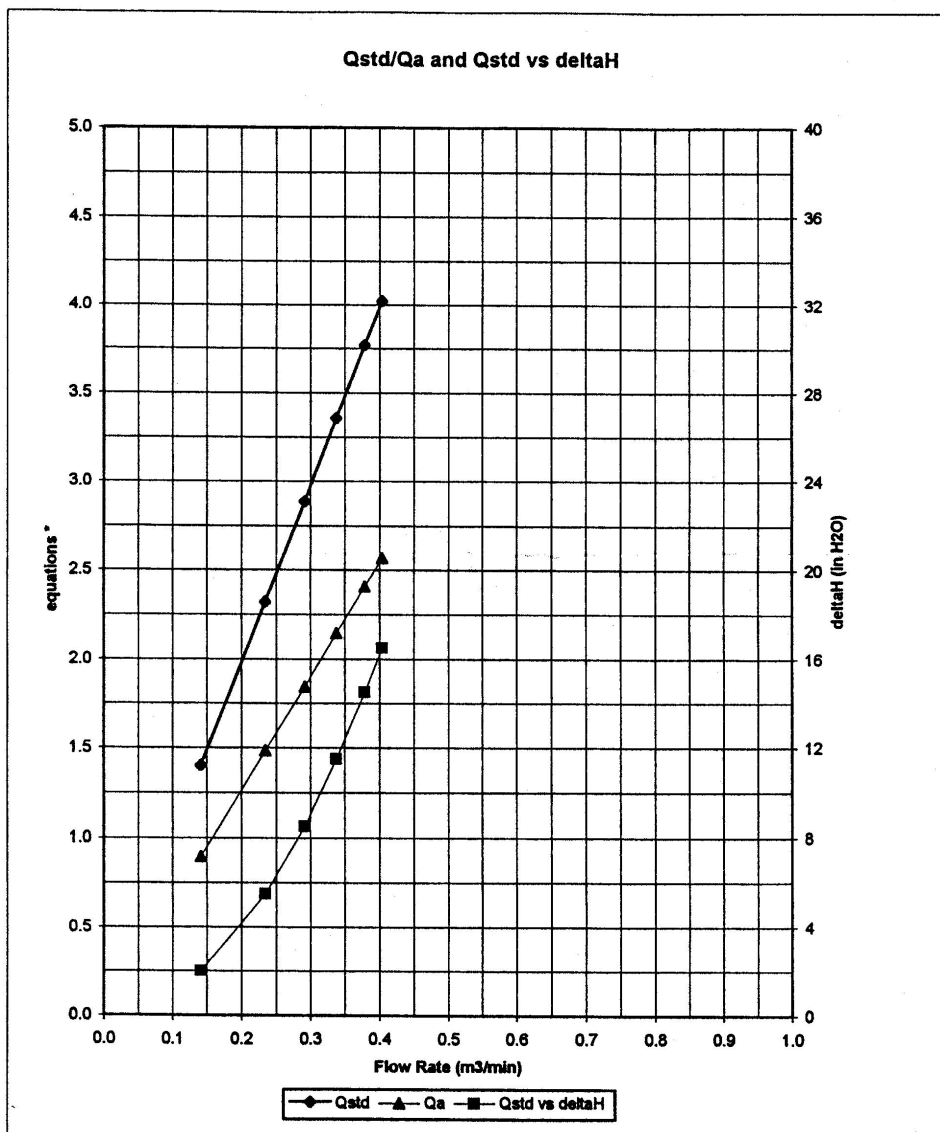
(A) Manometer deflection read in inches water: in. Hg. = in. H₂O/13.6
 (B) Stagnation Pressure (P₁) downstream of the filter. Re: Figure 3
 (C) Volumetric flow rates (Q₀) determined from prior orifice calibration using a Roots meter and corrected to appropriate (P₀, T₀) conditions. Re: Figure 4
 (D) Q̄₀: Q₀ based upon T̄₀, P̄₀ (average conditions) for atmospheric temperature and pressure, respectively.
 (E) Critical Flow Device* design flow rate condition: one microquartz filter in place and no other upstream obstructions.

*U.S. Patent No. 4,649,760

Figure E.2 Calibration Worksheet



AIR POLLUTION MONITORING EQUIPMENT



* y-axis equations:

Qstd series:
$$\sqrt{\Delta H \left(\frac{P_a}{P_{std}} \right) \left(\frac{T_{std}}{T_a} \right)}$$

Qa series:
$$\sqrt{(\Delta H (T_a / P_a))}$$

#5290

Figure E.3 Air Pollution Monitoring Equipment Graph

PROJECT NAME Calibration of Hi-vol Samplers NOTEBOOK NO. _____

Started 05-12-2010

Ambient Atm. measured in our lab is
 Ambient temperature in lab is 70.5°F or 21.38°C or $T_a = 294.54$ K

923 mbar or 92,300 Pa; 692.3 mmHg

Calibration kit is orifice transfer standard Model G28A SN: 2191

Q_{std} $m = 1.5710$ Q_A $m = 0.9840$
 $b = -0.023585$ $b = -0.015030$
 $c = 0.999986$ $c = 0.999980$

Sampler "A"

Run	ΔH_2O (in H_2O)	Stag Part mm H_2O mmHg	Q_a orifice	X-axis	Y-axis
1	2.26	3.85 7.19	1.0117	0.05895	0.98962
2	2.08	5.35 9.58	0.97127	0.05659	0.98557
3	1.96	7.50 14.00	0.94329	0.054963	0.97978
4	1.63	12.35 23.05	0.86156	0.050247	0.96670
5	1.30	17.65 32.94	0.77106	0.044928	0.95242

$y = 2.7175x + 0.8304$
 $R^2 = 0.99688$ (okay)

Equations used: $Q_a = \frac{\sqrt{(\Delta H_2O \cdot T_a)}}{Pa} - b$ $\therefore X = \frac{Q_a}{\sqrt{T_a}}$

$y = P_{std} = \frac{Pa - \Delta P_{std}}{Pa}$

Actual is $Q_{actual} = \frac{(P_{std} - b) \sqrt{T_a}}{m}$

Sampler "B"

Run	ΔH_2O in H_2O	Stag Part mm H_2O mmHg	Q_a	X-axis	Y-axis
1	3.50	6.05 11.29	1.255	0.0771	0.9836
2	3.41	8.50 15.80	1.239	0.0722	0.97708
3	3.32	13.50 20.10	1.223	0.0712	0.970686
4	3.15	14.50 27.02	1.191	0.0694	0.9601
5	3.00	19.25 35.93	1.163	0.0678	0.9481

$y = 0.5203x - 0.5061$
 $R^2 = 0.99867$

SIGNATURE _____ DATE _____ 20
 READ AND UNDERSTOOD _____ DATE _____ 20

Figure E.4 Calibration of Hi-vol Samples Hand Calculations

2 PROJECT NAME Calibration of Hi-vol Samplers NOTEBOOK NO.

Sampler "C"

Run	ΔH_{20}	Stag Port in H ₂ O	in Hg	Q _a	X axis	Y axis
1	3.53	6.05	11.29	1.261	0.0734	0.9837
2	3.44	7.95	14.44	1.245	0.0725	0.9786
3	3.34	9.20	17.17	1.226	0.0714	0.9752
4	3.20	10.00	19.78	1.219	0.0710	0.9714
5	2.77	14.10	25.05	1.120	0.0652	0.9485

$Y = 4.2455x + 0.6711$
 $R^2 = 0.99601$

Handcalc - example

$$Q_a \text{ (actual)} = \frac{\sqrt{(\Delta H_{20}) T_c / \rho_a} - b}{m}$$

$$Q_a = \frac{\sqrt{3.53(\text{in H}_2\text{O}) \cdot 294.54 \text{ K}} - (-0.015033)}{\frac{692.3 \text{ mmHg}}{0.9840}} = \frac{\sqrt{1.502} + 0.01503}{0.9840}$$

$$Q_a : 1.2607 \rightarrow \boxed{Q_a = 1.261 \text{ m}^3/\text{min}}$$

$$X = \frac{Q_a}{\sqrt{T_a}} = \frac{1.261}{\sqrt{294.54}} = \boxed{0.07348}$$

$$Y = P_{rat} = \frac{P_a - \Delta P_{20}}{P_a} = \frac{692.3 - 11.29}{692.3} = \boxed{0.98377}$$

PS

SIGNATURE _____ DATE _____ 2
 READ AND UNDERSTOOD _____ DATE _____ 2

Figure E.5 Calibration of Hi-vol Samplers Hand Calculations (cont.)

PROJECT NAME Test run of Hi-Vols NOTEBOOK NO. _____

05-14-2010 Performing a test run of Hi-vols to determine required run time (in the field). after 48 hrs in denator

Filter #	Weight (g)	Stand weight (g)	Total weight
Q0023531	4.4729	0.0000	4.4729
Q0023530	4.5163	0.0020	4.5604
Q0023529	4.5058	0.0000	4.5058
Q0023528	4.4791	0.0000	4.4791

Run times: Hi-vol B = 24 hrs → 4 hr chunks spread over 2 days
 Hi-vol C = 12 hrs → 6 hrs starting at 12 pm, 6 hrs starting at 12 AM
 ↳ expect a 0.065 g (not used)

Test run unit "B"

Filter tray B1
 location: MEC west side
 Temp: 68°F
 Δ initial Pressure: $(11.8 + 10.7) = 21.50$ in H₂O
 Filter # Q0023528
 Field blank filter # Q0023529
 Field blank filter tray - FB1

Approximate run times:

Monday	11:00 AM to 4:00 pm	(5 hrs)
	1:30 AM to 6:00 AM	(5 hrs)
Tuesday	10:00 AM to 3:00 pm	(5 hrs)
		15 hrs

Box output: $T = 68^\circ\text{F}$, 29.83 inHg, 1010 hPa
 inlet $Q = 1.231$ m³/min

Box Pressure: 30.09 inHg, 1017 hPa
 Box Temp: 53.1°F (284.87 K)
 Δ H₂O static head: 21.45

Q 0023528 = 4.5003 g
 Q 0023529 = 5.5051 g → F.B. = +/- 0.0007 g

SIGNATURE _____ DATE _____ 20
 READ AND UNDERSTOOD _____ DATE _____ 20

Figure E.6 Test Run of Hi-Vols Hand Calculations

4	PROJECT NAME	Particle Profiler Calibration	NOTEBOOK NO.
5-21-10	This project is to calibrate the particle profiler to a hi-vol sampler. Hi-vol's "B" & "C" will be used. The laser particle profiler will be referred to as LPP or Profiler.		
	Filter starting weights		
	#	(g)	
	Q0023517	= 4.4849	
	Q0023518	= 4.5173	
	Q0023519	= 4.4874	
	Q0023520	= 4.4914	
	Q0023521	= 4.5441	
	Q0023522	= 4.4808	
	Q0023523	= 4.4469	
	Q0023524	= 4.5342	
	Q0023525	= 4.4577	
5-21-10	2:40 pm	Temp = 72°F	
		Pressure = 29.74 in Hg, 1007 hPa, 755.40 mm Hg	
	Unit "C"	→ set to run ~ 40 hrs	
	Timer	= 933515	
	P _{sig}	= 21.0 in H ₂ O or 39.23 mm Hg	
	Filter #	= Q0023517	
	Plate #	= C1	
5-24-10	8 AM	Temp = 71°F	Pressure = 29.82 in Hg, 1009 hPa
	Timer	= 953463	ΔT = 20.168 min = 33.56 hrs
	P _{sig}	= 10.5 + 10.15 = 21.05 in H ₂ O or 39.3 mm Hg	
	Filter	= Q0023517, Plate C1	
	ending weight	= 4.4908 g	→ Avg Q ≈ 1.10 min, Cavg ≈ 2.15%
5-24-10	2nd set up	2 Hi-vol's & sampler	
	Pressure	= 29.89 in H ₂ O, 1012 hPa,	
	Temp	= 73°F	
	Unit C	Timer = 953732	
	P _{sig}	= 10.5 + 10.45 = 20.95 in H ₂ O	
	Filter #	= Q0023518	
	Plate #	= E1	
	Unit B	Timer = 362997	
	P _{sig}	= 10.10 + 10.10 = 21.2 in H ₂ O	
	Filter	= Q0023519	
	Plate	= F B1	
	SIGNATURE	_____	DATE _____ 20
	READ AND UNDERSTOOD	_____	DATE _____ 20

Figure E.7 Particular Profiler Calibration Hand Calculations

PROJECT NAME	Particle Profiler Calibration	NOTEBOOK NO.				
5-25-10 Env Run	Temp = 72°F					
	Pressure = 29.99 in Hg (1015 hPa)	762 mm Hg				
unit C	Timer = 96130.5 → Run time = 12.62 hrs					
	P _{std} = 10.5 + 10.5 = 21.0 in H ₂ O, P _{std Avg} = 20.975					
	end Filter weight = 4.48830 g					
	Δ Filter weight = 0.00090 g	} C = 9.79 E-7 g/m ³				
	Q = 1.2188 m ³ /min					
unit B	Timer = 37108.6 → Run time = 808.9 min 13.48 hrs					
	P _{std} = 10.6 + 10.65 = 21.25 in H ₂ O					
	end Filter weight = 4.51990 g	P _{std Avg} = 21.225				
	Δ Filter weight = 0.00260 g	} C = 2.62 E-6 g/m ³				
	Q = 1.22642 m ³ /min					
concentrations	<table border="1"> <tr> <td>"C" = 0.98 E-6 g/m³</td> <td rowspan="3">} Run 1</td> </tr> <tr> <td>"B" = 2.62 E-6 g/m³</td> </tr> <tr> <td>CFE = 0.92714 E-6 g/m³</td> </tr> </table>		"C" = 0.98 E-6 g/m ³	} Run 1	"B" = 2.62 E-6 g/m ³	CFE = 0.92714 E-6 g/m ³
"C" = 0.98 E-6 g/m ³	} Run 1					
"B" = 2.62 E-6 g/m ³						
CFE = 0.92714 E-6 g/m ³						
Run 25	Temp 72°F					
	Pressure 29.99 in Hg, 762 mm Hg					
unit C	Timer = 96132.9	end weight				
	P _{std} = 10.5 + 10.4 = 20.90 in H ₂ O	4.41978 g				
	Filter # = Q0023520					
	run time = 96895.9, 763 min					
	Δ Filter weight = 0.00280	} C = 3.137 E-6 g/m ³				
	Q = 1.17 m ³ /min					
unit B	Timer = 37116.7					
	P _{std} = 10.4 + 10.5 = 20.90 in H ₂ O	end weight				
	Filter # = Q0023522	4.4835 g				
	run time = 37919.7, 809 min					
	Δ Filter weight = 0.60270	} C = 2.78 E-6 g/m ³				
	Q = 1.20 m ³ /min					
Env	Temp = 74°					
Env	Pressure = 29.89 in Hg, 757.07 mm Hg					
concentrations	<table border="1"> <tr> <td>"C" = 3.14 g/m³</td> <td rowspan="3">}</td> </tr> <tr> <td>"B" = 2.78 g/m³</td> </tr> <tr> <td>CFE = 3.27 g/m³</td> </tr> </table>		"C" = 3.14 g/m ³	}	"B" = 2.78 g/m ³	CFE = 3.27 g/m ³
"C" = 3.14 g/m ³	}					
"B" = 2.78 g/m ³						
CFE = 3.27 g/m ³						
SIGNATURE _____	DATE _____	20				
READ AND UNDERSTOOD _____	DATE _____	20				

Figure E.8 Particular Profiler Calibration Hand Calculations (cont.)

6 PROJECT NAME _____ NOTEBOOK NO _____

Run 3: Temp 73°F
 Pressure: 29.82 in Hg
 96898.5
 unit C: Timer 37921.7, end Timer = 98499.5 $\Delta T = 16010$ min
 Filter Q 0023523
 Psta 10.7 + 10.45 = 20.75 in H₂O, 20.8 in H₂O
 End Filter weight = 4.4530 g
 Filter weight = 0.0060 g
 Psta end = 20.8 in H₂O
 37921.7 $Q = 1.1242$ m³/min

unit B: Timer ~~96898.5~~, end timer = 39547.3 $\Delta T = 1625.6$ min
 Filter Q 0023521
 Psta 10.5 + 11.0 = 21.0 in H₂O, 21.4 in H₂O
 End Filter weight = 4.5498 g
 Filter weight = 0.0058 g
 Psta end = 21.4 in H₂O
 Q = 1.1622 m³/min

END Temp: 72°F $T_{avg} = 72.5^\circ\text{F}, 295.65\text{ K}$
 END Pressure: 29.87 in Hg $P_{avg} = 29.85$ in Hg, 758 mmHg

unit C = 3.39 pp/m³
 unit B = 3.67 pp/m³
 LPC = 0.929

note LPC dust counting on 5-31-2010 @ 14:33

Run 4: Temp start = 72°F $T_{end} = 72^\circ\text{F}$ $T_{avg} = 72^\circ\text{F}$
 Pstart = 29.85 in Hg, P end = 29.92 in Hg $P_{avg} =$

unit B: Timer: 39547.3, end: 43212.7, $\Delta T = 3665.4$ min
 Psta start = 20.90 in H₂O
 Psta end = 21.10 in H₂O
 Filter Q 0023525
 Filter end weight = 4.4693 g $\Delta W = 0.0116$
 Q = 1.165 m³/min

unit C: Timer 98499.5, end timer = 02137.4, $\Delta T = 3637.8$ min
 Psta start = 21.25 in H₂O,
 Psta end = 21.30 in H₂O

SIGNATURE _____ DATE _____
 READ AND UNDERSTOOD _____ DATE _____

Figure E.9 Particular Profiler Calibration Hand Calculations (cont.)

PROJECT NAME	NOTEBOOK NO
unit "C" combined Filter # = Q0023624	
Filter end weight = 4.5462g	$\Delta W = 0.012g$
$Q = 1.12 \text{ m}^3/\text{min}$	
unit C = $3.53 \text{ E-}8 \text{ g/m}^3$	
unit B = $2.72 \text{ E-}6 \text{ g/m}^3$	
CPC =	
SIGNATURE _____ DATE _____ 20____	
READ AND UNDERSTOOD _____ DATE _____ 20____	

Figure E.10 Particular Profiler Calibration Hand Calculations (cont.)

APPENDIX F

Kernel Functions

BEN SEELY	KERNEL FUNCTIONS	11/19/10																																				
<p>KERNEL Function calculations</p> <p>taken from Dong et al., 2004, Marjamäki et al., 2005, and Szymanski et al., 2006 Wethington and Hornbuckle 2005.</p> $E_{i,j} = \left[1 + \left(\frac{(D_{50})_i}{D_{p,j}} \right)^{2B_i} \right]^{-1} \quad \text{for } i = 1, \dots, N \text{ and } j = 1, \dots, M$ <p>$(D_{50})_i$ = cut off diameter @ 50% efficiency on stage i.</p> <p>B_i = Steepness value for stage i.</p>																																						
<table border="1"> <thead> <tr> <th>STAGE i:</th> <th>$(D_{50})_i$ [μm]</th> <th>B_i [$\frac{\mu\text{m}}{\mu\text{m}}$]</th> </tr> </thead> <tbody> <tr><td>1</td><td>0.30</td><td>1.50</td></tr> <tr><td>2</td><td>0.53</td><td>1.30</td></tr> <tr><td>3</td><td>0.94</td><td>1.11</td></tr> <tr><td>4</td><td>1.7</td><td>1.10</td></tr> <tr><td>5</td><td>2.8</td><td>1.10</td></tr> <tr><td>6</td><td>4.8</td><td>1.05</td></tr> <tr><td>7</td><td>8</td><td>1.06</td></tr> <tr><td>8</td><td>12</td><td>1.06</td></tr> <tr><td>9</td><td>20</td><td>1.06</td></tr> <tr><td>10</td><td>32</td><td>1.16</td></tr> <tr><td>entrance</td><td>NA</td><td>NA</td></tr> </tbody> </table>			STAGE i :	$(D_{50})_i$ [μm]	B_i [$\frac{\mu\text{m}}{\mu\text{m}}$]	1	0.30	1.50	2	0.53	1.30	3	0.94	1.11	4	1.7	1.10	5	2.8	1.10	6	4.8	1.05	7	8	1.06	8	12	1.06	9	20	1.06	10	32	1.16	entrance	NA	NA
STAGE i :	$(D_{50})_i$ [μm]	B_i [$\frac{\mu\text{m}}{\mu\text{m}}$]																																				
1	0.30	1.50																																				
2	0.53	1.30																																				
3	0.94	1.11																																				
4	1.7	1.10																																				
5	2.8	1.10																																				
6	4.8	1.05																																				
7	8	1.06																																				
8	12	1.06																																				
9	20	1.06																																				
10	32	1.16																																				
entrance	NA	NA																																				
$K_{i,j} = E_{i,j} [1 - E_{i+1,j}] \dots [1 - E_{N,j}] \quad \text{for } i = 1 \text{ to } N-1 \text{ and } j = 1 \text{ to } M$ $K_{N,j} = E_{N,j} \quad \text{for } i = N \text{ and } j = 1 \text{ to } M.$																																						

Figure F.1 Kernel Function Hand Calculations

BEN SEELY	Kernel Functions	11/19/16
<p>Example Kernel functions</p> $E_{1,j} = \left[1 + \left(\frac{0.30 \mu\text{m}}{D_{p,j}} \right)^{2(1.50)} \right]^{-1} = \left[1 + \left(\frac{0.30}{D_{p,j}} \right)^3 \right]^{-1}$ $E_{2,j} = \left[1 + \left(\frac{0.53 \mu\text{m}}{D_{p,j}} \right)^{2(1.30)} \right]^{-1} = \left[1 + \left(\frac{0.53}{D_{p,j}} \right)^{2.6} \right]^{-1}$		

Figure F.2 Kernel Function Hand Calculations (cont.)

Table F.2 Kernel Function Results (cont.)

M(j)	N (i)										
	0.06	0.10	0.17	0.30	0.54	0.95	1.73	3.09	6.15	9.83	18.10
0.39	0.00	0.00	0.05	0.95	0.01	0.00	0.00	0.00	0.00	0.00	0.00
0.40	0.00	0.00	0.03	0.96	0.01	0.00	0.00	0.00	0.00	0.00	0.00
0.41	0.00	0.00	0.03	0.96	0.01	0.00	0.00	0.00	0.00	0.00	0.00
0.42	0.00	0.00	0.02	0.96	0.02	0.00	0.00	0.00	0.00	0.00	0.00
0.43	0.00	0.00	0.02	0.96	0.03	0.00	0.00	0.00	0.00	0.00	0.00
0.44	0.00	0.00	0.01	0.95	0.04	0.00	0.00	0.00	0.00	0.00	0.00
0.45	0.00	0.00	0.01	0.94	0.05	0.00	0.00	0.00	0.00	0.00	0.00
0.46	0.00	0.00	0.01	0.92	0.07	0.00	0.00	0.00	0.00	0.00	0.00
0.47	0.00	0.00	0.01	0.90	0.09	0.00	0.00	0.00	0.00	0.00	0.00
0.48	0.00	0.00	0.00	0.87	0.13	0.00	0.00	0.00	0.00	0.00	0.00
0.49	0.00	0.00	0.00	0.83	0.17	0.00	0.00	0.00	0.00	0.00	0.00
0.50	0.00	0.00	0.00	0.78	0.21	0.00	0.00	0.00	0.00	0.00	0.00
0.51	0.00	0.00	0.00	0.73	0.27	0.00	0.00	0.00	0.00	0.00	0.00
0.52	0.00	0.00	0.00	0.66	0.34	0.00	0.00	0.00	0.00	0.00	0.00
0.53	0.00	0.00	0.00	0.59	0.40	0.00	0.00	0.00	0.00	0.00	0.00
0.54	0.00	0.00	0.00	0.52	0.48	0.00	0.00	0.00	0.00	0.00	0.00
0.55	0.00	0.00	0.00	0.45	0.55	0.00	0.00	0.00	0.00	0.00	0.00
0.56	0.00	0.00	0.00	0.38	0.62	0.00	0.00	0.00	0.00	0.00	0.00
0.57	0.00	0.00	0.00	0.32	0.68	0.00	0.00	0.00	0.00	0.00	0.00
0.58	0.00	0.00	0.00	0.26	0.74	0.00	0.00	0.00	0.00	0.00	0.00
0.59	0.00	0.00	0.00	0.22	0.78	0.00	0.00	0.00	0.00	0.00	0.00
0.60	0.00	0.00	0.00	0.17	0.83	0.00	0.00	0.00	0.00	0.00	0.00
0.61	0.00	0.00	0.00	0.14	0.86	0.00	0.00	0.00	0.00	0.00	0.00
0.62	0.00	0.00	0.00	0.11	0.89	0.00	0.00	0.00	0.00	0.00	0.00
0.63	0.00	0.00	0.00	0.09	0.91	0.00	0.00	0.00	0.00	0.00	0.00
0.64	0.00	0.00	0.00	0.07	0.93	0.00	0.00	0.00	0.00	0.00	0.00
0.65	0.00	0.00	0.00	0.06	0.94	0.00	0.00	0.00	0.00	0.00	0.00
0.66	0.00	0.00	0.00	0.05	0.95	0.00	0.00	0.00	0.00	0.00	0.00
0.67	0.00	0.00	0.00	0.04	0.96	0.00	0.00	0.00	0.00	0.00	0.00
0.68	0.00	0.00	0.00	0.03	0.97	0.00	0.00	0.00	0.00	0.00	0.00
0.69	0.00	0.00	0.00	0.02	0.97	0.00	0.00	0.00	0.00	0.00	0.00
0.70	0.00	0.00	0.00	0.02	0.98	0.00	0.00	0.00	0.00	0.00	0.00
0.71	0.00	0.00	0.00	0.01	0.98	0.00	0.00	0.00	0.00	0.00	0.00
0.72	0.00	0.00	0.00	0.01	0.98	0.00	0.00	0.00	0.00	0.00	0.00
0.73	0.00	0.00	0.00	0.01	0.98	0.01	0.00	0.00	0.00	0.00	0.00
0.74	0.00	0.00	0.00	0.01	0.98	0.01	0.00	0.00	0.00	0.00	0.00
0.75	0.00	0.00	0.00	0.01	0.98	0.01	0.00	0.00	0.00	0.00	0.00
0.76	0.00	0.00	0.00	0.01	0.98	0.01	0.00	0.00	0.00	0.00	0.00
0.77	0.00	0.00	0.00	0.00	0.98	0.02	0.00	0.00	0.00	0.00	0.00
0.78	0.00	0.00	0.00	0.00	0.97	0.02	0.00	0.00	0.00	0.00	0.00
0.79	0.00	0.00	0.00	0.00	0.97	0.03	0.00	0.00	0.00	0.00	0.00
0.80	0.00	0.00	0.00	0.00	0.96	0.04	0.00	0.00	0.00	0.00	0.00
0.81	0.00	0.00	0.00	0.00	0.95	0.04	0.00	0.00	0.00	0.00	0.00
0.82	0.00	0.00	0.00	0.00	0.94	0.06	0.00	0.00	0.00	0.00	0.00
0.83	0.00	0.00	0.00	0.00	0.93	0.07	0.00	0.00	0.00	0.00	0.00
0.84	0.00	0.00	0.00	0.00	0.91	0.08	0.00	0.00	0.00	0.00	0.00
0.85	0.00	0.00	0.00	0.00	0.90	0.10	0.00	0.00	0.00	0.00	0.00

Table F.3 Kernel Function Results (cont.)

0.86	0.00	0.00	0.00	0.00	0.87	0.13	0.00	0.00	0.00	0.00	0.00
M(j)	N (i)										
	0.06	0.10	0.17	0.30	0.54	0.95	1.73	3.09	6.15	9.83	18.10
0.87	0.00	0.00	0.00	0.00	0.85	0.15	0.00	0.00	0.00	0.00	0.00
0.88	0.00	0.00	0.00	0.00	0.82	0.18	0.00	0.00	0.00	0.00	0.00
0.89	0.00	0.00	0.00	0.00	0.78	0.22	0.00	0.00	0.00	0.00	0.00
0.90	0.00	0.00	0.00	0.00	0.74	0.26	0.00	0.00	0.00	0.00	0.00
0.91	0.00	0.00	0.00	0.00	0.70	0.30	0.00	0.00	0.00	0.00	0.00
0.92	0.00	0.00	0.00	0.00	0.66	0.34	0.00	0.00	0.00	0.00	0.00
0.93	0.00	0.00	0.00	0.00	0.61	0.39	0.00	0.00	0.00	0.00	0.00
0.94	0.00	0.00	0.00	0.00	0.56	0.44	0.00	0.00	0.00	0.00	0.00
0.95	0.00	0.00	0.00	0.00	0.51	0.49	0.00	0.00	0.00	0.00	0.00
0.96	0.00	0.00	0.00	0.00	0.46	0.54	0.00	0.00	0.00	0.00	0.00
0.97	0.00	0.00	0.00	0.00	0.41	0.59	0.00	0.00	0.00	0.00	0.00
0.98	0.00	0.00	0.00	0.00	0.36	0.64	0.00	0.00	0.00	0.00	0.00
0.99	0.00	0.00	0.00	0.00	0.32	0.68	0.00	0.00	0.00	0.00	0.00
1.00	0.00	0.00	0.00	0.00	0.28	0.72	0.00	0.00	0.00	0.00	0.00
1.01	0.00	0.00	0.00	0.00	0.24	0.76	0.00	0.00	0.00	0.00	0.00
1.02	0.00	0.00	0.00	0.00	0.21	0.79	0.00	0.00	0.00	0.00	0.00
1.03	0.00	0.00	0.00	0.00	0.18	0.82	0.00	0.00	0.00	0.00	0.00
1.04	0.00	0.00	0.00	0.00	0.15	0.85	0.00	0.00	0.00	0.00	0.00
1.05	0.00	0.00	0.00	0.00	0.13	0.87	0.00	0.00	0.00	0.00	0.00
1.06	0.00	0.00	0.00	0.00	0.11	0.89	0.00	0.00	0.00	0.00	0.00
1.07	0.00	0.00	0.00	0.00	0.10	0.90	0.00	0.00	0.00	0.00	0.00
1.08	0.00	0.00	0.00	0.00	0.08	0.92	0.00	0.00	0.00	0.00	0.00
1.09	0.00	0.00	0.00	0.00	0.07	0.93	0.00	0.00	0.00	0.00	0.00
1.10	0.00	0.00	0.00	0.00	0.06	0.94	0.00	0.00	0.00	0.00	0.00
1.11	0.00	0.00	0.00	0.00	0.05	0.95	0.00	0.00	0.00	0.00	0.00
1.12	0.00	0.00	0.00	0.00	0.04	0.96	0.00	0.00	0.00	0.00	0.00
1.13	0.00	0.00	0.00	0.00	0.04	0.96	0.00	0.00	0.00	0.00	0.00
1.14	0.00	0.00	0.00	0.00	0.03	0.97	0.00	0.00	0.00	0.00	0.00
1.15	0.00	0.00	0.00	0.00	0.03	0.97	0.00	0.00	0.00	0.00	0.00
1.16	0.00	0.00	0.00	0.00	0.02	0.98	0.00	0.00	0.00	0.00	0.00
1.17	0.00	0.00	0.00	0.00	0.02	0.98	0.00	0.00	0.00	0.00	0.00
1.18	0.00	0.00	0.00	0.00	0.02	0.98	0.00	0.00	0.00	0.00	0.00
1.19	0.00	0.00	0.00	0.00	0.01	0.99	0.00	0.00	0.00	0.00	0.00
1.20	0.00	0.00	0.00	0.00	0.01	0.99	0.00	0.00	0.00	0.00	0.00
1.21	0.00	0.00	0.00	0.00	0.01	0.99	0.00	0.00	0.00	0.00	0.00
1.22	0.00	0.00	0.00	0.00	0.01	0.99	0.00	0.00	0.00	0.00	0.00
1.23	0.00	0.00	0.00	0.00	0.01	0.99	0.00	0.00	0.00	0.00	0.00
1.24	0.00	0.00	0.00	0.00	0.01	0.99	0.00	0.00	0.00	0.00	0.00
1.25	0.00	0.00	0.00	0.00	0.01	0.99	0.00	0.00	0.00	0.00	0.00
1.26	0.00	0.00	0.00	0.00	0.00	0.99	0.00	0.00	0.00	0.00	0.00
1.27	0.00	0.00	0.00	0.00	0.00	0.99	0.00	0.00	0.00	0.00	0.00
1.28	0.00	0.00	0.00	0.00	0.00	0.99	0.00	0.00	0.00	0.00	0.00
1.29	0.00	0.00	0.00	0.00	0.00	0.99	0.00	0.00	0.00	0.00	0.00
1.30	0.00	0.00	0.00	0.00	0.00	0.99	0.00	0.00	0.00	0.00	0.00
1.31	0.00	0.00	0.00	0.00	0.00	0.99	0.00	0.00	0.00	0.00	0.00
1.32	0.00	0.00	0.00	0.00	0.00	0.99	0.00	0.00	0.00	0.00	0.00
1.33	0.00	0.00	0.00	0.00	0.00	0.99	0.00	0.00	0.00	0.00	0.00

Table F.4 Kernel Function Results (cont.)

1.34	0.00	0.00	0.00	0.00	0.00	0.99	0.01	0.00	0.00	0.00	0.00
M(j)	N (i)										
	0.06	0.10	0.17	0.30	0.54	0.95	1.73	3.09	6.15	9.83	18.10
1.35	0.00	0.00	0.00	0.00	0.00	0.99	0.01	0.00	0.00	0.00	0.00
1.36	0.00	0.00	0.00	0.00	0.00	0.99	0.01	0.00	0.00	0.00	0.00
1.37	0.00	0.00	0.00	0.00	0.00	0.99	0.01	0.00	0.00	0.00	0.00
1.38	0.00	0.00	0.00	0.00	0.00	0.99	0.01	0.00	0.00	0.00	0.00
1.39	0.00	0.00	0.00	0.00	0.00	0.99	0.01	0.00	0.00	0.00	0.00
1.40	0.00	0.00	0.00	0.00	0.00	0.99	0.01	0.00	0.00	0.00	0.00
1.41	0.00	0.00	0.00	0.00	0.00	0.98	0.02	0.00	0.00	0.00	0.00
1.42	0.00	0.00	0.00	0.00	0.00	0.98	0.02	0.00	0.00	0.00	0.00
1.43	0.00	0.00	0.00	0.00	0.00	0.98	0.02	0.00	0.00	0.00	0.00
1.44	0.00	0.00	0.00	0.00	0.00	0.98	0.02	0.00	0.00	0.00	0.00
1.45	0.00	0.00	0.00	0.00	0.00	0.97	0.03	0.00	0.00	0.00	0.00
1.46	0.00	0.00	0.00	0.00	0.00	0.97	0.03	0.00	0.00	0.00	0.00
1.47	0.00	0.00	0.00	0.00	0.00	0.96	0.04	0.00	0.00	0.00	0.00
1.48	0.00	0.00	0.00	0.00	0.00	0.96	0.04	0.00	0.00	0.00	0.00
1.49	0.00	0.00	0.00	0.00	0.00	0.95	0.05	0.00	0.00	0.00	0.00
1.50	0.00	0.00	0.00	0.00	0.00	0.95	0.05	0.00	0.00	0.00	0.00
1.51	0.00	0.00	0.00	0.00	0.00	0.94	0.06	0.00	0.00	0.00	0.00
1.52	0.00	0.00	0.00	0.00	0.00	0.93	0.07	0.00	0.00	0.00	0.00
1.53	0.00	0.00	0.00	0.00	0.00	0.92	0.08	0.00	0.00	0.00	0.00
1.54	0.00	0.00	0.00	0.00	0.00	0.92	0.08	0.00	0.00	0.00	0.00
1.55	0.00	0.00	0.00	0.00	0.00	0.90	0.10	0.00	0.00	0.00	0.00
1.56	0.00	0.00	0.00	0.00	0.00	0.89	0.11	0.00	0.00	0.00	0.00
1.57	0.00	0.00	0.00	0.00	0.00	0.88	0.12	0.00	0.00	0.00	0.00
1.58	0.00	0.00	0.00	0.00	0.00	0.87	0.13	0.00	0.00	0.00	0.00
1.59	0.00	0.00	0.00	0.00	0.00	0.85	0.15	0.00	0.00	0.00	0.00
1.60	0.00	0.00	0.00	0.00	0.00	0.83	0.17	0.00	0.00	0.00	0.00
1.61	0.00	0.00	0.00	0.00	0.00	0.82	0.18	0.00	0.00	0.00	0.00
1.62	0.00	0.00	0.00	0.00	0.00	0.80	0.20	0.00	0.00	0.00	0.00
1.63	0.00	0.00	0.00	0.00	0.00	0.77	0.23	0.00	0.00	0.00	0.00
1.64	0.00	0.00	0.00	0.00	0.00	0.75	0.25	0.00	0.00	0.00	0.00
1.65	0.00	0.00	0.00	0.00	0.00	0.73	0.27	0.00	0.00	0.00	0.00
1.66	0.00	0.00	0.00	0.00	0.00	0.70	0.30	0.00	0.00	0.00	0.00
1.67	0.00	0.00	0.00	0.00	0.00	0.68	0.32	0.00	0.00	0.00	0.00
1.68	0.00	0.00	0.00	0.00	0.00	0.65	0.35	0.00	0.00	0.00	0.00
1.69	0.00	0.00	0.00	0.00	0.00	0.62	0.38	0.00	0.00	0.00	0.00
1.70	0.00	0.00	0.00	0.00	0.00	0.60	0.40	0.00	0.00	0.00	0.00
1.71	0.00	0.00	0.00	0.00	0.00	0.57	0.43	0.00	0.00	0.00	0.00
1.72	0.00	0.00	0.00	0.00	0.00	0.54	0.46	0.00	0.00	0.00	0.00
1.73	0.00	0.00	0.00	0.00	0.00	0.51	0.49	0.00	0.00	0.00	0.00
1.74	0.00	0.00	0.00	0.00	0.00	0.48	0.52	0.00	0.00	0.00	0.00
1.75	0.00	0.00	0.00	0.00	0.00	0.45	0.55	0.00	0.00	0.00	0.00
1.76	0.00	0.00	0.00	0.00	0.00	0.42	0.58	0.00	0.00	0.00	0.00
1.77	0.00	0.00	0.00	0.00	0.00	0.40	0.60	0.00	0.00	0.00	0.00
1.78	0.00	0.00	0.00	0.00	0.00	0.37	0.63	0.00	0.00	0.00	0.00
1.79	0.00	0.00	0.00	0.00	0.00	0.34	0.66	0.00	0.00	0.00	0.00
1.80	0.00	0.00	0.00	0.00	0.00	0.32	0.68	0.00	0.00	0.00	0.00
1.81	0.00	0.00	0.00	0.00	0.00	0.29	0.71	0.00	0.00	0.00	0.00

Table F.5 Kernel Function Results (cont.)

1.82	0.00	0.00	0.00	0.00	0.00	0.27	0.73	0.00	0.00	0.00	0.00
M(j)	N (i)										
	0.06	0.10	0.17	0.30	0.54	0.95	1.73	3.09	6.15	9.83	18.10
1.83	0.00	0.00	0.00	0.00	0.00	0.25	0.75	0.00	0.00	0.00	0.00
1.84	0.00	0.00	0.00	0.00	0.00	0.23	0.77	0.00	0.00	0.00	0.00
1.85	0.00	0.00	0.00	0.00	0.00	0.21	0.79	0.00	0.00	0.00	0.00
1.86	0.00	0.00	0.00	0.00	0.00	0.19	0.81	0.00	0.00	0.00	0.00
1.87	0.00	0.00	0.00	0.00	0.00	0.18	0.82	0.00	0.00	0.00	0.00
1.88	0.00	0.00	0.00	0.00	0.00	0.16	0.84	0.00	0.00	0.00	0.00
1.89	0.00	0.00	0.00	0.00	0.00	0.15	0.85	0.00	0.00	0.00	0.00
1.90	0.00	0.00	0.00	0.00	0.00	0.14	0.86	0.00	0.00	0.00	0.00
1.91	0.00	0.00	0.00	0.00	0.00	0.12	0.88	0.00	0.00	0.00	0.00
1.92	0.00	0.00	0.00	0.00	0.00	0.11	0.89	0.00	0.00	0.00	0.00
1.93	0.00	0.00	0.00	0.00	0.00	0.10	0.90	0.00	0.00	0.00	0.00
1.94	0.00	0.00	0.00	0.00	0.00	0.09	0.91	0.00	0.00	0.00	0.00
1.95	0.00	0.00	0.00	0.00	0.00	0.09	0.91	0.00	0.00	0.00	0.00
1.96	0.00	0.00	0.00	0.00	0.00	0.08	0.92	0.00	0.00	0.00	0.00
1.97	0.00	0.00	0.00	0.00	0.00	0.07	0.93	0.00	0.00	0.00	0.00
1.98	0.00	0.00	0.00	0.00	0.00	0.06	0.94	0.00	0.00	0.00	0.00
1.99	0.00	0.00	0.00	0.00	0.00	0.06	0.94	0.00	0.00	0.00	0.00
2.00	0.00	0.00	0.00	0.00	0.00	0.05	0.95	0.00	0.00	0.00	0.00
2.01	0.00	0.00	0.00	0.00	0.00	0.05	0.95	0.00	0.00	0.00	0.00
2.02	0.00	0.00	0.00	0.00	0.00	0.04	0.96	0.00	0.00	0.00	0.00
2.03	0.00	0.00	0.00	0.00	0.00	0.04	0.96	0.00	0.00	0.00	0.00
2.04	0.00	0.00	0.00	0.00	0.00	0.04	0.96	0.00	0.00	0.00	0.00
2.05	0.00	0.00	0.00	0.00	0.00	0.03	0.97	0.00	0.00	0.00	0.00
2.06	0.00	0.00	0.00	0.00	0.00	0.03	0.97	0.00	0.00	0.00	0.00
2.07	0.00	0.00	0.00	0.00	0.00	0.03	0.97	0.00	0.00	0.00	0.00
2.08	0.00	0.00	0.00	0.00	0.00	0.02	0.98	0.00	0.00	0.00	0.00
2.09	0.00	0.00	0.00	0.00	0.00	0.02	0.98	0.00	0.00	0.00	0.00
2.10	0.00	0.00	0.00	0.00	0.00	0.02	0.98	0.00	0.00	0.00	0.00
2.11	0.00	0.00	0.00	0.00	0.00	0.02	0.98	0.00	0.00	0.00	0.00
2.12	0.00	0.00	0.00	0.00	0.00	0.02	0.98	0.00	0.00	0.00	0.00
2.13	0.00	0.00	0.00	0.00	0.00	0.02	0.98	0.00	0.00	0.00	0.00
2.14	0.00	0.00	0.00	0.00	0.00	0.01	0.99	0.00	0.00	0.00	0.00
2.15	0.00	0.00	0.00	0.00	0.00	0.01	0.99	0.00	0.00	0.00	0.00
2.16	0.00	0.00	0.00	0.00	0.00	0.01	0.99	0.00	0.00	0.00	0.00
2.17	0.00	0.00	0.00	0.00	0.00	0.01	0.99	0.00	0.00	0.00	0.00
2.18	0.00	0.00	0.00	0.00	0.00	0.01	0.99	0.00	0.00	0.00	0.00
2.21	0.00	0.00	0.00	0.00	0.00	0.01	0.99	0.00	0.00	0.00	0.00
2.22	0.00	0.00	0.00	0.00	0.00	0.01	0.99	0.00	0.00	0.00	0.00
2.23	0.00	0.00	0.00	0.00	0.00	0.01	0.99	0.00	0.00	0.00	0.00
2.24	0.00	0.00	0.00	0.00	0.00	0.01	0.99	0.00	0.00	0.00	0.00
2.25	0.00	0.00	0.00	0.00	0.00	0.01	0.99	0.00	0.00	0.00	0.00
2.26	0.00	0.00	0.00	0.00	0.00	0.00	1.00	0.00	0.00	0.00	0.00
2.27	0.00	0.00	0.00	0.00	0.00	0.00	1.00	0.00	0.00	0.00	0.00
2.28	0.00	0.00	0.00	0.00	0.00	0.00	1.00	0.00	0.00	0.00	0.00
2.29	0.00	0.00	0.00	0.00	0.00	0.00	1.00	0.00	0.00	0.00	0.00
2.30	0.00	0.00	0.00	0.00	0.00	0.00	1.00	0.00	0.00	0.00	0.00
2.31	0.00	0.00	0.00	0.00	0.00	0.00	1.00	0.00	0.00	0.00	0.00

Table F.7 Kernel Function Results (cont.)

2.82	0.00	0.00	0.00	0.00	0.00	0.00	0.93	0.07	0.00	0.00	0.00
M(j)	N (i)										
	0.06	0.10	0.17	0.30	0.54	0.95	1.73	3.09	6.15	9.83	18.10
2.83	0.00	0.00	0.00	0.00	0.00	0.00	0.92	0.08	0.00	0.00	0.00
2.84	0.00	0.00	0.00	0.00	0.00	0.00	0.92	0.08	0.00	0.00	0.00
2.85	0.00	0.00	0.00	0.00	0.00	0.00	0.91	0.09	0.00	0.00	0.00
2.86	0.00	0.00	0.00	0.00	0.00	0.00	0.90	0.10	0.00	0.00	0.00
2.87	0.00	0.00	0.00	0.00	0.00	0.00	0.89	0.11	0.00	0.00	0.00
2.88	0.00	0.00	0.00	0.00	0.00	0.00	0.88	0.12	0.00	0.00	0.00
2.89	0.00	0.00	0.00	0.00	0.00	0.00	0.87	0.13	0.00	0.00	0.00
2.90	0.00	0.00	0.00	0.00	0.00	0.00	0.86	0.14	0.00	0.00	0.00
2.91	0.00	0.00	0.00	0.00	0.00	0.00	0.85	0.15	0.00	0.00	0.00
2.92	0.00	0.00	0.00	0.00	0.00	0.00	0.83	0.17	0.00	0.00	0.00
2.93	0.00	0.00	0.00	0.00	0.00	0.00	0.82	0.18	0.00	0.00	0.00
2.94	0.00	0.00	0.00	0.00	0.00	0.00	0.80	0.20	0.00	0.00	0.00
2.95	0.00	0.00	0.00	0.00	0.00	0.00	0.79	0.21	0.00	0.00	0.00
2.96	0.00	0.00	0.00	0.00	0.00	0.00	0.77	0.23	0.00	0.00	0.00
2.97	0.00	0.00	0.00	0.00	0.00	0.00	0.75	0.25	0.00	0.00	0.00
2.98	0.00	0.00	0.00	0.00	0.00	0.00	0.73	0.26	0.00	0.00	0.00
2.99	0.00	0.00	0.00	0.00	0.00	0.00	0.72	0.28	0.00	0.00	0.00
3.00	0.00	0.00	0.00	0.00	0.00	0.00	0.70	0.30	0.00	0.00	0.00
3.01	0.00	0.00	0.00	0.00	0.00	0.00	0.68	0.32	0.00	0.00	0.00
3.02	0.00	0.00	0.00	0.00	0.00	0.00	0.65	0.35	0.00	0.00	0.00
3.03	0.00	0.00	0.00	0.00	0.00	0.00	0.63	0.37	0.00	0.00	0.00
3.04	0.00	0.00	0.00	0.00	0.00	0.00	0.61	0.39	0.00	0.00	0.00
3.05	0.00	0.00	0.00	0.00	0.00	0.00	0.59	0.41	0.00	0.00	0.00
3.06	0.00	0.00	0.00	0.00	0.00	0.00	0.57	0.43	0.00	0.00	0.00
3.07	0.00	0.00	0.00	0.00	0.00	0.00	0.54	0.46	0.00	0.00	0.00
3.08	0.00	0.00	0.00	0.00	0.00	0.00	0.52	0.48	0.00	0.00	0.00
3.09	0.00	0.00	0.00	0.00	0.00	0.00	0.50	0.50	0.00	0.00	0.00
3.10	0.00	0.00	0.00	0.00	0.00	0.00	0.47	0.53	0.00	0.00	0.00
3.11	0.00	0.00	0.00	0.00	0.00	0.00	0.45	0.55	0.00	0.00	0.00
3.12	0.00	0.00	0.00	0.00	0.00	0.00	0.43	0.57	0.00	0.00	0.00
3.13	0.00	0.00	0.00	0.00	0.00	0.00	0.40	0.59	0.00	0.00	0.00
3.14	0.00	0.00	0.00	0.00	0.00	0.00	0.38	0.62	0.00	0.00	0.00
3.15	0.00	0.00	0.00	0.00	0.00	0.00	0.36	0.64	0.00	0.00	0.00
3.16	0.00	0.00	0.00	0.00	0.00	0.00	0.34	0.66	0.00	0.00	0.00
3.17	0.00	0.00	0.00	0.00	0.00	0.00	0.32	0.68	0.00	0.00	0.00
3.18	0.00	0.00	0.00	0.00	0.00	0.00	0.30	0.70	0.00	0.00	0.00
3.19	0.00	0.00	0.00	0.00	0.00	0.00	0.28	0.72	0.00	0.00	0.00
3.20	0.00	0.00	0.00	0.00	0.00	0.00	0.27	0.73	0.00	0.00	0.00
3.21	0.00	0.00	0.00	0.00	0.00	0.00	0.25	0.75	0.00	0.00	0.00
3.22	0.00	0.00	0.00	0.00	0.00	0.00	0.23	0.77	0.00	0.00	0.00
3.23	0.00	0.00	0.00	0.00	0.00	0.00	0.22	0.78	0.00	0.00	0.00
3.24	0.00	0.00	0.00	0.00	0.00	0.00	0.20	0.80	0.00	0.00	0.00
3.25	0.00	0.00	0.00	0.00	0.00	0.00	0.19	0.81	0.00	0.00	0.00
3.26	0.00	0.00	0.00	0.00	0.00	0.00	0.18	0.82	0.00	0.00	0.00
3.27	0.00	0.00	0.00	0.00	0.00	0.00	0.16	0.84	0.00	0.00	0.00
3.28	0.00	0.00	0.00	0.00	0.00	0.00	0.15	0.85	0.00	0.00	0.00
3.29	0.00	0.00	0.00	0.00	0.00	0.00	0.14	0.86	0.00	0.00	0.00

Table F.8 Kernel Function Results (cont.)

3.30	0.00	0.00	0.00	0.00	0.00	0.00	0.13	0.87	0.00	0.00	0.00
M(j)	N(i)										
	0.06	0.10	0.17	0.30	0.54	0.95	1.73	3.09	6.15	9.83	18.10
3.31	0.00	0.00	0.00	0.00	0.00	0.00	0.12	0.88	0.00	0.00	0.00
3.32	0.00	0.00	0.00	0.00	0.00	0.00	0.11	0.89	0.00	0.00	0.00
3.33	0.00	0.00	0.00	0.00	0.00	0.00	0.10	0.90	0.00	0.00	0.00
3.34	0.00	0.00	0.00	0.00	0.00	0.00	0.10	0.90	0.00	0.00	0.00
3.37	0.00	0.00	0.00	0.00	0.00	0.00	0.08	0.92	0.00	0.00	0.00
3.38	0.00	0.00	0.00	0.00	0.00	0.00	0.07	0.93	0.00	0.00	0.00
3.39	0.00	0.00	0.00	0.00	0.00	0.00	0.06	0.93	0.00	0.00	0.00
3.40	0.00	0.00	0.00	0.00	0.00	0.00	0.06	0.94	0.00	0.00	0.00
3.41	0.00	0.00	0.00	0.00	0.00	0.00	0.06	0.94	0.00	0.00	0.00
3.42	0.00	0.00	0.00	0.00	0.00	0.00	0.05	0.95	0.00	0.00	0.00
3.43	0.00	0.00	0.00	0.00	0.00	0.00	0.05	0.95	0.00	0.00	0.00
3.44	0.00	0.00	0.00	0.00	0.00	0.00	0.04	0.96	0.00	0.00	0.00
3.45	0.00	0.00	0.00	0.00	0.00	0.00	0.04	0.96	0.00	0.00	0.00
3.46	0.00	0.00	0.00	0.00	0.00	0.00	0.04	0.96	0.00	0.00	0.00
3.47	0.00	0.00	0.00	0.00	0.00	0.00	0.03	0.96	0.00	0.00	0.00
3.48	0.00	0.00	0.00	0.00	0.00	0.00	0.03	0.97	0.00	0.00	0.00
3.49	0.00	0.00	0.00	0.00	0.00	0.00	0.03	0.97	0.00	0.00	0.00
3.50	0.00	0.00	0.00	0.00	0.00	0.00	0.03	0.97	0.00	0.00	0.00
3.51	0.00	0.00	0.00	0.00	0.00	0.00	0.02	0.97	0.00	0.00	0.00
3.52	0.00	0.00	0.00	0.00	0.00	0.00	0.02	0.98	0.00	0.00	0.00
3.53	0.00	0.00	0.00	0.00	0.00	0.00	0.02	0.98	0.00	0.00	0.00
3.54	0.00	0.00	0.00	0.00	0.00	0.00	0.02	0.98	0.00	0.00	0.00
3.55	0.00	0.00	0.00	0.00	0.00	0.00	0.02	0.98	0.00	0.00	0.00
3.56	0.00	0.00	0.00	0.00	0.00	0.00	0.02	0.98	0.00	0.00	0.00
3.57	0.00	0.00	0.00	0.00	0.00	0.00	0.02	0.98	0.00	0.00	0.00
3.58	0.00	0.00	0.00	0.00	0.00	0.00	0.01	0.98	0.00	0.00	0.00
3.59	0.00	0.00	0.00	0.00	0.00	0.00	0.01	0.98	0.00	0.00	0.00
3.60	0.00	0.00	0.00	0.00	0.00	0.00	0.01	0.99	0.00	0.00	0.00
3.61	0.00	0.00	0.00	0.00	0.00	0.00	0.01	0.99	0.00	0.00	0.00
3.62	0.00	0.00	0.00	0.00	0.00	0.00	0.01	0.99	0.00	0.00	0.00
3.63	0.00	0.00	0.00	0.00	0.00	0.00	0.01	0.99	0.00	0.00	0.00
3.64	0.00	0.00	0.00	0.00	0.00	0.00	0.01	0.99	0.00	0.00	0.00
3.65	0.00	0.00	0.00	0.00	0.00	0.00	0.01	0.99	0.00	0.00	0.00
3.66	0.00	0.00	0.00	0.00	0.00	0.00	0.01	0.99	0.00	0.00	0.00
3.67	0.00	0.00	0.00	0.00	0.00	0.00	0.01	0.99	0.00	0.00	0.00
3.68	0.00	0.00	0.00	0.00	0.00	0.00	0.01	0.99	0.00	0.00	0.00
3.69	0.00	0.00	0.00	0.00	0.00	0.00	0.01	0.99	0.00	0.00	0.00
3.70	0.00	0.00	0.00	0.00	0.00	0.00	0.01	0.99	0.00	0.00	0.00
3.71	0.00	0.00	0.00	0.00	0.00	0.00	0.01	0.99	0.00	0.00	0.00
3.72	0.00	0.00	0.00	0.00	0.00	0.00	0.00	0.99	0.00	0.00	0.00
3.73	0.00	0.00	0.00	0.00	0.00	0.00	0.00	0.99	0.00	0.00	0.00
3.75	0.00	0.00	0.00	0.00	0.00	0.00	0.00	0.99	0.00	0.00	0.00
4.00	0.00	0.00	0.00	0.00	0.00	0.00	0.00	0.99	0.01	0.00	0.00
4.25	0.00	0.00	0.00	0.00	0.00	0.00	0.00	0.99	0.01	0.00	0.00
4.50	0.00	0.00	0.00	0.00	0.00	0.00	0.00	0.97	0.02	0.00	0.00
4.75	0.00	0.00	0.00	0.00	0.00	0.00	0.00	0.95	0.05	0.00	0.00
5.00	0.00	0.00	0.00	0.00	0.00	0.00	0.00	0.92	0.08	0.00	0.00

Table F.11 Kernel Function Results (cont.)

30.25	0.00	0.00	0.00	0.00	0.00	0.00	0.00	0.00	0.00	0.06	0.94
M(j)	N (i)										
	0.06	0.10	0.17	0.30	0.54	0.95	1.73	3.09	6.15	9.83	18.10
30.50	0.00	0.00	0.00	0.00	0.00	0.00	0.00	0.00	0.00	0.05	0.95
30.75	0.00	0.00	0.00	0.00	0.00	0.00	0.00	0.00	0.00	0.05	0.95
31.00	0.00	0.00	0.00	0.00	0.00	0.00	0.00	0.00	0.00	0.05	0.95
31.25	0.00	0.00	0.00	0.00	0.00	0.00	0.00	0.00	0.00	0.05	0.95
31.50	0.00	0.00	0.00	0.00	0.00	0.00	0.00	0.00	0.00	0.05	0.95
31.75	0.00	0.00	0.00	0.00	0.00	0.00	0.00	0.00	0.00	0.04	0.96
32.00	0.00	0.00	0.00	0.00	0.00	0.00	0.00	0.00	0.00	0.04	0.96
32.25	0.00	0.00	0.00	0.00	0.00	0.00	0.00	0.00	0.00	0.04	0.96
32.50	0.00	0.00	0.00	0.00	0.00	0.00	0.00	0.00	0.00	0.04	0.96
32.75	0.00	0.00	0.00	0.00	0.00	0.00	0.00	0.00	0.00	0.04	0.96
33.00	0.00	0.00	0.00	0.00	0.00	0.00	0.00	0.00	0.00	0.04	0.96
33.25	0.00	0.00	0.00	0.00	0.00	0.00	0.00	0.00	0.00	0.03	0.97
33.50	0.00	0.00	0.00	0.00	0.00	0.00	0.00	0.00	0.00	0.03	0.97
33.75	0.00	0.00	0.00	0.00	0.00	0.00	0.00	0.00	0.00	0.03	0.97
34.00	0.00	0.00	0.00	0.00	0.00	0.00	0.00	0.00	0.00	0.03	0.97
34.25	0.00	0.00	0.00	0.00	0.00	0.00	0.00	0.00	0.00	0.03	0.97
34.50	0.00	0.00	0.00	0.00	0.00	0.00	0.00	0.00	0.00	0.03	0.97
34.75	0.00	0.00	0.00	0.00	0.00	0.00	0.00	0.00	0.00	0.03	0.97

APPENDIX G

Sample RPD Calculation

Sample RPD Calculation

$$RPD = \frac{|C_{LPC} - C_{MOUDI}|}{\frac{C_{LPC} + C_{MOUDI}}{2}} * 100$$

Where:

RPD = relative percent difference

C_{LPC} = LPC TSP concentration

C_{MOUDI} = MOUDI TSP concentration

$$C_{LPC} = 0.59 \mu\text{g}/\text{m}^3$$

$$C_{MOUDI} = 0.68 \mu\text{g}/\text{m}^3$$

$$RPD = |0.59 \mu\text{g}/\text{m}^3 - 0.68 \mu\text{g}/\text{m}^3| / ((0.59 \mu\text{g}/\text{m}^3 + 0.68 \mu\text{g}/\text{m}^3)/2) * 100$$

$$RPD = |-0.09| / (0.635) * 100$$

$$RPD = 14.17 \%$$

APPENDIX H

Sample Calculation of LPC 1 to LPC 2 Calibration, Stat Sheets, and Charts

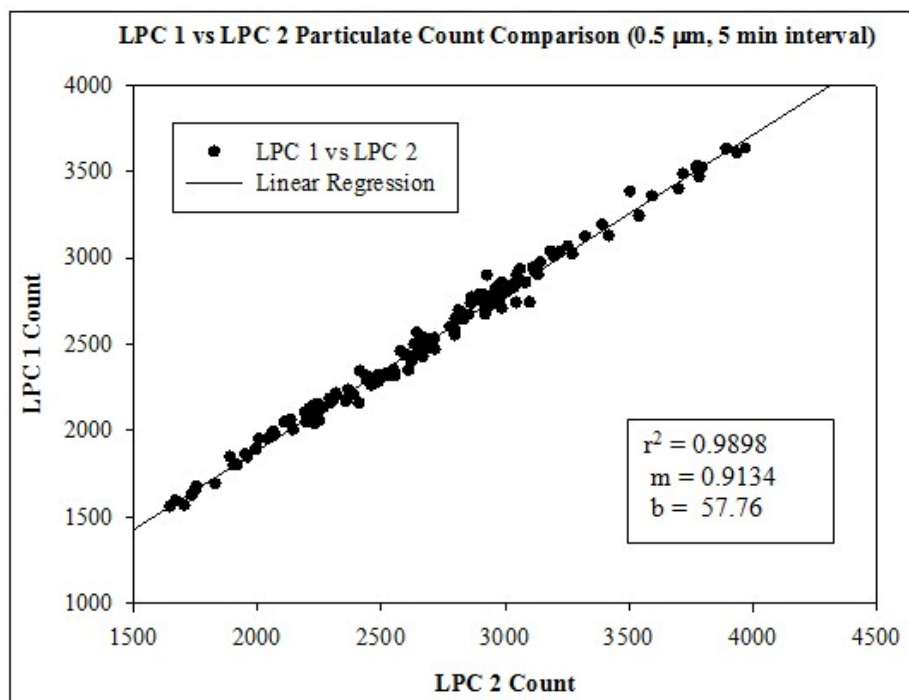


Figure H.1 LPC 1 vs LPC 2 Particulate Count Comparison (0.5 μm , 5 min Interval)

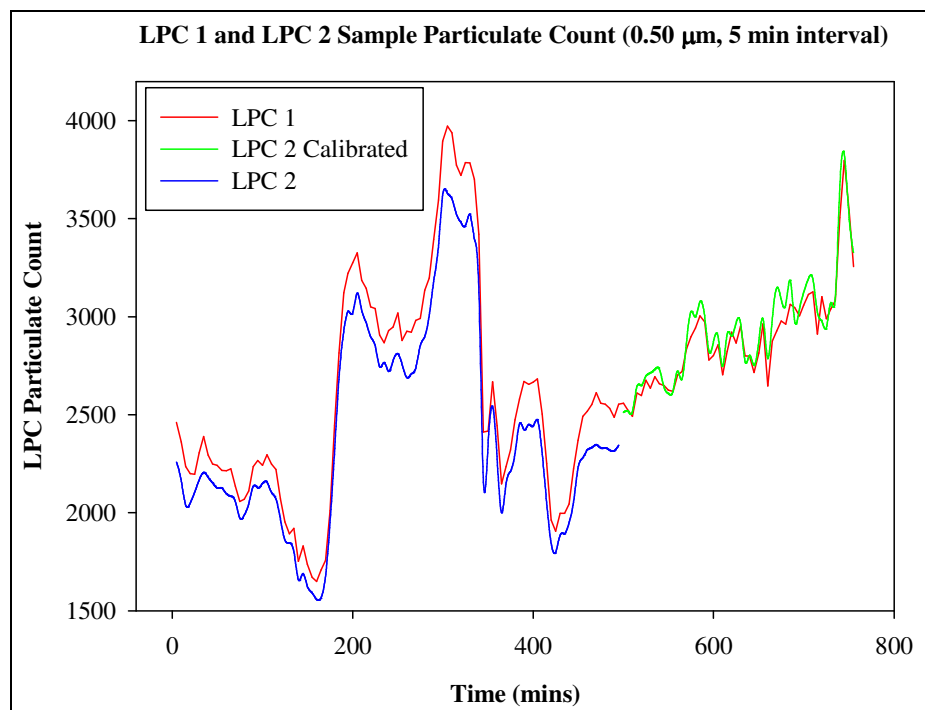


Figure H.2 LPC 1 and LPC 2 Sample Particulate Count (0.5 μm , 5 min Interval)

Table H.1 Mann-Whitney Rank Sum Test Results for 0.5 μm , 5 min interval.

t-test Wednesday, August 17, 2011, 3:27:42 PM

Data source: Data 2 in Summer LPC 1 to LPC 2.JNB

Normality Test: Failed ($P < 0.050$)
 Test execution ended by user request, Rank Sum Test begun

Mann-Whitney Rank Sum Test Wednesday, August 17, 2011, 3:27:42 PM

Data source: Data 2 in Summer LPC 1 to LPC 2.JNB

Group	N	Missing	Median	25%	75%
Col 5	155	4	2754.919	2396.802	3091.819
Col 2	155	4	2668.200	2273.050	2987.650

Mann-Whitney U Statistic= 10037.000

T = 24240.000 n(small)= 151 n(big)= 151 ($P = 0.072$)

The difference in the median values between the two groups is not great enough to exclude the possibility that the difference is due to random sampling variability; there is not a statistically significant difference ($P = 0.072$)

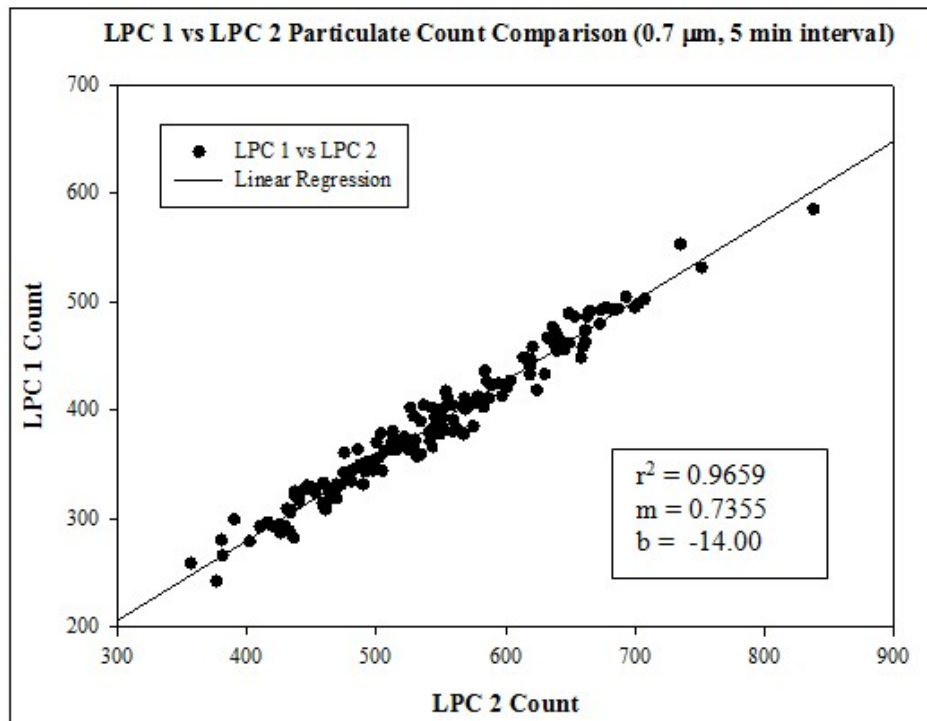


Figure H.3 LPC 1 vs LPC 2 Particulate Count Comparison (0.7 μm , 5 min Interval)

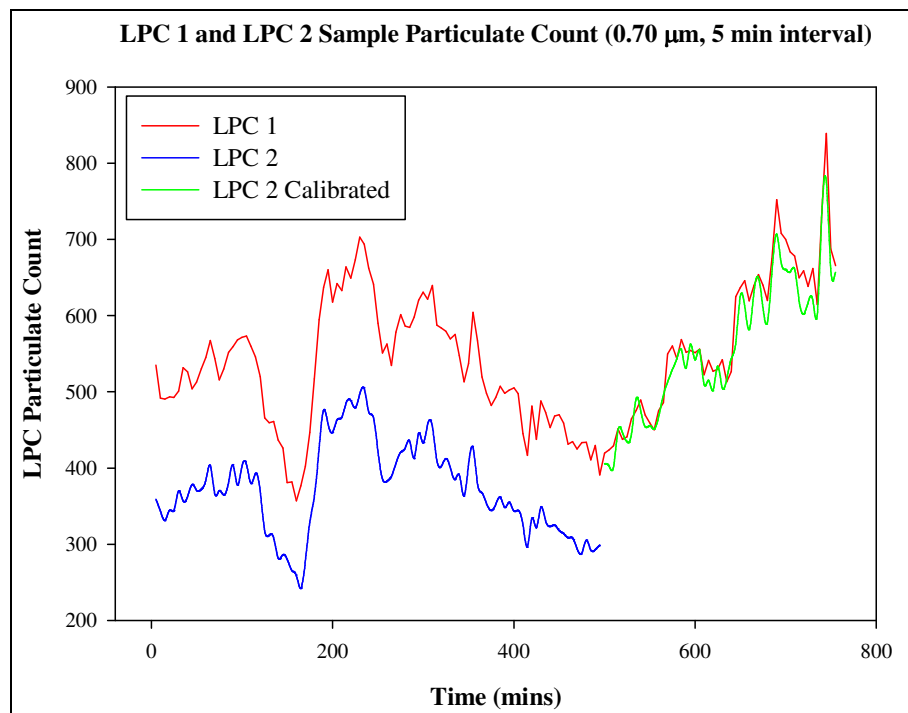


Figure H.4 LPC 1 and LPC 2 Sample Particulate Count (0.7 μm , 5 min Interval)

Table H.2 Mann-Whitney Rank Sum Test Results for 0.7 μm , 5 min interval.

t-test Wednesday, August 17, 2011, 4:37:03 PM

Data source: Data 3 in Summer LPC 1 to LPC 2.JNB

Normality Test: Failed (P < 0.050)

Test execution ended by user request, Rank Sum Test begun

Mann-Whitney Rank Sum Test Wednesday, August 17, 2011, 4:37:03 PM

Data source: Data 3 in Summer LPC 1 to LPC 2.JNB

Group	N	Missing	Median	25%	75%
Col 7	155	4	515.157	456.105	582.302
Col 2	155	4	541.400	475.350	616.900

Mann-Whitney U Statistic= 9918.000

T = 21394.000 n(small)= 151 n(big)= 151 (P = 0.051)

The difference in the median values between the two groups is not great enough to exclude the possibility that the difference is due to random sampling variability; there is not a statistically significant difference (P = 0.051)

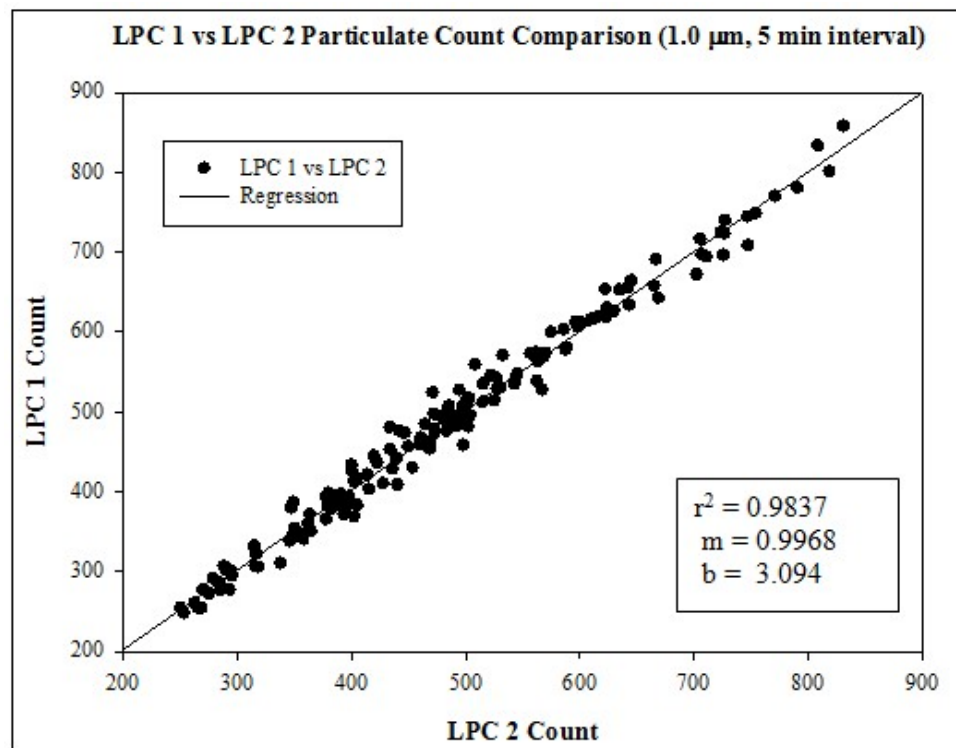


Figure H.5 LPC 1 vs LPC 2 Particulate Count Comparison (1.0 μm , 5 min Interval)

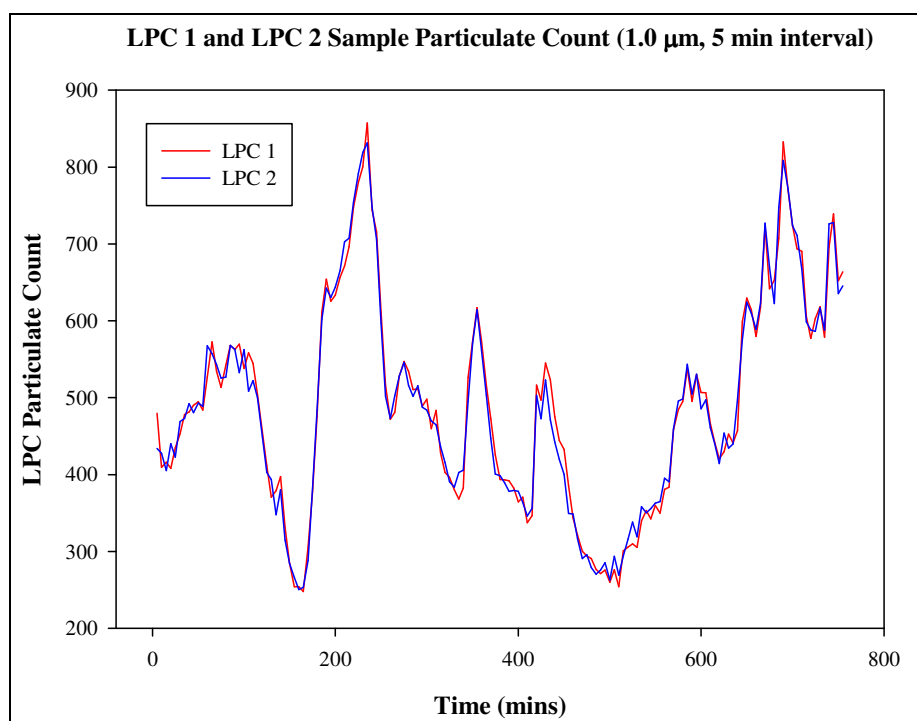


Figure H.6 LPC 1 and LPC 2 Sample Particulate Count (1.0 μm , 5 min Interval)

Table H.3 Mann-Whitney Rank Sum Test Results for 1.0 μ m, 5 min interval.

t-test Wednesday, August 17, 2011, 3:35:11 PM

Data source: Data 4 in Summer LPC 1 to LPC 2.JNB

Normality Test: Failed ($P < 0.050$)

Test execution ended by user request, Rank Sum Test begun

Mann-Whitney Rank Sum Test Wednesday, August 17, 2011, 3:35:11 PM

Data source: Data 4 in Summer LPC 1 to LPC 2.JNB

Group	N	Missing	Median	25%	75%
Col 2	155	4	483.800	382.700	576.200
Col 3	155	4	483.800	389.850	573.800

Mann-Whitney U Statistic= 11277.500

T = 22999.500 n(small)= 151 n(big)= 151 ($P = 0.872$)

The difference in the median values between the two groups is not great enough to exclude the possibility that the difference is due to random sampling variability; there is not a statistically significant difference ($P = 0.872$)

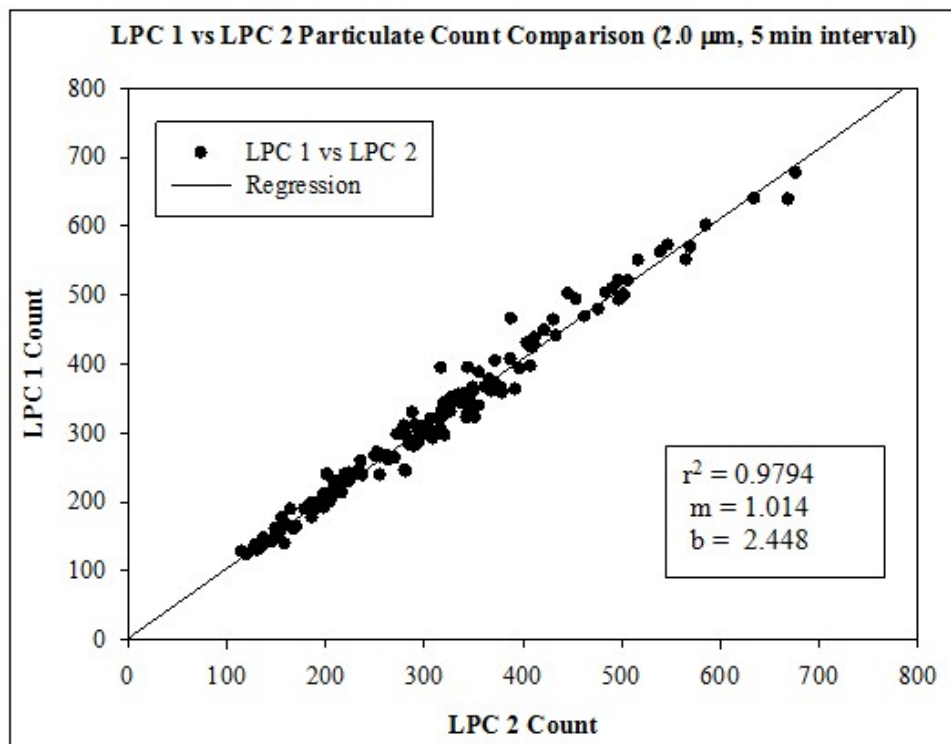


Figure H.7 LPC 1 vs LPC2 Particulate Count Comparison (2.0 μm , 5 min Interval)

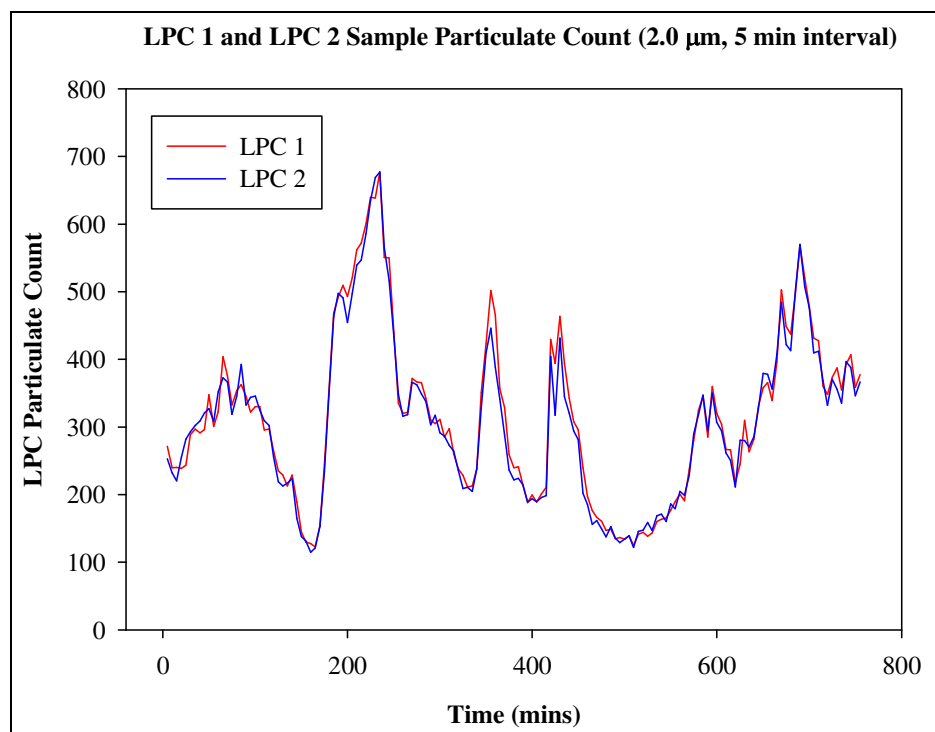


Figure H.8 LPC 1 and LPC2 Sample Particulate Count (2.0 μm , 5 min Interval)

Table H4 Mann-Whitney Rank Sum Test Results for 2.0 μ m, 5 min interval.

t-test Wednesday, August 17, 2011, 3:36:18 PM

Data source: Data 5 in Summer LPC 1 to LPC 2.JNB

Normality Test: Failed (P < 0.050)

Test execution ended by user request, Rank Sum Test begun

Mann-Whitney Rank Sum Test Wednesday, August 17, 2011, 3:36:18 PM

Data source: Data 5 in Summer LPC 1 to LPC 2.JNB

Group	N	Missing	Median	25%	75%
Col 2	155	4	304.800	220.300	373.100
Col 3	155	4	303.000	211.700	366.600

Mann-Whitney U Statistic= 11016.000

T = 23261.000 n(small)= 151 n(big)= 151 (P = 0.613)

The difference in the median values between the two groups is not great enough to exclude the possibility that the difference is due to random sampling variability; there is not a statistically significant difference (P = 0.613)

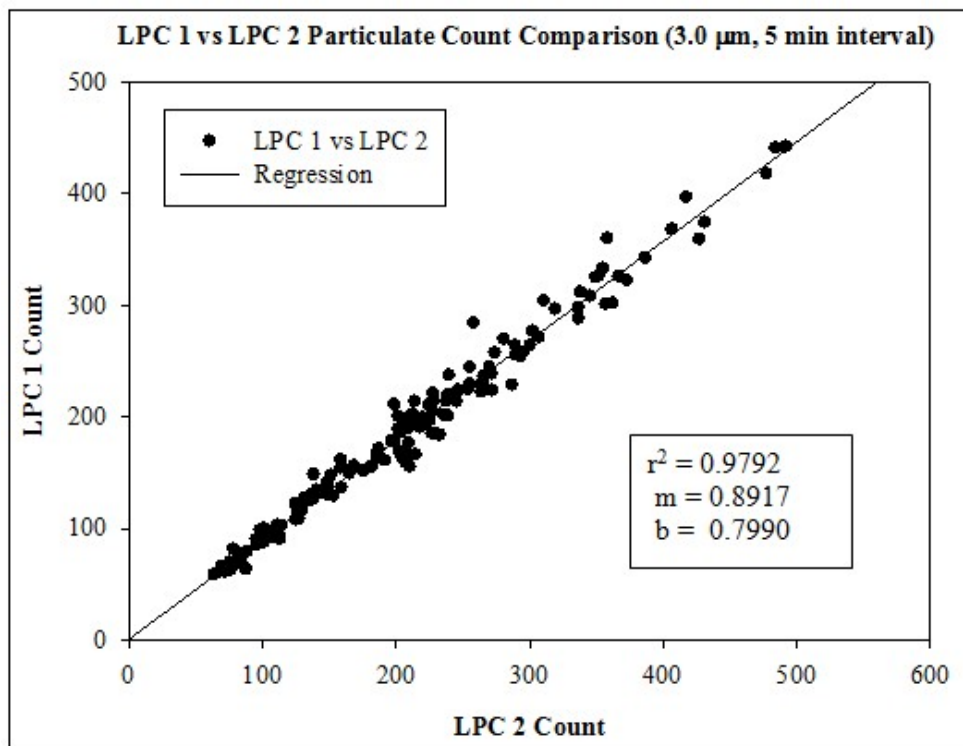


Figure H.9 LPC 1 vs LPC2 Particulate Count Comparison (3.0 μm , 5 min Interval)

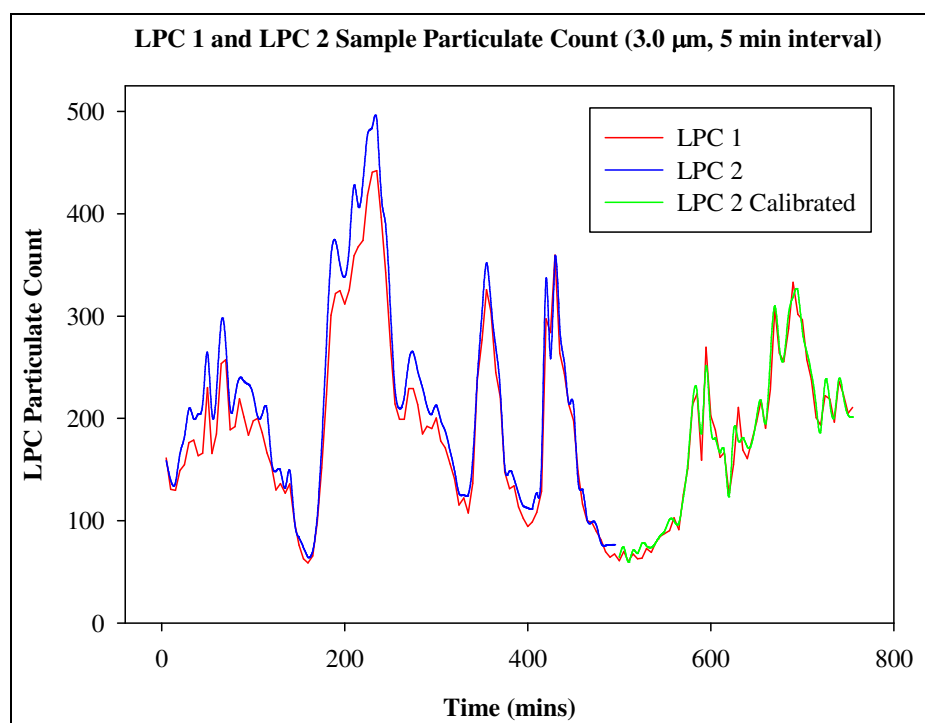


Figure H.10 LPC 1 and LPC 2 Sample Particulate Count (3.0 μm , 5 min Interval)

Table H.5 Mann-Whitney Rank Sum Test Results for 3.0 μm , 5 min interval.

t-test Wednesday, August 17, 2011, 3:51:17 PM

Data source: Data 6 in Summer LPC 1 to LPC 2.JNB

Normality Test: Failed (P < 0.050)

Test execution ended by user request, Rank Sum Test begun

Mann-Whitney Rank Sum Test Wednesday, August 17, 2011, 3:51:17 PM

Data source: Data 6 in Summer LPC 1 to LPC 2.JNB

Group	N	Missing	Median	25%	75%
Col 2	155	4	184.600	125.900	229.950
Col 5	155	4	186.912	122.139	236.672

Mann-Whitney U Statistic= 11376.000

T = 22852.000 n(small)= 151 n(big)= 151 (P = 0.975)

The difference in the median values between the two groups is not great enough to exclude the possibility that the difference is due to random sampling variability; there is not a statistically significant difference (P = 0.975)

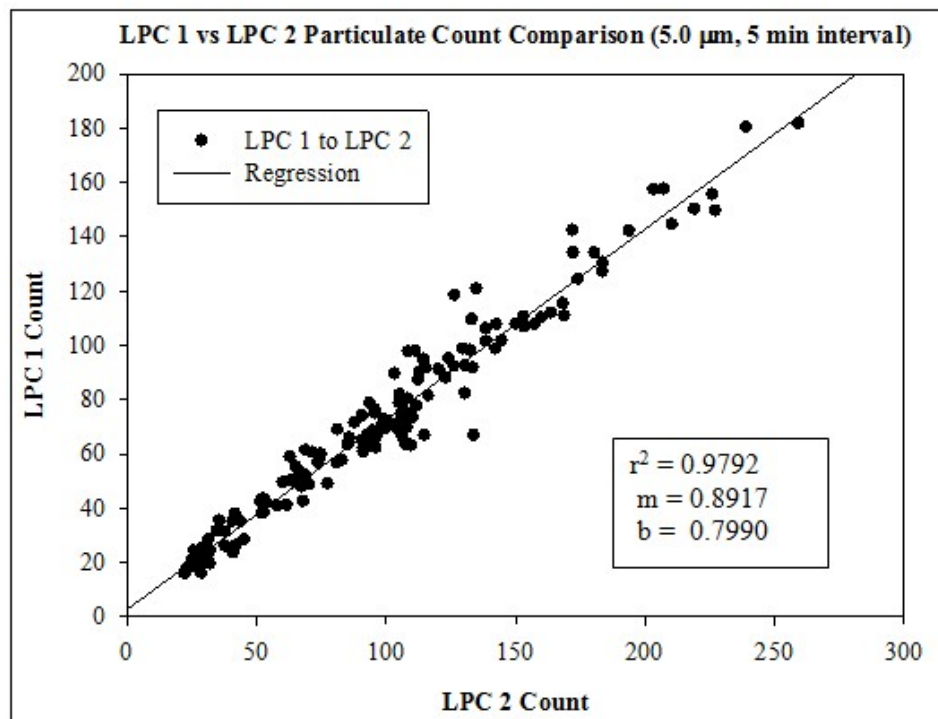


Figure H.11 LPC 1 vs LPC2 Particulate Count Comparison (5.0 μm , 5 min Interval)

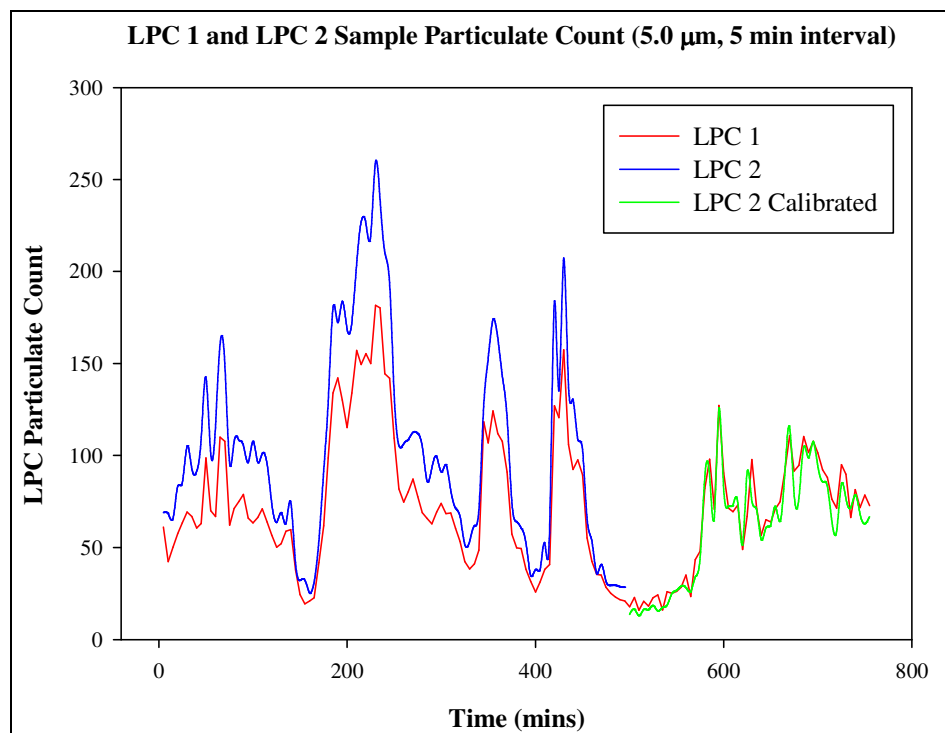


Figure H.12 LPC 1 and LPC2 Sample Particulate Count (5.0 μm , 5 min Interval)

Table H.6 Mann-Whitney Rank Sum Test Results for 5.0 μm , 5 min interval.

t-test

Wednesday, August 17, 2011, 3:53:44 PM

Data source: Data 7 in Summer LPC 1 to LPC 2.JNB**Normality Test:** Failed (P < 0.050)

Test execution ended by user request, Rank Sum Test begun

Mann-Whitney Rank Sum Test

Wednesday, August 17, 2011, 3:53:44 PM

Data source: Data 7 in Summer LPC 1 to LPC 2.JNB

Group	N	Missing	Median	25%	75%
Col 2	155	4	68.800	42.800	94.050
Col 7	155	4	64.741	39.779	85.852

Mann-Whitney U Statistic= 10438.000

T = 23839.000 n(small)= 151 n(big)= 151 (P = 0.205)

The difference in the median values between the two groups is not great enough to exclude the possibility that the difference is due to random sampling variability; there is not a statistically significant difference (P = 0.205)

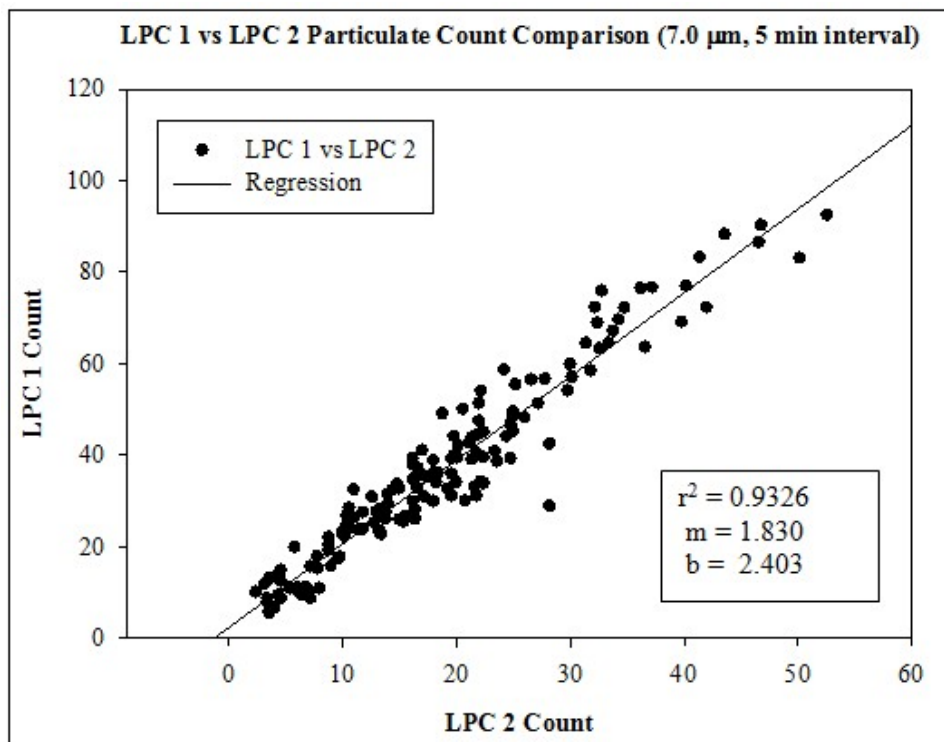


Figure H.13 LPC 1 vs LPC2 Particulate Count Comparison (7.0 μm, 5 min Interval)

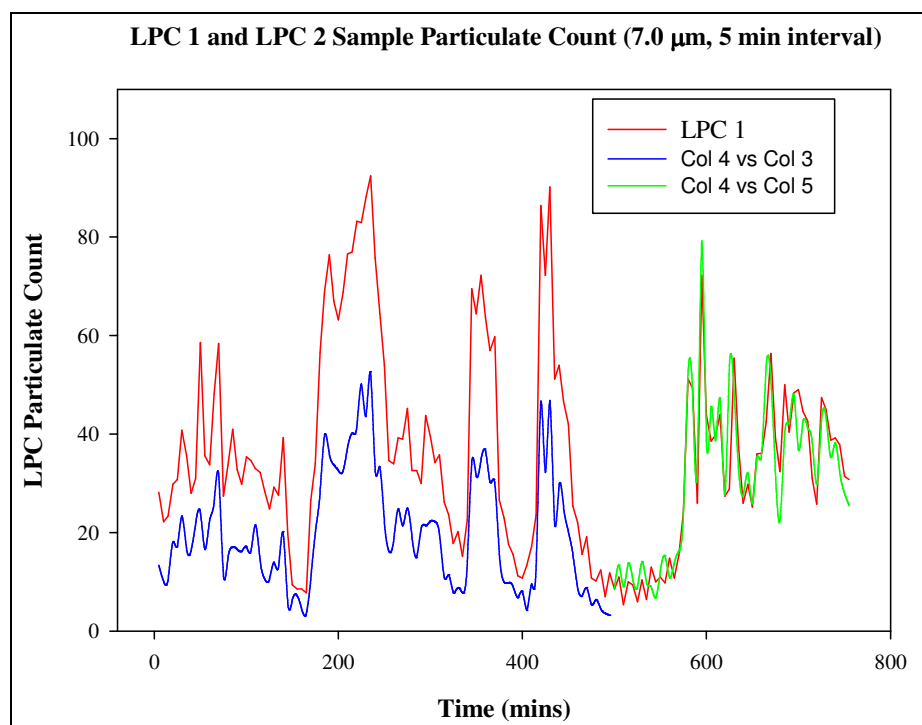


Figure H.14 LPC 1 and LPC2 Sample Particulate Count (7.0 μm, 5 min Interval)

Table H.7 Mann-Whitney Rank Sum Test Results for 7.0 μm , 5 min interval.

t-test						Wednesday, August 17, 2011, 4:19:22 PM
Data source:	Data 8.0 in Summer LPC 1 to LPC 2.JNB					
Normality Test:	Failed (P < 0.050)					
Test execution ended by user request, Rank Sum Test begun						
Mann-Whitney Rank Sum Test						Wednesday, August 17, 2011, 4:19:22 PM
Data source:	Data 8.0 in Summer LPC 1 to LPC 2.JNB					
Group	N	Missing	Median	25%	75%	
Col 5	155	4	33.147	20.794	46.964	
Col 2	155	4	33.000	22.300	47.200	
Mann-Whitney U Statistic= 11290.000						
T = 22987.000 n(small)= 151 n(big)= 151 (P = 0.885)						
The difference in the median values between the two groups is not great enough to exclude the possibility that the difference is due to random sampling variability; there is not a statistically significant difference (P = 0.885)						

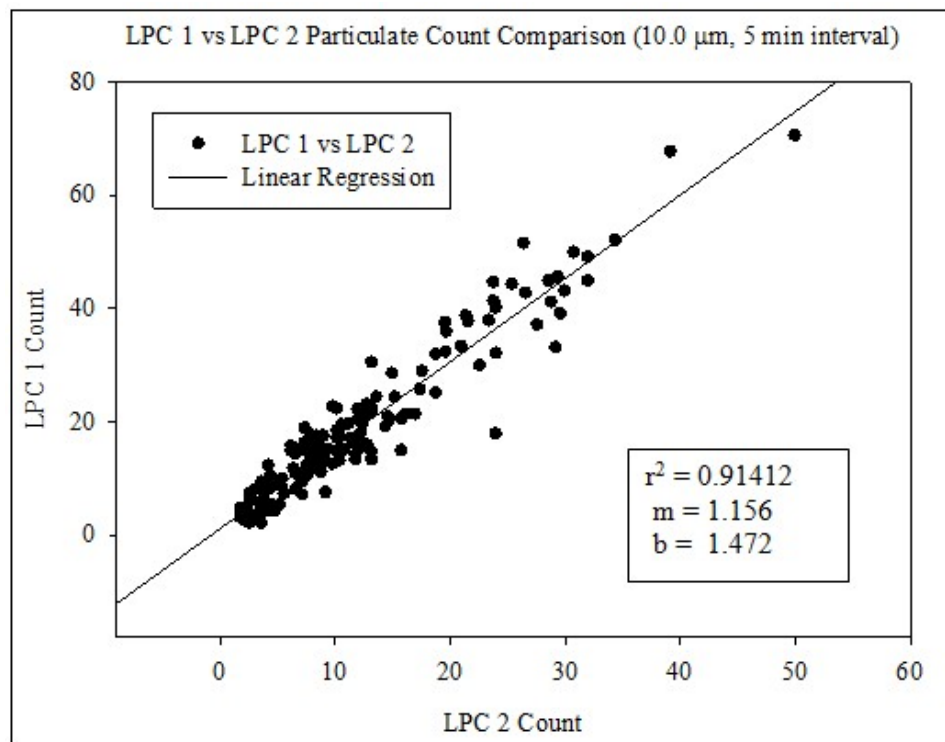


Figure H.15 LPC 1 vs LPC2 Particulate Count Comparison (10.0 μm , 5 min Interval)

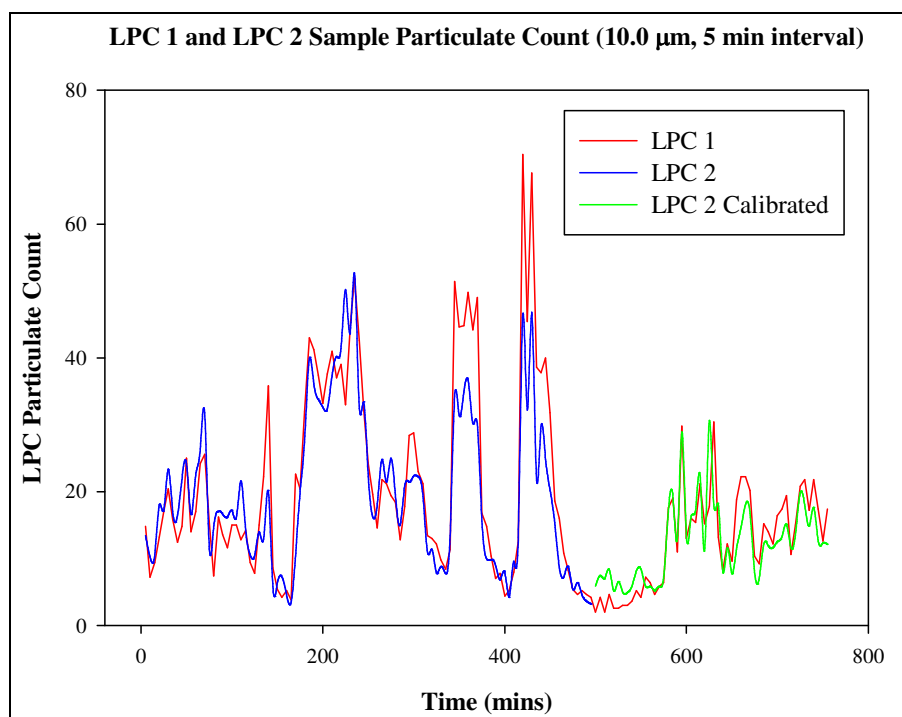


Figure H.16 LPC 1 and LPC2 Sample Particulate Count (10.0 μm , 5 min Interval)

Table H.8 Mann-Whitney Rank Sum Test Results for 10.0 μm , 5 min interval.

t-test Wednesday, August 17, 2011, 4:51:17 PM

Data source: Data 9 in Summer LPC 1 to LPC 2.JNB

Normality Test: Failed (P < 0.050)

Test execution ended by user request, Rank Sum Test begun

Mann-Whitney Rank Sum Test Wednesday, August 17, 2011, 4:51:17 PM

Data source: Data 9 in Summer LPC 1 to LPC 2.JNB

Group	N	Missing	Median	25%	75%
Col 8	155	4	13.712	9.092	20.353
Col 2	155	4	15.200	9.250	22.500

Mann-Whitney U Statistic= 10716.000

T = 22192.000 n(small)= 151 n(big)= 151 (P = 0.367)

The difference in the median values between the two groups is not great enough to exclude the possibility that the difference is due to random sampling variability; there is not a statistically significant difference (P = 0.367)

APPENDIX I

Student T-Test Trip Blank Results

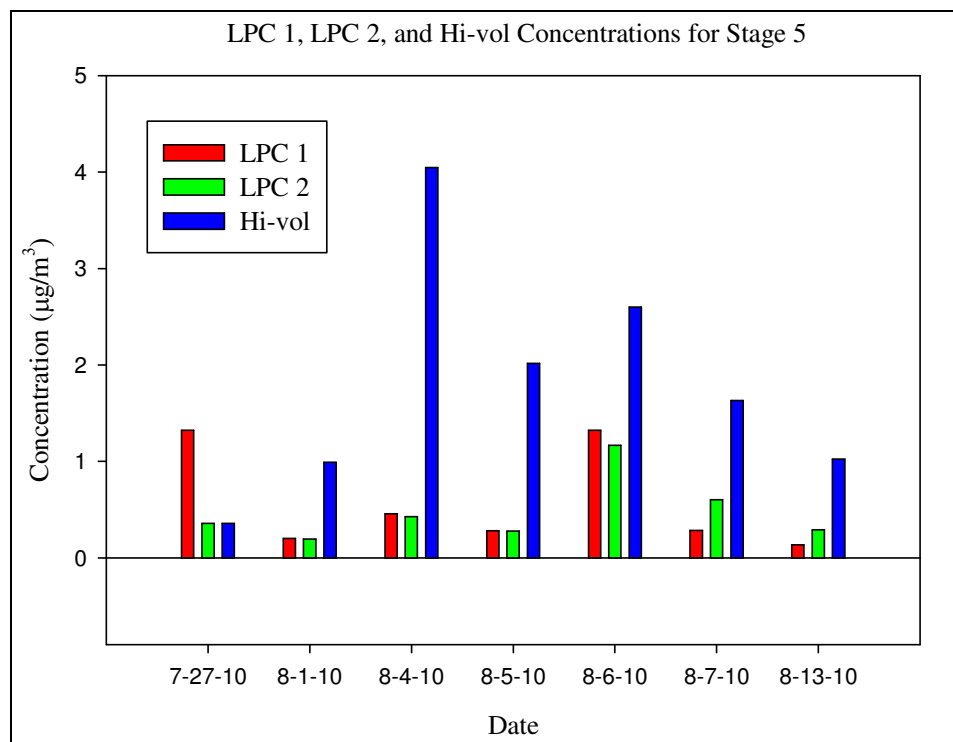


Figure I.1 LPC 1, LPC 2, and Hi-vol Concentrations for Stage 5

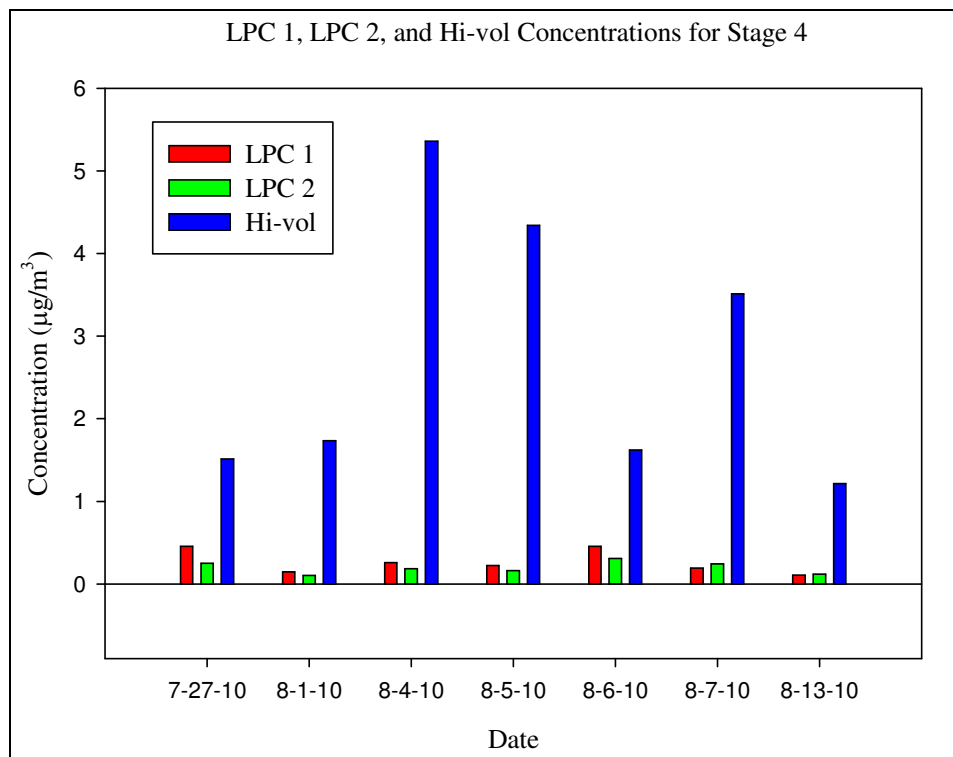


Figure I.2 LPC 1, LPC 2, and Hi-vol Concentrations for Stage 4

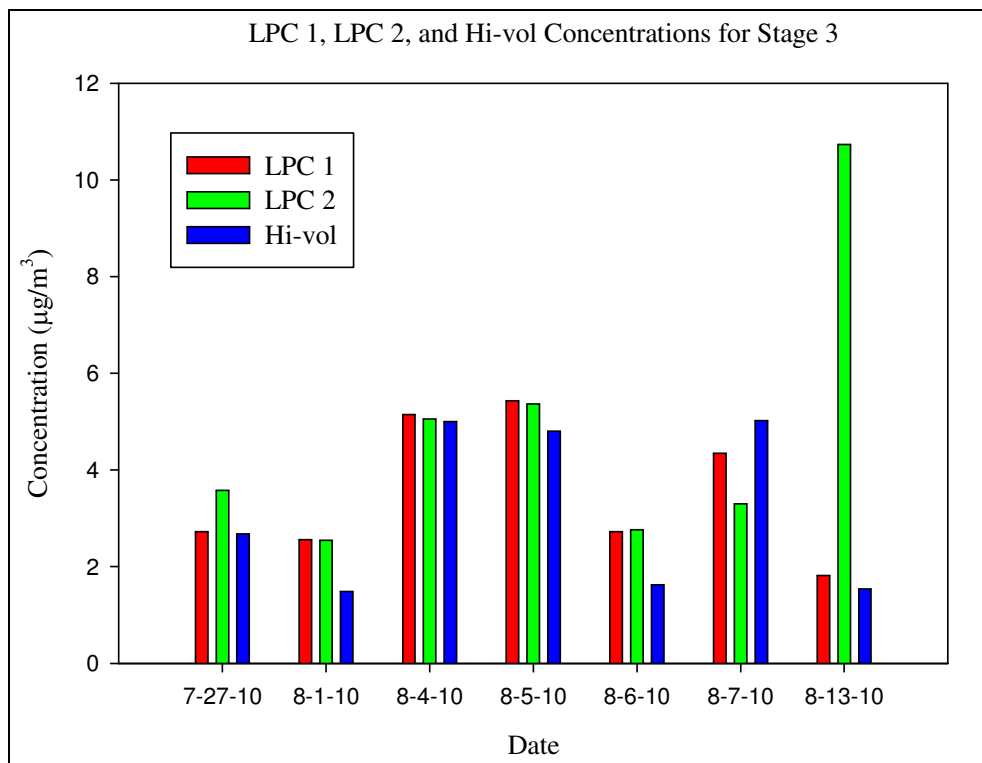


Figure I.3 LPC 1, LPC 2, and Hi-vol Concentrations for Stage 3

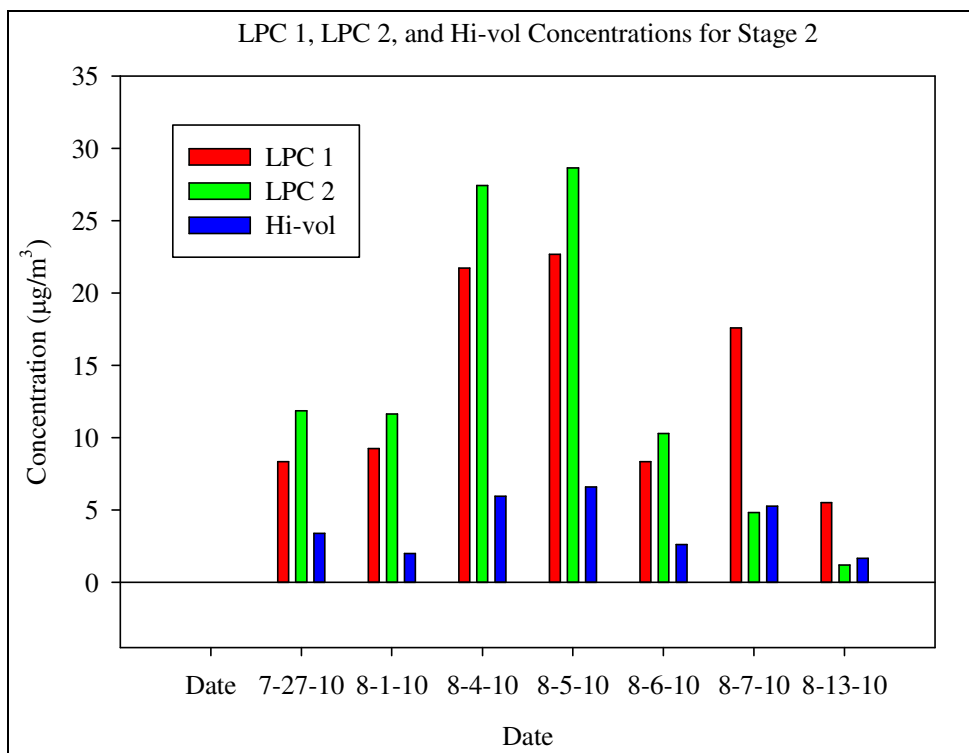


Figure I.4 LPC 1, LPC 2, and Hi-vol Concentrations for Stage 2

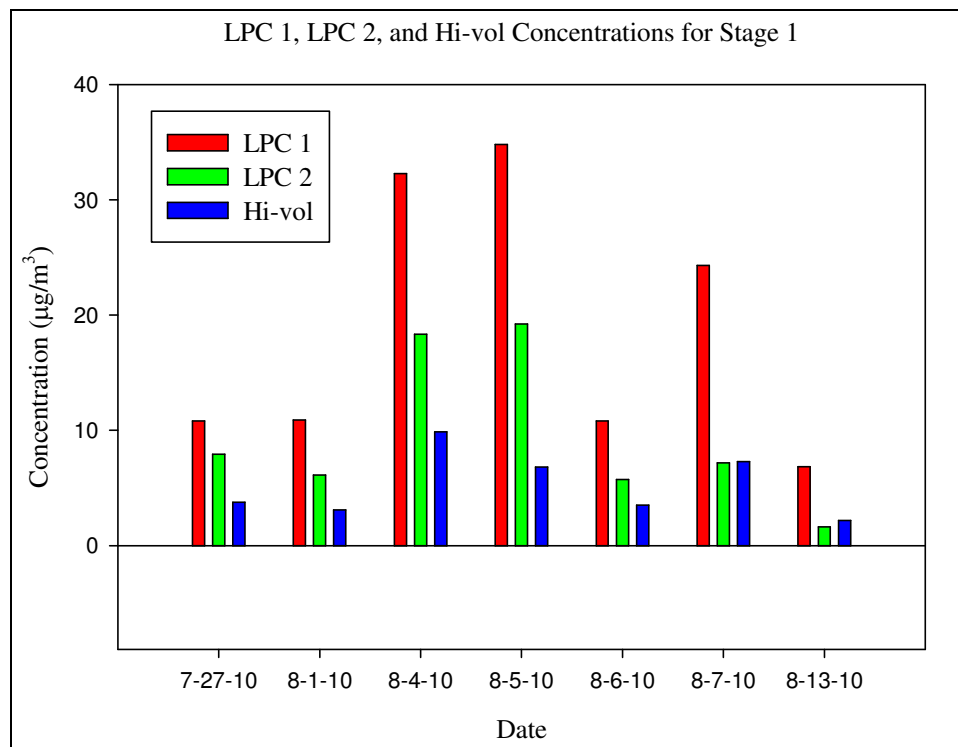


Figure I.5 LPC 1, LPC 2, and Hi-vol Concentrations for Stage 1

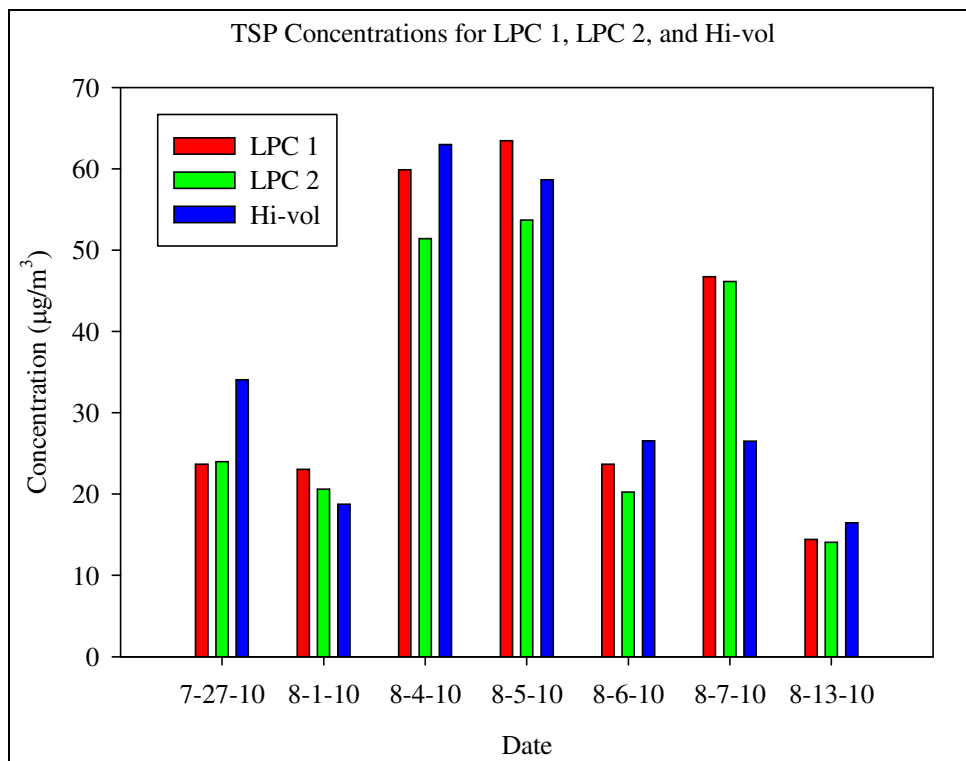


Figure I.6 TSP Concentrations for LPC 1, LPC 2, and Hi-vol

APPENDIX J

Student T-Test Trip Blank Results

Table J.1 Hi-vol trip blank results

Date	Start Weight (mg)	End Weight (mg)	Rel. Difference
10-25	4.4229	4.4231	0.0002
10-22	4.4203	4.4202	0.0001
10-27	4.4189	4.4185	0.0004
10-28	4.4284	4.4288	0.0004
11-02	4.4268	4.4276	0.0008
11-03	4.4171	4.4169	0.0002
11-04	4.4049	4.4052	0.0003

Table J.2 T-Test

t-test	Monday, October 03, 2011, 1:59:38 PM				
Data source: Data 2 in LPC pump calibration.JNB					
Normality Test:	Passed (P = 0.055)				
Equal Variance Test:	Passed (P = 0.925)				
Group Name	N	Missing	Mean	Std. Dev	SEM
Col 3	9	2	4.420	0.00778	0.00294
Col 4	9	2	4.420	0.00791	0.00299
Difference	-0.000143				
t = -0.0341 with 12 degrees of freedom. (P = 0.973)					
95 percent confidence interval for difference of means: -0.00928 to 0.00899					
The difference in the mean values of the two groups is not great enough to reject the possibility that the difference is due to random sampling variability. There is not a statistically significant difference between the input groups (P = 0.973).					
Power of performed test with alpha = 0.050: 0.050					
The power of the performed test (0.050) is below the desired power of 0.800.					
Less than desired power indicates you are less likely to detect a difference when one actually exists.					
Negative results should be interpreted cautiously.					
